

Modelling of the hydromechanical behaviour of
unsaturated swelling soils

*A dissertation submitted for the
Degree of Master of Science*

Maria Camila Olarte Garzón

April 2023

University of Brasilia, Brasilia

Faculty of Technology

Department of Civil and Environmental Engineering

Publication: G.DM 391/2023

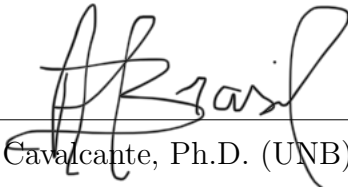
UNIVERSITY OF BRASILIA
FACULTY OF TECHNOLOGY
DEPARTMENT OF CIVIL AND ENVIRONMENTAL

MODELLING OF THE HYDROMECHANICAL BEHAVIOUR OF UNSATURATED SWELLING SOILS

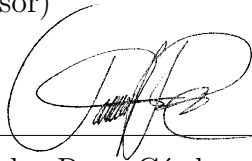
MARIA CAMILA OLARTE GARZÓN

DISSERTATION SUBMITTED TO THE DEPARTMENT OF CIVIL ENGINEERING
OF THE UNIVERSITY OF BRASILIA AS PART OF THE NECESSARY REQUIRE-
MENTS TO OBTAIN THE DEGREE OF MASTER OF SCIENCE.

APROVED BY:

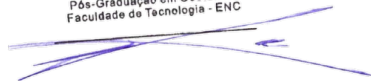


André Luís Brasil Cavalcante, Ph.D. (UNB)
(Supervisor)



Juan Carlos Ruge Cárdenas, Ph.D. (UMNG)
(External Examiner)

JUAN FÉLIX RODRÍGUEZ REBOLLEDO
Professor, Eng. Civil, MSc, PhD
Pós-Graduação em Geotecnia
Faculdade de Tecnologia - ENC



Juan Félix Rodríguez Rebolledo, Ph.D. (UNB)
(Internal Examiner)

BRASILIA/DF, April, 2023

CATALOGUING DATA

OLARTE GARZÓN, MARIA CAMILA

Modelling of the hydromechanical behaviour of unsaturated swelling soils. Brasilia/DF, 2023. viii, 103p., 210 x 297 mm (FEC/FT/UnB), Master of Science, Geotechnics, 2023.

University of Brasilia, Faculty of Technology, Department of Civil and Environmental Engineering.

- | | |
|------------------------------|---------------------------|
| 1. Hydromechanical behaviour | 2. Swelling soils |
| 3. Unsaturated media | 4. Mathematical modelling |
| I. FEC/FT/UnB | II. MASTER |

BIBLIOGRAPHIC REFERENCE

Olarte, M.C. (2023). Modelling of the hydromechanical behaviour of unsaturated swelling soils. Master's dissertation. Publication PPG. G.DM 391/2023, Department of Civil and Environmental Engineering, University of Brasilia, Brasilia/DF, 103p.

ASSIGNMENT OF RIGHTS

Author: Maria Camila Olarte Garzón

Title: Modelling of the hydromechanical behaviour of unsaturated swelling soils.

Degree: Master of Science Year: 2023

Permission is granted to University of Brasilia to reproduce copies of this Master's dissertation and to loan or sell such copies for academic and scientific purposes only. The author reserves other publication rights, and no part of this Master's dissertation may be reproduced without the author's written permission.



Maria Camila Olarte Garzón

University of Brasilia (UnB)

Brasilia - DF CEP 70919-970

Dedication

To my beloved Luciana

Acknowledgements

I thank the Great Architect of the Universe and creator of natural perfection for guiding and enlightening me in moments of intellectual darkness. To the benign Nature that extraordinarily allows me to find something to learn everywhere: *"Nature is the source of all true knowledge. She has her own logic, her own laws, she has no effect without cause nor invention without necessity. - Leonardo da Vinci"*

To my family; my parents, my sister, and my beloved niece Luciana, for being my balm and my safe place. As difficult as reality can be at times, my most precious possession is sharing life's journey with you.

To the post-graduate program in Geotechnics at the University of Brasilia for believing in me and my abilities when I was accepted into the master's course. To the CNPq and CAPES for supporting me financially in Brazil.

I am deeply grateful to Professor André Luís Brasil Cavalcante for being my master and the most significant support I had throughout this academic process. Your guidance, with admirable commitment and selflessness, was the main axis that allowed me to complete this work successfully. I will always be grateful.

To my dear friends Joshy, Wendy, Anderson and Mayara, for accompanying me on this journey and giving me the most sincere and selfless friendship. Thank you for turning the smallest moment into the greatest memory, and for making my life so beautiful, so full of color and laughter.

To all the professors of the PPG of the University of Brasilia, and to all those who were part of my academic life. If I have seen further it is by standing on the shoulders of giants.

ABSTRACT

Olarte Garzon, M.C., (2023). **Modelling of the hydromechanical behaviour of unsaturated swelling soils**. Master's dissertation, University of Brasilia, Faculty of Technology, Department of Civil and Environmental Engineering, Brasilia DF, 103p.

Expansive soils are materials composed mainly of active minerals, such as montmorillonite, which tend to undergo volumetric changes due to moisture content migration. Different geotechnical engineering practices, such as the design of a dam core or the compaction of the subgrade, require a thorough analysis and prediction of the expansion phenomenon under unsaturated transient conditions. The main problem in evaluating the mechanical response of this type of soil lies in the nonlinear nature of most of the unsaturated properties, which requires sophisticated tools that include parameters that are difficult to obtain. This study performs a mathematical analysis to understand the hydromechanical behaviour of swelling soils under unsaturated transient flow. The implementation of two mathematical models based on the [Richards \(1931\)](#) equation with a simplified coupling is applied to evaluate the approach. Based on experimental results obtained from soil-column tests, the behaviour of the resulting model under different suction and moisture content conditions is explored. Four cases of analytical solutions are established to build a model-specific response framework, each with restrictive assumptions tailored to an initial and two boundary conditions. In this case, the hydromechanical predictions in unsaturated flow are adjusted considering the variations of the void ratio along the swelling process to account for the impact of volumetric deformations on the model parameters. Finally, a parametric calibration with literature results is performed to evaluate the parametric sensitivity and the range of volumetric variation in which the model is constrained. The results indicate a high statistical proximity between the numerical estimation and the experimental data, with correlation factors higher than 97%, both in the wetting and drying paths of the void ratio *versus log* suction curve. Likewise, the predictions of the analytical solutions for cases 1 and 3 are consistent for each parameter analyzed and work for unimodal and bimodal Soil Water Retention Curves.

RESUMO

Olarte Garzon, M.C., (2023). **Modelagem do comportamento hidromecânico de solos expansivos não saturados**. Dissertação de Mestrado, Universidade de Brasília, Faculdade de Tecnologia, Departamento de Engenharia Civil e Ambiental, Brasília DF, 103p.

Os solos expansivos são materiais compostos principalmente por minerais ativos, como a montmorilonita, que tendem a sofrer alterações volumétricas devido à migração do teor de umidade. Diferentes práticas de engenharia geotécnica, como o projeto de um núcleo de barragem ou a compactação do solo, requerem uma análise minuciosa e previsão do fenômeno de expansão sob condições transientes não saturadas. O principal problema na avaliação da resposta mecânica deste tipo de solo reside na natureza não linear da maioria das propriedades não saturadas, o que requer ferramentas sofisticadas que incluem parâmetros de difícil obtenção. Este estudo realiza uma análise matemática para entender o comportamento hidromecânico de solos expansivos sob fluxo transiente não saturado. A implementação de dois modelos matemáticos baseados na equação Richards (1931) com um acoplamento simplificado é aplicada para avaliar a abordagem. Com base em resultados experimentais obtidos em ensaios de grandes colunas, explora-se o comportamento do modelo resultante em diferentes condições de sucção e conteúdo volumétrico d'água. Quatro casos de soluções analíticas são estabelecidos para construir uma estrutura de resposta específica do modelo, cada um com suposições restritivas adaptadas a uma condição inicial e duas condições de contorno. Neste caso, as previsões hidromecânicas em fluxo não saturado são ajustadas considerando as variações do índice de vazios ao longo do processo de expansão, para dar conta do impacto das deformações volumétricas nos parâmetros do modelo. Por fim, uma calibração paramétrica com resultados da literatura é realizada para avaliar a sensibilidade paramétrica e a faixa de variação volumétrica na qual o modelo está restrito. Os resultados indicam uma grande proximidade estatística entre a estimativa numérica e os dados experimentais, com fatores de correlação superiores a 97%, tanto nas trajetórias de umedecimento quanto de secagem da curva de índice de vazios *versus* \log de sucção. Da mesma forma, as previsões das soluções analíticas para os casos 1 e 3 são consistentes para cada parâmetro analisado e funcionam para Curvas de Retenção de Água unimodais e bimodais.

RESUMEN

Olarte Garzon, M.C., (2023). **Modelación del comportamiento hidromecánico de arcillas expansivas no saturadas**. Trabajo de grado de Maestría, Universidad de Brasilia, Facultad de Tecnología, Departamento de Ingeniería Civil y Ambiental, Brasilia DF, 103p.

Los suelos expansivos son materiales compuestos principalmente por minerales activos como la montmorillonita, que tienden a sufrir cambios volumétricos debido a cambios en el contenido de humedad. Diferentes prácticas de ingeniería geotécnica, como el diseño de núcleos de presas o la compactación de la subrasante en pavimentos, requieren un análisis y una predicción exhaustivos del fenómeno de expansividad en condiciones transientes no saturadas. El principal problema para evaluar la respuesta mecánica de este tipo de suelos radica en la naturaleza no lineal de la mayoría de las propiedades no saturadas, lo que requiere herramientas sofisticadas que incluyen parámetros de difícil obtención. Este estudio realiza un análisis matemático para comprender el comportamiento hidromecánico de suelos expansivos bajo flujo transiente no saturado. Es aplicada la implementación de dos modelos matemáticos basados en la ecuación [Richards \(1931\)](#) con un acoplamiento simplificado para evaluar el enfoque. Con base en resultados experimentales obtenidos de ensayos de columnas de suelos, se explora el comportamiento del modelo resultante bajo diferentes condiciones de succión y contenido volumétrico de agua. Se establecen cuatro casos de soluciones analíticas para construir un marco de respuesta específico del modelo, cada uno con suposiciones restrictivas adaptadas a una condición inicial y dos condiciones de contorno. En este caso, las predicciones hidromecánicas en flujo no saturado se ajustan considerando las variaciones de la relación de vacíos a lo largo del proceso de expansión para tener en cuenta el impacto de las deformaciones volumétricas en los parámetros del modelo. Finalmente, se realiza una calibración paramétrica con resultados de la literatura para evaluar la sensibilidad paramétrica y el rango de variación volumétrica a la que se restringe el modelo. Los resultados indican una alta proximidad estadística entre la estimación numérica y los datos experimentales, con factores de correlación superiores al 97%, tanto en la trayectoria de humedecimiento como en la de secado de la curva relación de vacíos *versus log* de succión. Asimismo, las estimaciones de las soluciones analíticas para los Casos 1 y 3 son consistentes para cada parámetro analizado, y funcionan para curvas de retención de agua unimodales y bimodales.

Contents

1	INTRODUCTION	1
1.1	MOTIVATION	1
1.2	OBJECTIVES	2
1.3	METHODOLOGY	3
1.4	DISSERTATION OUTLINE	4
2	STATE OF THE ART	5
2.1	EXPANSIVE SOILS	5
2.1.1	Understanding of microscopic mechanisms of swelling	5
2.1.2	Hydromechanical behaviour of swelling soils	8
2.1.3	The place of swelling clays in soil mechanics	12
2.1.4	Problems of expansive soils	13
2.2	MOVEMENT OF WATER	15
2.2.1	Flow in unsaturated porous medium	19
2.3	RICHARDS EQUATION (1931)	20
2.3.1	Cavalcante and Zornberg (2017) model	22
2.3.2	Askar and Jin (2000) model	25
3	METHODS AND MATERIALS	28
3.1	METHODS	28
3.1.1	Mathematical model formulation	28
3.1.2	Analytical solutions	29
3.1.3	Validation with experimental results	30
3.1.4	Parametric calibration	32
3.2	MATERIALS	33
4	RESULTS	37
4.1	MATHEMATICAL MODEL FORMULATION	37
4.2	ANALYTICAL SOLUTIONS	41

4.2.1	Case 1: Imposed constant moisture to the upper boundary of a semi-infinite column	43
4.2.2	Case 2: Imposed constant moisture to the upper boundary of a column of finite length	45
4.2.3	Case 3: Imposed constant discharge velocity to the upper boundary of a semi-infinity column	47
4.2.4	Case 4: Imposed constant discharge velocity to the upper boundary of a column of finite length	48
4.3	DECISION JUSTIFICATION ON CASE CHOICE	50
4.4	VALIDATION WITH EXPERIMENTAL RESULTS	51
4.5	PARAMETRIC CALIBRATION	65
4.5.1	Wetting path	65
4.5.2	Drying path	66
5	CONCLUDING REMARKS	70
5.1	CONCLUSIONS	70
5.2	LIMITATIONS OF THE MODEL	71
5.3	RECOMMENDATIONS	71
	REFERENCES	73
A	MATHEMATICAL DERIVATION	82
A.1	DEFINITION OF $k_z(\theta)$	82
A.2	DEFINITION OF $\psi(\theta)$	83
A.3	DEFINITION OF $e(\theta)$	85

List of Figures

1.1	Methodology of the dissertation.	3
2.1	Schematic of swelling process.	7
2.2	Schematic of an unsaturated expansive soil.	8
2.3	Unimodal soil-water retention curve.	10
2.4	Swell evolution.	11
2.5	Water content-void ratio swell-shrink paths of a clay soil.	11
2.6	Water flow: (a) REV; (b) water flow in and out of the REV.	16
2.7	Physical representation of parameters δ , θ_s , and θ_r	25
3.1	Summary of steps of the methodology to be implemented.	28
3.2	Schematic of model formulation for swelling soils in unsaturated porous media.	29
3.3	Formulation of the analytical solution for model of swelling soils.	30
3.4	Schematic diagram of the soil column test.	31
3.5	$e - \log \psi$ curve.	33
3.6	Particle Size Distribution of the soil.	34
3.7	Soil Water Retention Curve.	35
3.8	Soil k -function.	36
4.1	Synthesized scheme: (a) hydrological cycle; (b) functions $k(\theta)$ and v_0 with respect to time.	41
4.2	Graphical representation of the behaviour of θ_0 , θ_i , v_0 and $v_{0,max}$ with respect to time.	42
4.3	Predicted volumetric water content for Case 2 using $\delta=0.639 \text{ kPa}^{-1}$: (a) time history at different locations; (b) profiles at increasing times.	50
4.4	Predicted void ratio for Case 2 using $\delta=0.639 \text{ kPa}^{-1}$: (a) time history at different locations; (b) profiles at increasing times.	51
4.5	Predicted swelling for Case 4 using $\delta=0.639 \text{ kPa}^{-1}$: (a) time history at different locations; (b) profiles at increasing times.	51
4.6	Fitting SWRC to obtain the δ value.	53
4.7	Fitting of bimodal SWRC to obtain the δ value.	54

4.8	Comparison of the experimental results of unsaturated hydraulic conductivity with the k -function fitting model.	55
4.9	Sensitivity of hydraulic parameter (δ) in the $e - \log \psi$ curve.	56
4.10	Predicted volumetric water content for Case 1 using $\delta=0.639 \text{ kPa}^{-1}$: (a) time history at different locations; (b) profiles at increasing times.	57
4.11	Experimental results for time history of volumetric water content.	58
4.12	Predicted suction for Case 1 using $\delta=0.639 \text{ kPa}^{-1}$: (a) time history at different locations; (b) profiles at increasing times.	58
4.13	Experimental results for time history of total suction.	59
4.14	Predicted unsaturated hydraulic conductivity for Case 1 using $\delta=0.639 \text{ kPa}^{-1}$: (a) time history at different locations; (b) profiles at increasing times.	60
4.15	Predicted saturation degree for Case 1 using $\delta=0.639 \text{ kPa}^{-1}$: (a) time history at different locations; (b) profiles at increasing times.	60
4.16	Predicted void ratio for Case 1 using $\delta=0.639 \text{ kPa}^{-1}$: (a) time history at different locations; (b) profiles at increasing times.	61
4.17	Predicted swelling for Case 1 using $\delta=0.639 \text{ kPa}^{-1}$: (a) time history at different locations; (b) profiles at increasing times.	62
4.18	Predicted results for Case 1 using $\delta=0.639 \text{ kPa}^{-1}$: (a) time history of void ratio rates (b) void ratio gradient profiles.	62
4.19	Predicted void ratio for Case 3 using $\delta=0.639 \text{ kPa}^{-1}$: (a) time history at different locations; (b) profiles at increasing times.	63
4.20	Predicted swelling for Case 3 using $\delta=0.639 \text{ kPa}^{-1}$: (a) time history at different locations; (b) profiles at increasing times.	64
4.21	Predicted results for Case 3 using $\delta=0.639 \text{ kPa}^{-1}$: (a) time history of void ratio rates (b) void ratio gradient profiles.	64
4.22	$e - \log \psi$ curve (wetting path) comparison between model simulation and experiment data (Nowamooz & Masrouri, 2010).	65
4.23	$e - \log \psi$ curve (drying path) comparison between model simulation and experiment data (Al-Dakheeli & Bulut, 2019).	67
4.24	$e - \log \psi$ curve (drying path) comparison between model simulation and experiment data (Zhao et al., 2021).	68
4.25	$e - \log \psi$ curve (drying path) comparison between model simulation and experiment data (Sarker & Wang, 2022).	69

List of Tables

2.1	Cases study of buildings damaged by expansive soils.	15
3.1	Initial and boundary conditions for each case.	30
3.2	Physical properties of soil.	33
3.3	Summary of hydraulic fitting parameters of soil.	35
4.1	Parameters of the analyzed model.	52
4.2	Sensitivity of the δ parameter for unimodal and bimodal SWRC.	53
4.3	\bar{R} , \bar{D}_z and \bar{a}_s components obtained from the experimental fitting.	56
4.4	Parametric values used in the analytical solutions for Cases 1 and 3.	56
4.5	Calibration parameters for the wetting path.	65
4.6	Statistical fit and estimated \bar{R} component for the wetting path.	66
4.7	Calibration parameters for the drying path.	67
4.8	Statistical fit and estimated \bar{R} component for the drying path.	69

List of acronyms

Latin expressions

in situ Latin expression that means in the original place

Initialism

AEV *Air Entry Value*
REV Representative Volume Element
SWRC *Soil Water Retention Curve*

Greek symbols

δ	Fitting hydraulic parameter	$[M^{-1}LT^2]$
Δ	Differential	
γ_d	Dry unit weight	$[ML^{-3}]$
θ	Volumetric water content	$[L^3L^{-3}]$
θ_r	Residual volumetric water content	$[L^3L^{-3}]$
θ_s	Saturated volumetric water content	$[L^3L^{-3}]$
θ_i	Initial volumetric water content	$[L^3L^{-3}]$
θ_0	Volumetric water content at the upper boundary	$[L^3L^{-3}]$
ρ_w	Density of water	$[ML^{-3}]$
ϕ	Hydraulic head	$[L]$
Φ	Energy per unit mass of fluid	$[L^2T^{-2}]$
ψ	Suction	$[ML^{-1}T^{-2}]$
ε_{sw}	Swelling deformation	$[LL^{-1}]$

Abbreviations

a_s	Unsaturated advective seepage	$[LT^{-1}]$
\bar{a}_s	Constant unsaturated advective component	$[LT^{-1}]$
D_x	Unsaturated water diffusivity at x -direction	$[L^2T^{-1}]$
D_y	Unsaturated water diffusivity at y -direction	$[L^2T^{-1}]$
D_z	Unsaturated water diffusivity at z -direction	$[L^2T^{-1}]$
\bar{D}_z	Constant unsaturated water diffusivity component	$[L^2T^{-1}]$
e	Void ratio	$[L^3L^{-3}]$
e_{max}	Maximum void ratio	$[L^3L^{-3}]$
e_{min}	Minimum void ratio	$[L^3L^{-3}]$
g	Gravitational acceleration	$[LT^{-2}]$
k_s	Saturated hydraulic conductivity	$[LT^{-1}]$
k_{sx}	Saturated hydraulic conductivity in the x -direction	$[LT^{-1}]$
k_{sy}	Saturated hydraulic conductivity in the y -direction	$[LT^{-1}]$
k_{sz}	Saturated hydraulic conductivity in the z -direction	$[LT^{-1}]$
k_x	Unsaturated hydraulic conductivity in the x -direction	$[LT^{-1}]$
k_y	Unsaturated hydraulic conductivity in the y -direction	$[LT^{-1}]$
k_z	Unsaturated hydraulic conductivity in the z -direction	$[LT^{-1}]$
L	Length of the column	$[L]$
LL	Liquid Limit	
PL	Plastic Limit	
PI	Plasticity Index	
R^2	Coefficient of determination	
\bar{R}	Constant swelling component	
Sr	Degree of saturation	$[L^3L^{-3}]$
Sg	Specific gravity	$[ML^3M^{-1}L^{-3}]$
t	Time	$[T]$
v_0	Initial discharge velocity	$[LT^{-1}]$
v_x	Discharge velocity in the x -direction	$[LT^{-1}]$
v_y	Discharge velocity in the y -direction	$[LT^{-1}]$
v_z	Discharge velocity in the z -direction	$[LT^{-1}]$
w_{opt}	Optimum moisture content	$[MM^{-1}]$

Chapter 1

INTRODUCTION

1.1 MOTIVATION

Expansive soils are materials composed primarily of active minerals such as montmorillonite, which tend to undergo volumetric variations due to moisture changes. Several geotechnical engineering practices require a thorough understanding of how water interaction can affect the mechanical response of expansive soils, especially for applications such as dam core compaction. However, the deformations produced by these swelling and shrinkage mechanisms are mainly inelastic, which limits the application of most classical elastoplastic theories to this type of soil ([Al-Yaqoub et al., 2017](#)).

Water flow in soils is highly nonlinear, and most closed analytical solutions are only possible in cases where the simplified flow uses restrictive assumptions. The equation attributed to [Richards \(1931\)](#), which describes the flow through unsaturated porous media, combines three basic conservation principles: i) the Darcy-Buckingham law, ii) the continuity equation, and iii) the Bernoulli equation ([Fredlund & Rahardjo, 1993](#)). Using this equation, the air pressure is assumed to be a constant variable, and the water motion can be described using the generalized Darcy's law ([Darcy, 1856](#)). However, the highly nonlinear partial differential form ([List & Radu, 2016](#)) of the Richards equation limits the operation of numerical analysis schemes.

Currently, most numerical models of unsaturated flow employ the Richards equation form based on suction or volumetric water content. In recent years a large number of different finite element or finite difference solution techniques have been proposed with each of these equation forms ([Šimnek et al., 2006](#); [Zha et al., 2013](#)). However, just as in some cases, the numerical solution can easily converge, there are conditions under which some will not for various reasons.

Some exact one-dimensional solutions of the Richards equation for closed cases were derived in specialized forms from constitutive relations that allow describing the soil water retention mechanism and the unsaturated hydraulic conductivity functions. The proposal of [Cavalcante & Zornberg \(2017\)](#) is based on the use of constant parameters with physical meaning that represent the soil water retention and the unsaturated hydraulic conductivity functions for transient flows, with analytical solutions of the Richards equation for one-dimensional closed cases. The constitutive model proposed by [Askar & Jin \(2000\)](#) allows evaluating the behaviour of expansive soils in unsaturated conditions, assuming a unique and non-hysteretic dependence of the void ratio, total suction, and unsaturated hydraulic conductivity, on the volumetric water content. This is a model based on [Richards \(1931\)](#) equation for one-dimensional flows, in which the equation neglects the influence of volume variation on unsaturated hydraulic conductivity and on the diffusivity function.

In this work, the behaviour of unsaturated swelling soils under transient conditions was evaluated using a combination of the models of [Askar & Jin \(2000\)](#) and [Cavalcante & Zornberg \(2017\)](#). The mathematical model obtained allows the evaluation of the hydromechanical behaviour of swelling soils using six parameters that are easy to get experimentally: i) a fitting hydraulic parameter (δ), ii) the saturated volumetric water content (θ_s), iii) the residual volumetric water content (θ_r), iv) the saturated hydraulic conductivity (k_s), v) and the maximum and minimum void ratios (e_{max} and e_{min} respectively). Four analytical solutions are proposed to explore the parametric sensitivity, each with one initial and two boundary conditions. The predictions obtained after analytical implementation are compared with laboratory results of soil-column tests to examine the model's functionality. Finally, to explore the range of applicability of the model, data available in the literature is used to build a complete parametric analysis framework.

1.2 OBJECTIVES

The general objective of this research is to perform a analytical and mathematical approach to simulate the hydromechanical behaviour of swelling soils.

The specific objectives focus on the following aspects:

- Develop a model taking into account the unsaturated flow model under transient condition proposed by [Cavalcante & Zornberg \(2017\)](#), and the assumptions proposed by [Askar & Jin \(2000\)](#) to readjust Richards equation.
- Validate the proposed model employing the results of soil-column tests in the literature, the overall behaviour of expansive soils and the parameters that directly influence their hydromechanical response.

- Develop a sensitivity analysis of the model using analytical solutions for closed cases with restrictive assumptions.
- Establish a complete parametric comparison field in order to identify the range of model functionality for soils with different void ratios.

The analytical scheme will be used to solve the Richards equation implementing a new mathematical approach that focuses on solving the limitations of this equation when applied to swelling soils.

1.3 METHODOLOGY

The main problem the research focuses on is the difficulty in mathematically defining the expansivity phenomenon. The dissertation is divided into seven fundamental parts: i) Introduction, ii) Literature review, iii) Methodology, iv) Mathematical model, v) Analytical solutions, vi) Parametric calibration, and vii) Conclusions. Fig. 1.1 presents a synthesized scheme of the methodology to be followed for the research development.

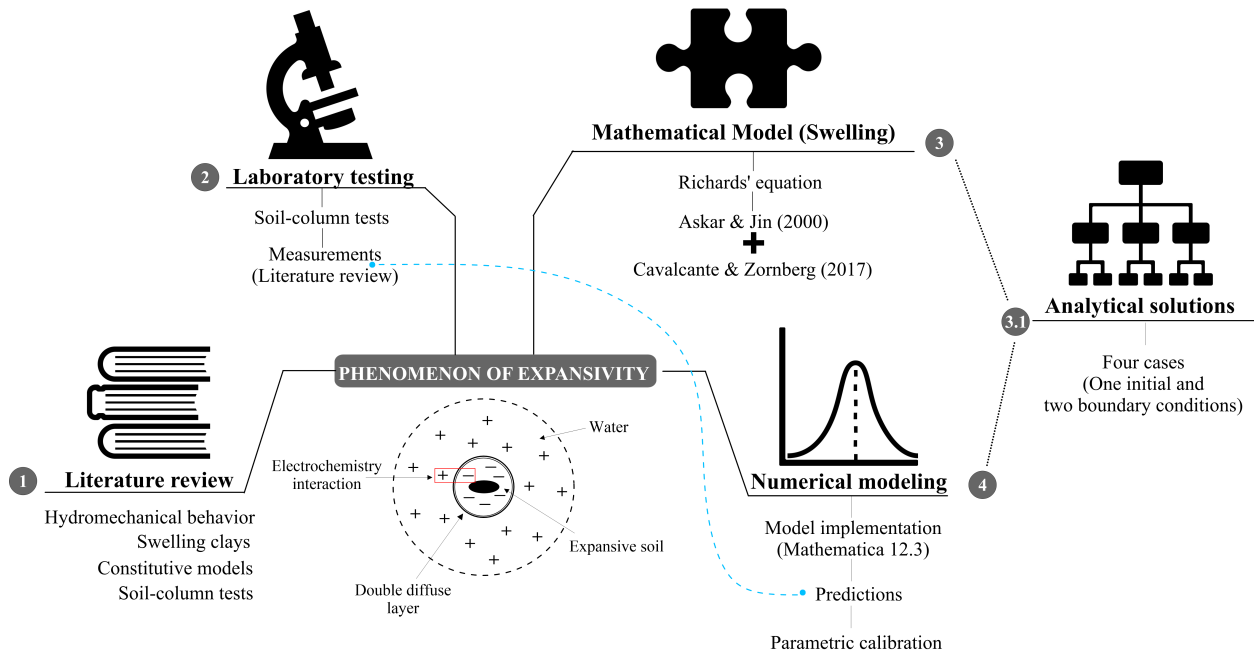


Figure 1.1: Methodology of the dissertation.

In the literature review a wide spectrum related to the hydromechanical behaviour of swelling soils is covered, as well as the evaluation of the swelling mechanism employing soil-column tests, the implementation of both the model and the analytical solutions in *Wolfram Mathematica 12.3*, and the comparison of experimental results to calibrate the model. The mathematical approach is based on the solution of Richards equation for the unsaturated

flow in capillary media, and the routing of this work is established to calibrate the proposed model using of experimental and theoretical results to calibrate the model.

1.4 DISSERTATION OUTLINE

This document is presented as a requirement for obtaining the Master's degree in Geotechnics, and is divided into four chapters. The Chapter 1 consists of this introduction.

In Chapter 2, basic theoretical concepts and state-of-the-art related to the understanding of swelling from a microstructural perspective will be discussed, as well as the hydromechanical behaviour of soils with volumetric change characteristics. The knowledge of the problem of expansive soils and the constitutive models developed to estimate their hydromechanical response are explored. Since the aim is to perform a coupled model, the water movement in unsaturated porous media and the derivation of the approaches used are presented in this chapter.

In Chapter 3, the research methodology is presented. Here the results obtained by [Azevedo \(2016\)](#) in soil-column tests are presented, as well as the physical characteristics of the tested material. Additionally, the four stages addressed in Chapter 4 are explained at a theoretical and strictly procedural level.

In Chapter 4, the mathematical derivation of the model is presented, as well as the parameters used, established from the definition of the advective, dispersive flow, and swelling components as constants (Appendix A). Four analytical solutions with different initial and boundary conditions are implemented to explore the hydromechanical behaviour of the swelling soils in time and space.

The results obtained by introducing the experimental test data into the model formulation and the analytical solutions are also presented. In this case, the behaviour of the soil is analyzed in Case 1, where the initial volumetric content is constant, and in Case 3, where the discharge velocity is invariable. The last phase of this chapter presents the parametric calibration of the model and its degree of accuracy when compared to literature results performed on soils with different void ratios.

In Chapter 5, a retrospective analysis is performed to identify the limitations of the model, as well as the conclusions generated from the research development, recommendations and suggestions for future mathematical approaches. Finally, the limitations presented by using the proposed model are addressed. It is necessary to consider that since this is a simplified analysis based on flow analysis, the mechanical spectrum is established by relating the volumetric change to the shear strength.

Chapter 2

STATE OF THE ART

2.1 EXPANSIVE SOILS

2.1.1 Understanding of microscopic mechanisms of swelling

The categorization of expansive soil is given to any material whose volumetric changes are sensitive to variations in moisture content. These characteristics of swelling or shrinkage by adsorption and evaporation of water result in a highly problematic soil type (Nelson & Miller, 1997). Most soils exhibiting this behaviour contain reticulate-type clay minerals that are part of the smectite family, where montmorillonite is an important member of this group (Asuri & Keshavamurthy, 2016). The size and shape of clay lamellae within the microstructure are determined by the arrangement of crystalline fabric and the organization of other elements, such as hydrogen, sodium, calcium, and magnesium (Jones & Jefferson, 2012). In saturated condition, the behaviour of these clay sheet assemblages, generally called "*tactoids*", is dominated by mineralogy.

The nature of expansivity understood on a global scale, is not a completely reversible process, since both shrinkage and swelling can cause isolated responses, even if they occur consecutively. To exemplify this phenomenon, during the expansion process, the bonds between particles are weakened by violent cation exchange and form lumps that become shrinkage cracks in the dry season. When saturated, these cracks do not return to their original state, facilitating water access during the new swelling phase and imparting heterogeneity to the soil (Holtz & Kovacs, 1981). Therefore, due to the adverse dynamics of the expansivity phenomenon, when clay layer assemblages become saturated by external moisture fluctuations, the molecular bonds weaken and alter the shear strength of the soil (Fredlund & Rahardjo, 1993; Sheng et al., 2008).

Upon contact with water, the expansivity response spectrum on a microporous scale can be explained and analyzed using the diffuse double layer (DDL) theory. Clay particles are surface-active materials because of their electronegativity, so the hydromechanical behaviour depends on the accumulation of ionic countercharge at the soil-water boundary (OlarTE et al., 2021). While the colloidal suspension occurs, an adsorbed water hydrosphere containing soluble cations of different charges, also called exchangeable cations, is created on the lamellar surface. These cations balance the clay’s negative charges, and the DDL preserves their electrical neutrality. Therefore, the greater the thickness of the DDL, the greater the cation exchange capacity of the material, which translates as a more significant fluctuation in the structural, hydraulic, volumetric, physicochemical, and mechanical properties of expansive soils (Fukue et al., 2001).

Since the discovery of the properties of the crystalline structure of fine soils in the early 1930s, knowledge of molecular dynamics in the clay/water system has increased rapidly. Understanding the phenomenon of expansivity at the nanoscale requires basic applications of the law of charge since, under induced saturation, expansion processes are generated by reducing attractive forces relative to repulsive forces. When the soil/water interface is established, the stresses induced by the water molecules easily dominate the Van der Waals forces of attraction (Van der Waals, 1873), ultimately leading to swelling. The repulsive or electrical surface forces depend on the thickness of the DDL, which may increase when the concentration of exchangeable ions is reduced or when the dielectric constant is increased. However, Van der Waals forces are independent of these factors (Yong & Warkentin, 1966).

A key aspect in the understanding of expansive soils is the identification of the mechanisms involved in swelling, which, according to Low (1961), can be of two types: i) crystalline swelling, caused by hydration of cations in the crystalline tissue, and ii) osmotic swelling, produced by ionic imbalance at the contact interface between clay and aqueous molecules. The osmotic fraction takes place in DDL and is strongly linked to the ionic concentration, pH, mineralogy, and type of exchangeable ion (Van Olphen, 1986). Thus, in the face of moisture variations, the different mechanisms that interfere in the expansion process interact simultaneously and depend directly on the charge potential at the surface ψ_0 [$ML^2A^{-1}T^{-3}$] and the distance from the clay plate (x) [L]. Fig. 2.1 explains the expansion process using the DDL theory.

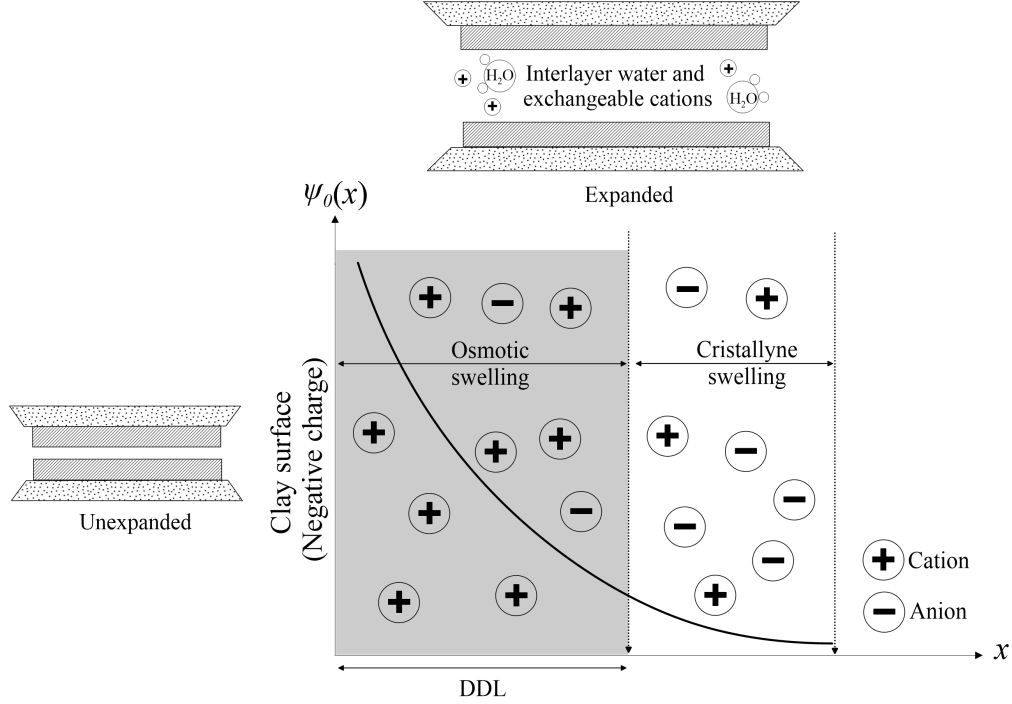


Figure 2.1: Schematic of swelling process.

In addition to DDL, the specific surface area (SSA) allows for determining many of the physicochemical properties of materials employing a ratio between the surface area (A_s) [L^2] and the mass (M) [M] of a clay particle. SSA is an essential parameter for understanding the interaction processes during the state transformations of soil: from semisolid to plastic and finally to liquid. Unlike coarse-grained soils, where the dominant forces are mainly of physical origin, in fine-grained soils, the relevance of capillary and electrical forces increases because grain size decreases and SSA increases (Santamarina et al., 2002).

Because of their microscopic size, clay minerals have a considerable effect on the permeability, strength, stiffness, and bearing condition of soil. Their abundant presence allows them to form stabilizing buttresses on the surface of the main constituent mineral, making them a critical control point in swelling and shrinkage processes. Like phyllosilicates, clay minerals are remarkably anisotropic and can develop different types of SSA. Generally, according to Macht et al. (2011), there are predominantly two types of surface: i) basal, where charges are inherited by isomorphous substitution, and ii) lateral, where SSA is dependent on *in-situ* pH.

In unsaturated condition, although the response of expansive soils, especially talking about the swelling mechanism, is still dependent on moisture content variations, suction ψ [$ML^{-1}T^{-2}$] acquires a significant domain fraction in the hydromechanical spectrum. The concept of unsaturated behaviour in expansive soils can be defined from the water retention

curve on a scale where the soil constituents are observable, i.e., on a macroporous scale (Ikeagwuani & Nwonu, 2019). However, Fityus & Buzzi (2009) pointed out that the field of unsaturated soil mechanics covering expansive soils does not address the basic aspects of volume change during constitutive modelling. A synthesized scheme of the expansive modulus in unsaturated condition is presented in Fig. 2.2. In this new space, the interference of air pressure (u_a) in the process results in a ψ -controlled environment. The variable (V_v) [L^3] is the total volume of voids, (V_s) [L^3] is the total volume of solid particles, (V_{siv}) [L^3] is the volume of saturated interlaminar voids, (V_{EM}) [L^3] is the volume of expansive solids, and (V_{NM}) [L^3] is the volume of nonexpansive solids.

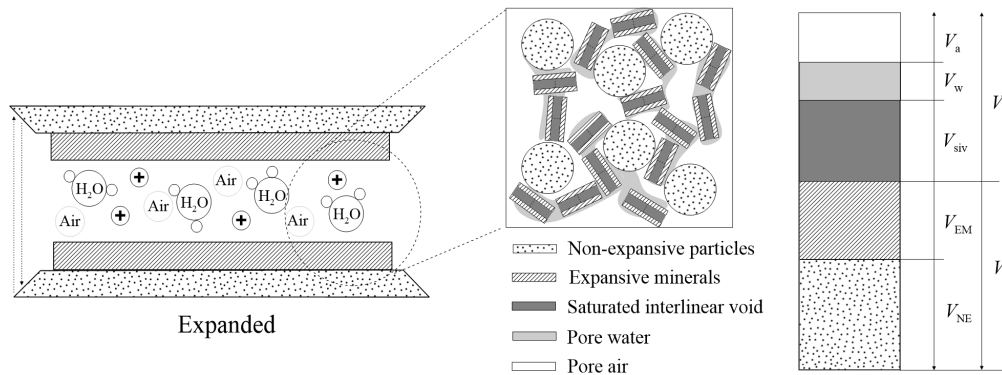


Figure 2.2: Schematic of an unsaturated expansive soil.

In the empirical field of soil mechanics, three conditions are established for test specimens: i) undisturbed (with intact internal structure), ii) remodeled (when the soil has consolidated), and iii) compacted (imposition of degrees of compaction). However, soils prepared under these conditions clearly generate different particle size distributions and pore networks, so the swelling/shrinkage cycles may occur with different amplitudes and generate different responses. Therefore, numerous constitutive approaches have been developed in recent decades to evaluate the behaviour of expansive soils in each of these three conditions and in saturated and unsaturated states.

2.1.2 Hydromechanical behaviour of swelling soils

The influence of suction (ψ) on the hydromechanical behaviour of soils is generally recognized and investigated as a critical factor governing the unsaturated state. The pioneering study to evaluate the mechanical response of unsaturated soils was carried out by Bishop et al. (1960) using results from controlled suction triaxial tests. The ψ can be measured or applied experimentally in different ways (e.g., filter paper, axis translation technique, triaxial equipment, among others). Theoretically, the Soil Water Retention Curve (SWRC), or soil characteristic curve according to Fredlund & Rahardjo (1993), establishes that the

parameters ψ and volumetric water content (θ) [L^3L^{-3}] are related to each other in a porous medium.

For unsaturated mechanics, both ψ and θ are unique fundamental properties of the SWRC, although they are related to different mechanisms. In the empirical framework, ψ values are related to piezometric heads and θ values to the degree of saturation (Sr) [L^3L^{-3}]. However, in descriptive processes evaluating water-air interaction, the behaviour of the SWRC is constantly adjusted using predictive models (Cornelis et al., 2005). A particular feature of the SWRC is that the θ is generally higher in the drying path, which generates a hysteretic behaviour concerning the wetting path. The mechanisms responsible for the presence of hysteresis between curves are generally microstructural (e.g., nonuniformity in interconnected pores, and capillary condensation, among others). The knowledge of hysteresis in the drying/wetting history is vital to understanding the hydromechanical behaviour of soils, both from a stress-strain perspective (Likos & Lu, 2004) and a purely hydraulic one (Parker & Lenhard, 1987).

The fundamental concept encompassing the SWRC description establishes two main saturation domains. In the pendular regime ($Sr < 20\%$), water is organized as thin films on the particle surface, which contributes to retention, capillary condensation (by meniscus formation), and increased ψ values. At higher saturation ($20\% < Sr < 90\%$), interstitial water molecules form a fabric of liquid bridges in partially filled pores and bubbles in saturated pores (Hernández et al., 2022). In this retention system, known as the funicular state, ψ is low and strongly depends on the geometry of the solid network, including the porosimetry and grain size distribution. Most empirical models or strictly mathematical equations attempt to reproduce part of the SWRC by including some reference parameters such as the saturated volumetric water content (θ_s) [L^3L^{-3}] defined at full saturation ($Sr = 100\%$), the value of ψ at which the first partially saturated voids arise called the air entry value (AEV), and the residual volumetric water content (θ_r) [L^3L^{-3}] where the value of $Sr = 0\%$.

The graphical-mathematical form of the SWRC is generally hyperbolic (Van Genuchten, 1980), and only at the points corresponding to θ_s and θ_r is it possible to apply the effective stress principle of Terzaghi (1923). The data pairs corresponding to ψ and θ collected from the laboratory are generally fitted in the SWRC using the constitutive equations proposed by Brooks & Corey (1964), Van Genuchten (1980), Fredlund & Xing (1994), and Cavalcante & Zornberg (2017). The mathematical derivation of each model usually includes different calibration parameters, as well as flow concepts associated with the Richards equation. Fig. 2.3 presents the SWRC in its typical unimodal form for a drying and wetting paths and the saturation domains.

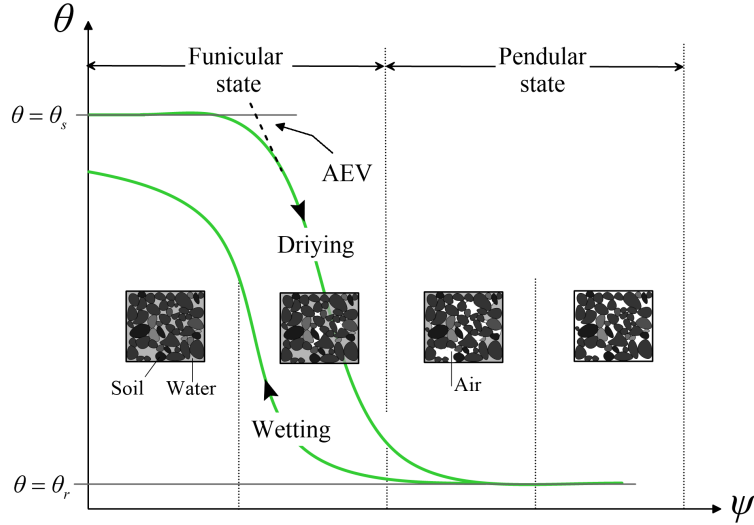


Figure 2.3: Unimodal soil-water retention curve.

There is a wide variety of stress and wetting conditions that expansive soils experience *in situ*, which can alter their hydromechanical response. Loading and unloading cycles due to the imposition of external stresses or water table fluctuations, in addition to seasonal variations, induce changes in ψ and, therefore, in shear strength. Most studies investigating the hydromechanical behaviour of expansive soils start from the stress-strain relationship under different values of ψ . [Bendahgane et al. \(2017\)](#) evaluated the fluctuation in the void ratio (e) [$L^3 L^{-3}$] of expansive material employing wetting and drying paths obtained by controlled suction testing. [Tang et al. \(2011\)](#) analyse the hydromechanical response of expansive soils using one-dimensional compression tests under constant θ conditions.

An effective way to understand the hydromechanical behaviour of expansive soils is by using a time-deformation relationship, where the deformation caused by swelling (ε_{sw}) [LL^{-1}] is expressed as a percentage increase in height. During the swelling process, three main stages are established: i) inter-vacuum swelling (*ivsw*), produced by expansive minerals within voids created by larger non-expansive particles, ii) primary swelling (*psw*), where about 80% of the swelling occurs, and iii) secondary swelling (*ssw*), reached at the point where swelling shows a linear relationship with time (t) [T]. The typical t - ε_{sw} relationship is presented in [Fig. 2.4](#).

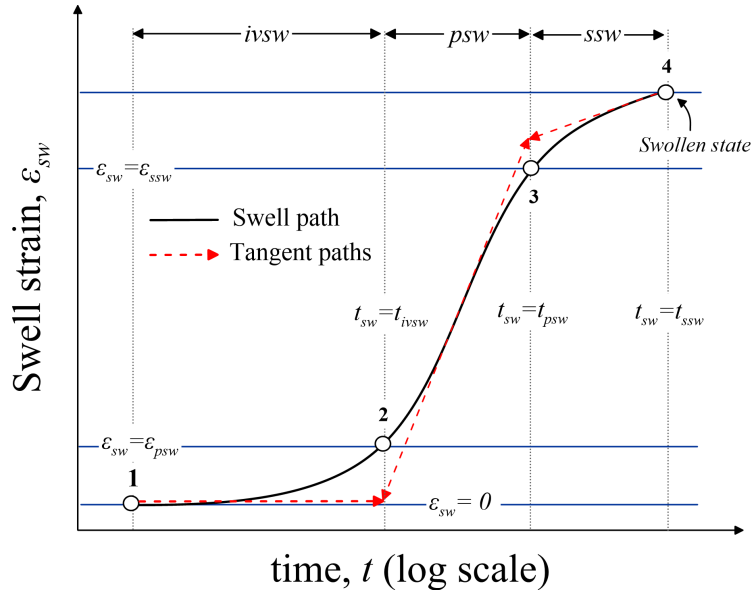


Figure 2.4: Swell evolution.

In an initially dry clay soil subject to wetting, the swelling process starts with a mainly structural process, where the pores fill with water without accompanying volumetric changes. The volume begins to increase when the variation in volume (ΔV) is equal to the variation in water volume (Δw). Progressively, when the soil reaches the "residual phase" phase, ΔV is more significant than Δw . Finally, the swelling process ceases when ΔV is equal to Δw . However, the swelling characteristics can deviate significantly from the idealized form presented in Fig. 2.5.

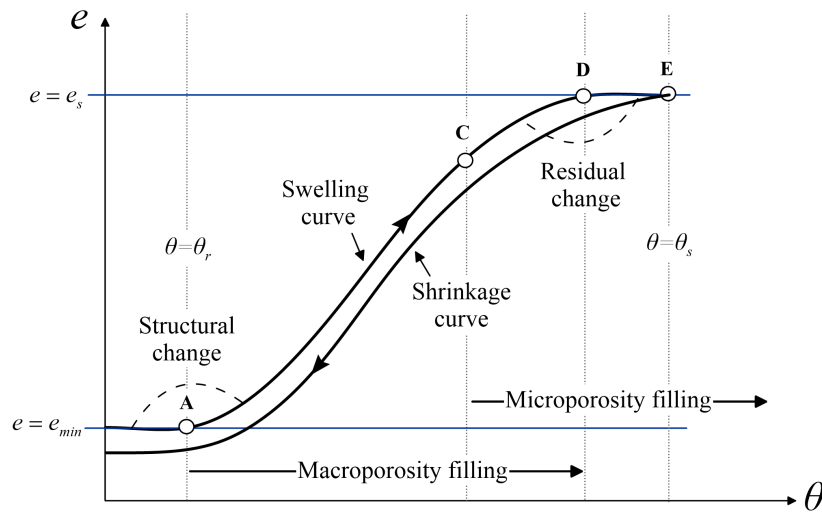


Figure 2.5: Water content-void ratio swell-shrink paths of a clay soil.

In general, when wetting occurs on a microporous scale, the water movement can consider several phases. At the beginning of saturation, the water flow follows the path from point A to point C, where point A is located at the structural swelling (inter-vacuum swelling) at θ_r . When the soil begins to wet from low degrees of saturation, the water flow first enters the macropores, which are fully saturated in the residual zone.

Unlike micropores, where the water flow is dominated by electrochemical forces, macropores responds to the action of gravity. After short periods, the soil water content in the swelling stage reaches a residual value for a void ratio equal to e_s , i.e., a value close to saturation. The inverse path to swelling corresponds to shrinkage, which builds the expansion phenomenon. As in the SWRC for the drying and wetting paths, the swell-shrink paths present a slight degree of hysteresis between them, mainly due to the volumetric change between phases.

2.1.3 The place of swelling clays in soil mechanics

The first studies of expansive soils carried out around the 1950s by [Aitchison & Holmes \(1953\)](#) and [Norrish \(1954\)](#) were strongly influenced by the need to understand the hydrodynamic behaviour and hydrostatics of soil-water boundaries. Gradually, considerable scientific output was reported to broaden the field of swelling and shrinkage processes within classical soil mechanics ([Holtz & Gibbs, 1956](#); [Miller, 1975](#); [Parcher & Liu, 1965](#); [Philip, 1969](#)). The first international forum devoted to the consideration of expansive soils, significantly recognized by researchers, was held at Texas AM University in 1965. From then on, a series of exclusive congresses in this field were held worldwide in different countries ([Al-Rawas & Goosen, 2006](#)).

Initially, what was known about the understanding of this phenomenon borrowed some concepts from soil science and the effects of cations. However, the structure of expansive clays is extensively complex, so many of the models that were developed to explain this phenomenon in a timely manner were derived from the DDL theory, attributed to [Gouy \(1910\)](#) and [Chapman \(1913\)](#) in its basic form ([Liu, 2013](#); [Phillips & Tripathy, 2011](#); [Sridharan & Jayadeva, 1982](#); [Yong et al., 1962](#); [Zhang et al., 1993](#)). Additionally, according to [Mašin & Khalili \(2015\)](#), the group of constitutive approaches derived from the DDL principle is exclusively applicable to scenarios where an ensemble of smectite particles is suspended in monovalent electrolyte solutions at low concentrations.

A fundamental aspect in estimating the behaviour of expansive soils lies in understanding the functioning of the microstructure and organization of the saturated and unsaturated pore space. In fully saturated condition, the value of ψ is transferred to a "net stress" state and the degree of saturation (S_r) reaches the value of unity. Therefore, in theory, expansion problems could be treated using the effective stress principle of [Terzaghi \(1923\)](#).

However, the assumptions made by Terzaghi in the original form of the expression do not include cation exchange and the influence of electrochemical forces, so this principle is not fully applicable to the mechanical equilibrium of expansive soils. Some constitutive models estimating expansivity in saturated condition were proposed by Hueckel (1992), and Mašín & Khalili (2015).

Some geotechnical applications make special use of compacted expansive soils (e.g. nuclear waste storage, dam cores) or as replacements in situations where non-expansive materials are in short supply (e.g. road subgrade). In these cases, it is of vital importance to determine the expansive potential of soil in order to evaluate its stabilization methods and placement requirements. Models that evaluate the expansion of soils under these conditions are generally complex, requiring sophisticated mathematical implementations (Alonso et al., 1999; Dormieux et al., 1995). Erguler & Ulusay (2003), employing experimental results, produced predictive multivariate regressions under any parametric combination.

Currently, there are models with punctual approaches, i.e., focused on the calculation of a specific variable: i) experimental models to evaluate expansion pressure (Low & Margheim, 1979), ii) swelling deformation produced by constant load tests (Buzzi, 2010; Buzzi et al., 2007, 2011), iii) continuous thermodynamic models to relate water potential to expansion pressure (Dueck & Börgesson, 2007; Lempinen, 2011), among others. The models cited above use constitutive relationships to estimate the isotropic behaviour of expansive soils, in addition to sophisticated mathematical formulations, resulting in an accommodation of the concepts of charge and electrochemical equilibrium.

In the case of soils in unsaturated condition, most of the commonly used proposed models establish an inversely proportional relationship between ψ and S_r . This assumption was originally proposed by Alonso et al. (1990) in the well-known Barcelona Basic Model (BBM) and subsequently adapted by numerous researchers (Gens & Alonso, 1992; Sheng et al., 2008; Wheeler et al., 2003). However, the volumetric content incorporated in these models is significantly lower than the range over which expansive soils, in natural condition, remain saturated. The models cited above, in specific situations such as compacted bentonite samples (Loret et al., 2002) are able to estimate the swelling and shrinkage behaviour. This is because, the compaction process imparts artificially large pore distributions in the soil, resulting in unsaturated conditions.

2.1.4 Problems of expansive soils

Buildings founded on expansive soils are subject to strong movements due to non-uniform moisture fronts, which generate cracking related to severe deformations. This damage can range from cracks in pavements to differential settlements that cause irreparable displacements in foundation mechanisms (footings or piles) and superstructure elements (Langroudi

& Yasrobi, 2009). Damage to lightly loaded buildings has been reported around the globe, most frequently in countries such as Australia (Li & Cameron, 2002), China (Shi et al., 2002), India (Ameta et al., 2007), South Africa (Williams et al., 1985), United Kingdom (Eyo et al., 2017), Colombia (Gongora et al., 2008), Peru (Castro Cuba Valencia, 1992), and the United States (Houston et al., 2011). The main reference used to understand differential settlement in expansive soils was published by Skempton & MacDonald (1956) and later updated by Grant et al. (1974). In this study, 98 buildings in United States were evaluated that experienced damage from light to severe scales under numerous degrees of settlement. Table 2.1 presents a summary of case studies of buildings affected by expansive soils in different parts of the world.

It is easy to infer that the pathology of expansive soils is one of the most studied within the geotechnical field given that, it is this type of soil that is found in most of the territory of the United States. The American Society of Civil Engineers estimates that one in four homes has been or is affected by expansive soils today (Snethen et al., 1975). In the United States alone, the annual cost of recorded damage from expansive soils extends to a value of \$ 15 billion per year, i.e., an amount greater than the damage generated by all weather events combined. The annual capital investment devoted to solving this problem in countries such as China and the United Kingdom approaches amounts of \$ 15 billion and 446 million, respectively (Lytton, 1970). In countries such as Australia, where approximately 20 % of the country is covered by expansive soils, Considine (1984) reports that about 50,000 houses are affected annually by expansive soils. In Latin America, Mexico has the most affected area, since it has a considerable region of expansive soils, with about 12 % of the total territory (Padilla-Corona, 2008).

Table 2.1: Cases study of buildings damaged by expansive soils.

Author	Country	Year	Engineering structure	Cause	Analysis method
Li & Cameron (2002)	Australia	1990	Single storey, articulated masonry veneer dwelling	Edge heaving as a result of water ponding in the courtyard	3D back analysis by finite-element method
Day (1992)	USA	1991	Buildings H and J at the Calavo Woods Apartments	Foundation displacement caused by difference in moisture content	Subsurface exploration
Li et al. (2014)	Australia	1998	Single storey, articulated masonry veneer dwelling	Overwatering of the lawn and leaking sewer pipe and/or storm water pipe	3D back analysis
Ewing (2011)	USA	2002	Residence built (Eudora Welty house)	Differential settlement of foundation	Structural works such as piers and beams
Padilla-Corona (2008)	Mexico	2008	Educative centers having one or two levels buildings	Differential settlement caused by difference in moisture content	Stratigraphic profiles and laboratory index tests
Lew (2010)	Brazil	2010	Residence built	High swelling potential due to the presence of expansive-clay minerals	Foundation structural analysis
Anastasopoulos (2013)	Greece	2011	5-storey RC building	Differential settlement of foundation	Numerical analyses taking account of the construction sequence
Li & Guo (2017)	Australia	2011	Single story, partially articulated masonry dwelling	Tree root drying	Numerical analysis
Zumrawi (2015)	Sudan	2015	Buildings of single or two storey and light structures	Uplift forces resulting from heave caused by the swelling of soils	Visual inspection

2.2 MOVEMENT OF WATER

In the context of hydrodynamics, one of the most familiar equations in theoretical physics is the equation of continuity. The general solution of the equation illustrates the balance of mass entering and leaving a representative volume element (REV). Thus, there can be no mass increase or loss when an infinitesimal point is filled with water, regardless of the flow paths. The main axiom applied in this conservation principle states that a quantity of matter associated with a location in the REV is invariant in time. Employing the divergence

theorem, it's possible to isolate the continuity equation in the basic form by applying the conservation theory of mass in a fluid volume inside the REV. In this way, it is obtained:

$$\frac{d}{dt}M_R = - \int_{\partial R} \rho_w \vec{v} \cdot \vec{n} dS = - \int_R \text{div}(\rho_w \vec{v}) dV = \frac{d}{dt} \int_R \rho_w dV_w = 0 \quad (2.1)$$

where R denotes the region occupied by the REV at a time instant t , $\rho_w [ML^{-3}]$ is the density of water, $\vec{v} [LT^{-1}]$ is the velocity vector defining the velocity field within the REV, $V [L^{-3}]$ the total volume, and $V_w [L^{-3}]$ the total water volume. Using the concept of volumetric moisture content (θ), Eq. 2.1 can be expressed as:

$$\int_R \frac{\partial}{\partial t}(\rho_w \theta) dV + \int_R \text{div}(\rho_w \vec{v}) dV = 0 \quad (2.2)$$

To fulfill Eq. 2.2, it is necessary to verify that for any fixed region R , the expression granted there must be zero. The mass balance caused by the outflow and inflow of a fluid is defined by assuming a REV located at a point (x,y,z) on a cartesian plane as presented in Fig. 2.6. In this three-dimensional space, the volume differential (dV) is represented as $dx dy dz$.

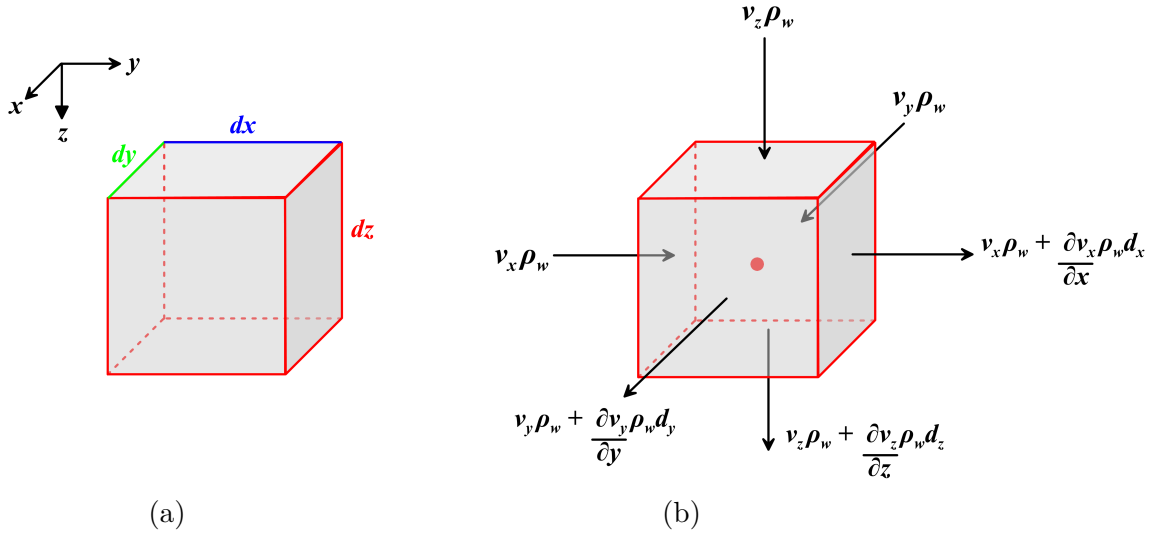


Figure 2.6: Water flow: (a) REV; (b) water flow in and out of the REV.

The conservation law guarantees that the sum of the three mass flow quantities is equal to the change in water content in the REV. Mass flow can be defined mathematically in two parts. The first part is the amount of mass entering the REV, $\dot{m}_{in} [MT^{-1}]$ at a time t is defined as:

$$\dot{m}_{in} = v_x \rho_w (dzdy) + v_y \rho_w (dxdz) + v_z \rho_w (dxdy) \quad (2.3)$$

where v_x , v_y , and v_z are the discharge velocities in the x , y , z directions respectively, [LT^{-1}]. The second part corresponds to the amount of mass leaving the REV, \dot{m}_{out} [MT^{-1}] at a time t :

$$\begin{aligned} \dot{m}_{out} = & \left(v_x \rho_w + \frac{\partial(\rho_w v_x)}{\partial x} dx \right) (dzdy) + \left(v_y \rho_w + \frac{\partial(\rho_w v_y)}{\partial y} dy \right) (dxdz) \\ & + \left(v_z \rho_w + \frac{\partial(\rho_w v_z)}{\partial z} dz \right) (dxdy) \end{aligned} \quad (2.4)$$

Therefore, using the difference between Eq. 2.3 and Eq. 2.4 it is possible to define the mass storage in the REV, [MT^{-1}] :

$$\dot{m}_{storage} = \left[-\frac{\partial(\rho_w v_x)}{\partial x} - \frac{\partial(\rho_w v_y)}{\partial y} - \frac{\partial(\rho_w v_z)}{\partial z} \right] dV \quad (2.5)$$

On the other hand, the mass storage by the voids inside the REV for any time t is equal to:

$$\dot{m}_{storage dv} = \frac{\partial(\rho_w \theta)}{\partial t} dV \quad (2.6)$$

Equating Eq. 2.5 with Eq. 2.6 gives:

$$\frac{\partial(\rho_w \theta)}{\partial t} = -\frac{\partial(\rho_w v_x)}{\partial x} - \frac{\partial(\rho_w v_y)}{\partial y} - \frac{\partial(\rho_w v_z)}{\partial z} \quad (2.7)$$

In the case of incompressible fluids in the transient state, ρ_w is constant in time and space. Using algebraic management, the Eq. 2.7 takes the form of the continuity equation applied to any fluid under these conditions:

$$\frac{\partial \theta}{\partial t} = -\frac{\partial v_x}{\partial x} - \frac{\partial v_y}{\partial y} - \frac{\partial v_z}{\partial z} \quad (2.8)$$

The previous case is restricted exclusively to homogeneous, incompressible Newtonian fluids traveling slowly through the voids of rigid porous media in steady state. Following the first mechanistic approaches by [Hubbert \(1956\)](#) and [Hall \(1956\)](#), it is possible to derive Darcy's law for anisotropic porous media from the Navier-Stokes equation. To perform this

procedure, it is assumed that the flow is laminar, incompressible, predominantly viscous, and the permeability tensor is symmetric. Furthermore, it is shown that there is a one-to-one relationship between the viscous forces and the local velocity fields. Thus, the water flow can be expressed for a saturated medium by:

$$v = -(k_x k_y k_z) \nabla \Phi \quad (2.9)$$

where $\nabla \Phi [L^2 T^{-2}]$ is the net driving force, expressed here as the gradient of the total hydraulic potential, and $k_x(\psi)$, $k_y(\psi)$, and $k_z(\psi)$ are the unsaturated hydraulic conductivity functions in each of the x , y and z directions, respectively, $[L T^{-1}]$. Eq. 2.9 was initially derived empirically by Darcy (1856) and named after him. Mechanistic theory considers Darcy's law (Eq. 2.9) as an equation to define the macroscopic momentum since it is the Navier-Stokes equation that expresses the momentum balance applied to the transport of Newtonian fluids. Numerous mathematical approaches have been presented in the last decades to theoretically analyze the flow through porous media, either based on stochastic processes (Scheidegger, 2020), geometric models (Bachmat, 1965) or formal averaging processes (Neuman, 1977). The principle of conservation of energy applied to fluids is described using the relationship between pressure and velocity in a non-viscous incompressible Newtonian fluid, as:

$$\phi = \frac{\vec{v} \cdot \vec{v}}{2g} - z + \frac{u_w}{\rho_w} \quad (2.10)$$

where $\phi [L]$ is a variable denoting a measure of specific energy per unit weight of the fluid, called the hydraulic head, $g [L T^{-2}]$ is the gravitational acceleration, and $u_w [M T^{-2} L^{-1}]$ is the pore pressure. However, the fluid energy can be associated either with the ϕ or with the fluid potential (i.e., energy per unit mass of fluid), denoted by Φ , and mathematically defined by:

$$\Phi = -z g + \frac{\psi}{\rho_w} \quad (2.11)$$

The Eq. 2.10 is called Bernoulli's equation and allows to establish the theoretical basis of hydraulic calculation, which solves the practical engineering problem related to force and energy. Three individual fragments constitute the energy state of a fluid in Bernoulli's equation: i) the velocity head ($\frac{\vec{v} \cdot \vec{v}}{2g}$) that controls the kinetic energy of the fluid, ii) a portion of the potential energy stored in the form of gravitational energy (z), and iii) a fraction of the potential energy stored in the form of fluid pressure ($\frac{u_w}{\rho_w}$). According to Bear (1972), the

portion representing the kinetic energy can be neglected when the velocity modulus is very small, which is the case in soils.

The mathematical demonstration of Eqs. 2.8, 2.9, and 2.10 exhibited the principles of conservation of mass, conservation of linear momentum, and conservation of energy, respectively. Although, there is an additional principle: the equation of conservation of angular momentum. However, there is no way to write an expression that complies with this principle due to the definition must include the fundamental assumption that the flow is irrotational and the tensors that make the water move must be isotropic.

2.2.1 Flow in unsaturated porous medium

The main problem in evaluating unsaturated flow in porous media is that, like any type of motion, it is governed by the same conservation laws, the axioms of which are usually expressed using mathematical terms (Liakopoulos, 1964). Flowing water must satisfy the continuity equation, the equation of state, and the dynamic equations of motion for any position x , at any time t . However, in porous media, the intervention of capillary forces generates a highly nonlinear equation of motion, as the variables t and x become dependent on ψ and θ . In other words, the nature of the equation for unsaturated porous media requires two functions to determine solutions at $t > 0$: $k(\theta)$ and $\psi(\theta)$.

Buckingham (1907) was the first to recognize water movement in unsaturated soils, using a unique relationship between discharge and suction gradients. In his monograph published in 1907, the concepts of matrix potential, water retention curve, pressure loading, and unsaturated hydraulic conductivity were distinguished as soil properties. By defining the concept of capillary potential, Buckingham provided a new paradigm for soil mechanics that unified saturated and unsaturated flow mechanisms, including in the mathematical basis an equation equivalent to the law that Darcy (1856) employed in saturated sands half a century earlier. In modern notation, Darcy's law is generally referred to as Darcy-Buckingham law, due to k is a function of θ . The Darcy-Buckingham law in one dimension is:

$$v_z = -\frac{k_z(\theta)}{\rho_w g} \left[\frac{\partial \psi}{\partial z} - \rho_w g \right] \quad (2.12)$$

Eq. 2.12 is applicable to the saturated condition when ψ reaches values less than or equal to 0 and unsaturated at $\psi > 0$. According to the Darcy-Buckingham law, the main difference between a saturated and an unsaturated medium in terms of water movement is that the pressure is determined by capillary forces and k depends on θ . A particular approach to Eq. 2.12 was published by Childs & Collis-George (1950) in which the geometry of the porous medium is related to the unsaturated conductivity using the pore size distribution curve.

Subsequently, the general behaviour of the $k(\theta)$ functions was established by Moore et al. (1939).

Although in the case of flow in saturated soils, the hydraulic conductivity can be considered constant, in reality, several extrinsic and intrinsic factors must be analyzed. Airflow through pores, aggregate dispersion, and even bacterial action can directly affect k values in saturated materials. The complexity in unsaturated media is due to the sum of the above factors plus the anisotropic variation due to volumetric water content. Presumably, k is assumed to be a single-valued function of θ . However, it is now known that both ψ and θ are not related to each other by univocal functions, so hysteresis effects are generated, inducing difficulties in mathematical analysis. Richards (1931) and Gardner (1936) introduced functional relationships for k in the Darcy-Buckingham law, establishing $k(\theta)$ and $k(\psi)$.

Experimentally it has been evaluated that the hysteresis loops produced in the $k(\theta)$ plane are much less significant than in $k(\psi)$, so many models ignore the hysteresis in $k(\psi)$ and base the mathematical formulation exclusively in terms of $k(\theta)$. Some simple mathematical formulations use adjustment coefficients to calibrate measurement data for either $k(\theta)$ or $k(\psi)$ (Brooks & Corey, 1964; Gardner, 1958; Wind, 1955). These approaches are used with restrictive assumptions, and the coefficients vary considerably between models, as no single relationship is valid for all soil types. Mualem (1986) presents an extensive summary of the concepts of $k(\theta)$ and $k(\psi)$, and their application within unsaturated soil mechanics.

2.3 RICHARDS EQUATION (1931)

The Richards equation (Richards, 1931) is a mathematical simplification that describes the flow of water in an unsaturated condition under the action of gravitational force. The study of this equation requires the inclusion of the concept of capillarity and a mathematical definition in porous media. However, due to the complexity of the equations of thermodynamics applied to flow in capillary media, it is necessary to generate mathematical simplifications adapted to specific cases. Despite its ease of derivation, the Richards equation is one of the most challenging equations to solve accurately in hydrosciences since its complex nature is derived mainly from the high nonlinearity of the moisture retention curves.

The first analytical solution of the Richards equation was developed by Philip (1957, 1969) using a time expansion method, in which infiltration is assumed to be a sorption process with some degree of gravity-generated perturbation. From this point on, numerous approaches were developed in order to apply the Richards equation considering simplified hydraulic conditions (Cavalcante et al., 2013; Hogarth & Parlange, 2000; Parlance et al., 1992; Sander et al., 1988; Swamee et al., 2014). However, most of these works demand the

involvement of non-transient flow, and the solutions are presented as integrals that require the implementation of numerical models (Chen et al., 2003, 2001).

In essence, the Richards equation is a mass conservation principle that employs the continuity equation (Eq. 2.8) and Bernoulli's equation (Eqs. 2.10 and 2.11) and is based on the fact that the Darcy-Buckingham law (Eq. 2.12) is valid for describing the motion of water. As the Richards equation is applied to unsaturated porous media, its solution depends on two highly nonlinear soil water constitutive relations: $k(\theta)$ and $\psi(\theta)$. However, these functions are not readily computable and can have very high slopes and hysteresis, as well as being discontinuous at low saturation values (Farthing & Ogden, 2017). To be demonstrated numerically, it is necessary to define the discharge velocity components using the Darcy-Buckingham law:

$$v_x = -\frac{k_x(\psi)}{g} \frac{\partial \Phi}{\partial x} \quad (2.13)$$

$$v_y = -\frac{k_y(\psi)}{g} \frac{\partial \Phi}{\partial y} \quad (2.14)$$

$$v_z = -\frac{k_z(\psi)}{g} \frac{\partial \Phi}{\partial z} \quad (2.15)$$

Substituting the Bernoulli's equation in terms of Φ (Eq. 2.11) into Eqs. (2.13)-(2.15), the discharge velocity in x , y and z directions can be rewritten as:

$$v_x = -\frac{k_x(\psi)}{\rho_w g} \frac{\partial \psi}{\partial x} \quad (2.16)$$

$$v_y = -\frac{k_y(\psi)}{\rho_w g} \frac{\partial \psi}{\partial y} \quad (2.17)$$

$$v_z = -k_z(\psi) \left(\frac{1}{\rho_w g} \frac{\partial \psi}{\partial z} - 1 \right) \quad (2.18)$$

The main difference between the continuity equation and Darcy-Buckingham law when evaluating the flow into and out of REV is that, according to Biot (1941), the former is expressed in absolute velocities (Eq. 2.8), and the latter uses relative velocities [Eqs. (2.16)-(2.18)]. Now, by substituting Eqs. (2.16)-(2.18) into Eq. 2.8 it is possible to obtain the 3D version of Richards equation for unsaturated soils under transient flow:

$$\frac{\partial \theta}{\partial t} = \frac{\partial}{\partial x} \left[\frac{k_x(\psi)}{\rho_w g} \frac{\partial \psi}{\partial x} \right] + \frac{\partial}{\partial y} \left[\frac{k_y(\psi)}{\rho_w g} \frac{\partial \psi}{\partial y} \right] + \frac{\partial}{\partial z} \left[k_z(\psi) \left(\frac{1}{\rho_w g} \frac{\partial \psi}{\partial x} - 1 \right) \right] \quad (2.19)$$

In Eq. 2.19 θ and ψ are dependent variables, so it is possible to rewrite this equation in terms of either $\psi = f(\theta)$ or $\theta = f(\psi)$. However, in some cases it is more convenient to express the Richard's equation in terms of θ rather than ψ , because $\psi = f(\theta)$ is less nonlinear. In order to use θ as an independent variable, it is necessary to replace $\partial\psi/\partial x$, $\partial\psi/\partial y$, and $\partial\psi/\partial z$ with $(\partial\psi/\partial\theta)(\partial\theta/\partial x)$, $(\partial\psi/\partial\theta)(\partial\theta/\partial y)$, and $(\partial\psi/\partial\theta)(\partial\theta/\partial z)$ respectively. Therefore, the concept of unsaturated water diffusivity must be employed ($D(\theta)$) ($[L^2T^{-1}]$), which for the x , y and z directions is defined as:

$$D_x(\theta) = - \frac{k_x(\theta)}{\rho_w g} \frac{\partial \psi}{\partial \theta} \quad (2.20)$$

$$D_y(\theta) = - \frac{k_y(\theta)}{\rho_w g} \frac{\partial \psi}{\partial \theta} \quad (2.21)$$

$$D_z(\theta) = - \frac{k_z(\theta)}{\rho_w g} \frac{\partial \psi}{\partial \theta} \quad (2.22)$$

When Eqs. (2.20)-(2.22) are substituted into Eq. 2.19, the conventional θ -form of the Richards equation is obtained:

$$\frac{\partial \theta}{\partial t} = \frac{\partial}{\partial x} \left(D_x(\theta) \frac{\partial \theta}{\partial x} \right) + \frac{\partial}{\partial y} \left(D_y(\theta) \frac{\partial \theta}{\partial y} \right) + \frac{\partial}{\partial z} \left(D_z(\theta) \frac{\partial \theta}{\partial z} - k_z(\theta) \right) \quad (2.23)$$

In the solution of Eq. 2.19 θ is a continuous variable, which is valuable for evaluating the nature of water flow in homogeneous soil. However, although the θ -form of the Richards equation is usually employed, models based on this equation do not adequately simulate internodal flow in heterogeneous soils because θ is discontinuous between layer interfaces (Assouline, 2013).

2.3.1 Cavalcante and Zornberg (2017) model

The closed analytical solution of the Richards equation proposed by Cavalcante & Zornberg (2017) is based on the principle that constitutive models are adopted to represent the hydraulic conductivity and suction functions in the unsaturated condition for transient flows. The formulation adopted by the authors considers negligible volumetric changes, so the flow occurs in an unsaturated porous medium where the porosity is constant. The assumption

included, although it limits the application of the model in soil mechanics, is perfectly applicable to cemented soils in arid to sub-humid climates. Before finding a solution for Eq. 2.23, it is necessary to perform a linearization process using the concepts of unsaturated hydraulic conductivity (k_z) and unsaturated advective seepage, a_s ($[LT^{-1}]$), expressed as follows:

$$\frac{\partial k_z(\theta)}{\partial z} = \frac{\partial k_z(\theta)}{\partial \theta} \frac{\partial \theta}{\partial z} = a_s(\theta) \frac{\partial \theta}{\partial z} \quad (2.24)$$

Substituting Eq.2.24 into Eq. 2.23, the Richards equation can be rewritten as:

$$\frac{\partial \theta}{\partial t} = \frac{\partial}{\partial x} \left(D_x(\theta) \frac{\partial \theta}{\partial x} \right) + \frac{\partial}{\partial y} \left(D_y(\theta) \frac{\partial \theta}{\partial y} \right) + \frac{\partial}{\partial z} \left(D_z(\theta) \frac{\partial \theta}{\partial z} \right) - a_s(\theta) \frac{\partial \theta}{\partial z} \quad (2.25)$$

To solve Eq. 2.25, it is necessary to define two functions $k_z(\theta)$ and $\psi(\theta)$ for which the nonlinear terms of D_x , D_y , D_z and a_s are constants. For this, the model proposes a mathematical relationship for $\psi(\theta)$:

$$\psi(\theta) = \frac{1}{\delta} \ln \left(\frac{\theta - \theta_r}{\theta_s - \theta_r} \right) \quad (2.26)$$

where θ_s is the saturated volumetric water content $[L^3L^{-3}]$, θ_r is the residual volumetric water content $[L^3L^{-3}]$, and δ is a fitting hydraulic parameter of the model $[M^{-1}LT^2]$. In the other hand, the relationship for $k_z(\theta)$ is defined for the directions x, y and z as:

$$k_x(\theta) = k_{sx} \frac{(\theta - \theta_r)}{(\theta_s - \theta_r)} \quad (2.27)$$

$$k_y(\theta) = k_{sy} \frac{(\theta - \theta_r)}{(\theta_s - \theta_r)} \quad (2.28)$$

$$k_z(\theta) = k_{sz} \frac{(\theta - \theta_r)}{(\theta_s - \theta_r)} \quad (2.29)$$

where k_s is the saturated hydraulic conductivity $[LT^{-1}]$. The main advantage of analytically solving the Richards equation using θ as an independent variable is that the function $k_z(\theta)$ has less hysteresis than $k_z(\psi)$, and (D_z) varies less if the independent variable is θ and not ψ . Additionally, adopting the definition of Eq. 2.20, 2.26, and 2.27 the term $D_x(\theta)$ becomes constant for the x direction:

$$\bar{D}_x = \frac{k_{sx}}{\rho_w g(\theta_s - \theta_r)\delta} \quad (2.30)$$

Combining Eq. 2.21, 2.26, and 2.28, the unsaturated diffusivity constant at y -direction can be expressed as:

$$\bar{D}_y = \frac{k_{sy}}{\rho_w g(\theta_s - \theta_r)\delta} \quad (2.31)$$

Finally, using Eq. 2.22, 2.26, and 2.29, the unsaturated diffusivity constant at z -direction is equal to:

$$\bar{D}_z = \frac{k_{sz}}{\rho_w g(\theta_s - \theta_r)\delta} \quad (2.32)$$

The physical meaning of the a_s corresponds to the slope of the unsaturated hydraulic conductivity function when expressed as a function of θ ($k_z(\theta)$). However, employing Eq. 2.29 and 2.24, it is possible to convert the parameter a_s into a constant and define it as:

$$\bar{a}_s = \frac{k_{sz}}{(\theta_s - \theta_r)} \quad (2.33)$$

From the definitions of \bar{D}_x , \bar{D}_y , \bar{D}_z , and \bar{a}_s the Richards equation can be expressed as:

$$\frac{\partial \theta}{\partial t} = \bar{D}_x \frac{\partial^2 \theta}{\partial x^2} + \bar{D}_y \frac{\partial^2 \theta}{\partial y^2} + \bar{D}_z \frac{\partial^2 \theta}{\partial z^2} - \bar{a}_s \frac{\partial \theta}{\partial z} \quad (2.34)$$

There are three particularities when globally evaluating the equation proposed by the authors: i) for steady-state conditions, Eq. 2.34 is set to 0, which facilitates the application of the Richards equation when $dv/dt = 0$, ii) the parameters have a physical interpretation, and iii) for the case of a one-dimensional unsaturated flow in the z -direction, the constants \bar{D}_z and \bar{a}_s are analogous to the coefficient of longitudinal hydrodynamic dispersion (D_h) ($[L^2T^{-1}]$), and the average linear velocity (v_s) ($[LT^{-1}]$) respectively in the advection-dispersion contaminant transport equation.

Therefore, the pollutant advection-dispersion phenomenon is directly related to the transport of water in an unsaturated porous medium, facilitating the obtaining of solutions for other types of phenomena in which there is a solution to the dispersion-advection equation. However, solutions must be used from one case to another, considering different physical interpretations for each scenario. The model proposes a fitting equation for SWRC as a function of absolute suction value for soils with a unimodal pore distribution:

$$\theta(|\psi|) = \theta_r + (\theta_s - \theta_r)e^{-|\psi|^\delta} \quad (2.35)$$

The graphical representation of Eq. 2.35 is shown in Fig. 2.7, where the parameter δ is proportional to the initial slope of the SWRC, i.e., the slope at saturation.

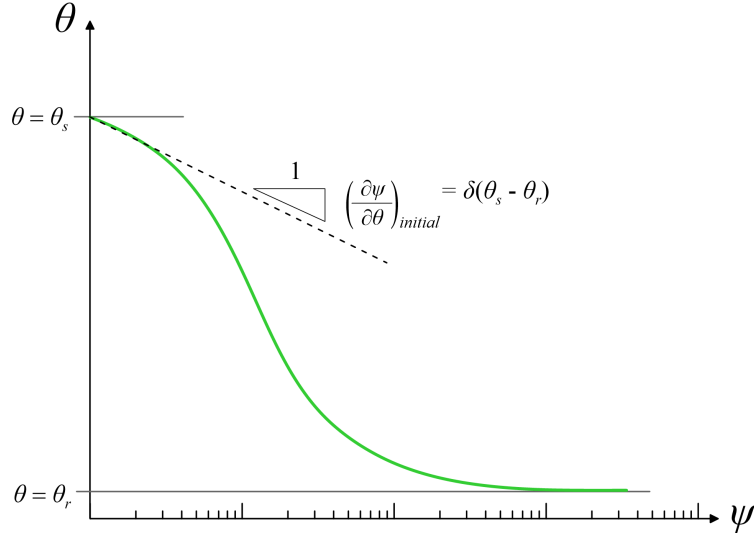


Figure 2.7: Physical representation of parameters δ , θ_s , and θ_r .

2.3.2 Askar and Jin (2000) model

The objective of the model proposed by Askar & Jin (2000) focuses on the application of the Richards equation (Eq. 2.23) to expansive soils. The model proposes a relationship between θ and volumetric variations, expressed through the general flow equation. The mathematical formulation of the model considers the volumetric changes during the expansion phenomenon and its effect on the void ratio (e). Assuming that a soil element represented by a cube of side z [L], with initial volume (V_0) [L^3], and initial volume of water (V_{w0}) [L^3] begins to swell by the inflow of water from a (θ_0) [L^3L^{-3}] at a time t_0 , the volume change (ΔV_w) [L^3] when the cube reaches a value of V , V_w and θ at a time t is equal to:

$$\Delta V_w = V_w - V_{w0} = \theta V - \theta_0 V_0 \quad (2.36)$$

To obtain the volume of water per unit area ($\Delta w'$) [L], Eq. 2.36 is divided by z^2 [L^2]:

$$\Delta w' = \frac{\Delta V_w}{A} = \frac{\theta V - \theta_0 V_0}{A} = \frac{\theta V}{z^2} - \frac{\theta_0 V_0}{z^2} \quad (2.37)$$

Bronswijk (1990) proposes a mathematical expression to define the changes in the geometry of clay soils when subjected to wetting and drying cycles. The simple general equation describes the conversion of volumetric changes from a three-dimensional plane to a one-dimensional plane in swelling soils as:

$$\left(1 + \frac{\Delta V}{V}\right) = \left(1 + \frac{\Delta z}{z}\right)^{r_s} \quad (2.38)$$

where r_s is a dimensionless geometry factor, and for 3D conditions, r_s takes the value of 3, and in the 1D case the value of 1. Using Eq. 2.38 for one-dimensional analysis ($r_s = 1$) and $V = z^3 [L^3]$:

$$\Delta V = V - V_0 = \left[\left(1 + \frac{\Delta z}{z}\right) - 1 \right] z^3 \quad (2.39)$$

Substituting Eq. 2.39 into Eq. 2.37, and expressing in terms of V_0 :

$$\Delta w' = \frac{V_0}{z^2}(\theta - \theta_0) + \theta \Delta z \quad (2.40)$$

Eq. 2.40 is based on the assumption that vertical soil movement leads to changes in soil layer thickness. This assumption requires that horizontal cracks remain stable or negligible. During the swelling process, e changes from e_0 to e at t_0 to t , and since $r_s = 1$ (one-dimensional) the ΔV is restricted exclusively to Δz so that $\Delta V = \Delta z z^2$. Therefore, ΔV can be expressed in terms of Δe as:

$$z^2 \Delta z = \Delta e V_s \quad (2.41)$$

where V_s is the volume of solids $[L^3]$. Now, substituting Eq. 2.41 into 2.40, it is possible to obtain the equation describing the increase in $\Delta w'$ due to Δe :

$$\Delta w' = \frac{V_0 \Delta \theta}{z^2} + \frac{\theta \Delta e V_s}{z^2} \quad (2.42)$$

According to Eq. 2.37, the Eq. 2.42 can be expressed in terms of V_w as:

$$\Delta V_w = (V - \Delta V) \Delta \theta + \theta \Delta e \left(\frac{V}{1 + e} \right) \quad (2.43)$$

The continuity equation in a one-dimensional analysis is restricted exclusively to the z -direction. Therefore, using the 1D-form of Eq. 2.8 in Eq. 2.36 it is obtained:

$$\frac{\partial \left(\frac{\Delta V_w}{V} \right)}{\partial t} = -\frac{\partial v_z}{\partial z} \quad (2.44)$$

Substituting Eq. 2.44 into Eq. 2.43:

$$-\frac{\partial v_z}{\partial z} = \frac{\partial}{\partial t} \left(\frac{(V - \Delta V)\Delta\theta}{V} + \frac{\theta\Delta e}{V} \left(\frac{V}{1+e} \right) \right) \quad (2.45)$$

According to Askar & Jin (2000) the term $((V - \Delta V)\Delta\theta)/V$ is too small and can be neglected, so Eq. 2.45 can be rewritten as follows:

$$-\frac{\partial v_z}{\partial z} = \left(\frac{\partial\theta}{\partial t} + \frac{\theta}{1+e} \frac{\partial e}{\partial t} \right) \quad (2.46)$$

In the case of non-swelling soils, the term $(\theta/1+e)/(\partial e/\partial t)$ is equal to 0, which returns the continuity equation, and therefore the Richards equation, to its original form. Employing Darcy-Buckingham law (Eq. 2.12), and the definitions of D_x , D_y , and D_z (Eqs. (2.20 to 2.22)), the swelling-Richards equation is expressed as follows:

$$\frac{1}{1+e} \frac{\partial}{\partial t} [(1+e)\theta] = \frac{\partial}{\partial x} \left(D_x(\theta) \frac{\partial\theta}{\partial x} \right) + \frac{\partial}{\partial y} \left(D_y(\theta) \frac{\partial\theta}{\partial y} \right) + \frac{\partial}{\partial z} \left(D_z(\theta) \frac{\partial\theta}{\partial z} \right) - \frac{\partial k_z(\theta)}{\partial z} \quad (2.47)$$

Chapter 3

METHODS AND MATERIALS

3.1 METHODS

The methods used can be divided into four stages: i) mathematical formulation of the model, ii) analytical solutions, iii) validation with experimental results, and iv) parametric calibration. Fig. 3.1 presents the summary of the steps of the methodology to be executed during the work. The final model obtained is one-dimensional and allows evaluating the hydromechanical response of expansive soils, where the swelling path is mainly considered. The results recorded after the mathematical modelling process are compared with laboratory test data of soil columns with specific boundary conditions. The parametric calibration evaluates the model's field of action in different soil typologies using results reported in the literature. In this way, the behaviour of the data of the $e-\psi$ curve allows establishing of the model's limitations and the values of e at which the model presents a numerical limit.

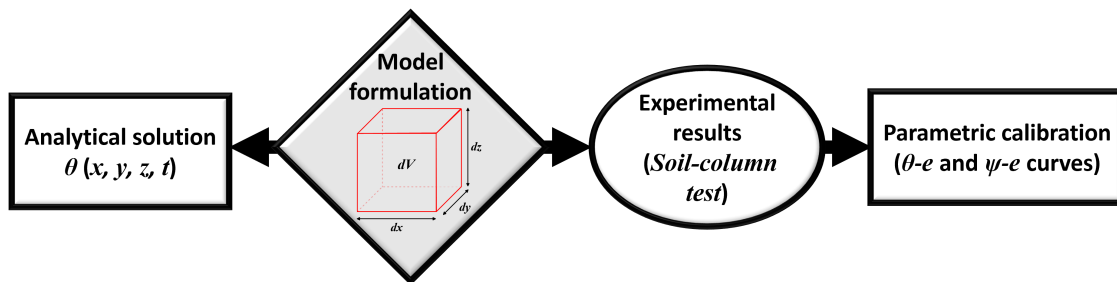


Figure 3.1: Summary of steps of the methodology to be implemented.

3.1.1 Mathematical model formulation

The mathematical development established in this work is based on the lines of research followed by [Askar & Jin \(2000\)](#); [Cavalcante & Zornberg \(2017\)](#); [Richards \(1931\)](#). The model

is initially formulated from the theoretical arguments of water movement in unsaturated porous media, introducing the concepts of swelling and shrinkage of soils due to moisture changes. The definition of the unsaturated hydraulic conductivity and suction functions in terms of volumetric water content and water movement in a REV results in a stable and convenient formulation. This first orientation gives a hydraulic justification to the original approach. Then, the model is developed from mechanical arguments on expansion behaviour.

It is established that transient flow in unsaturated porous media generates volumetric changes expressed in variations in the soil void ratio. This first argument takes into consideration the principle of mass conservation. In the classical [Richards \(1931\)](#) equation, it is assumed that all changes in θ are dependent on variations in Sr , which translates into soil porosity (n) [L^3L^{-3}] remaining conservatively constant for all wetting or drying paths. The model presented by [Cavalcante & Zornberg \(2017\)](#) is one-dimensional and can be applied to column test results, where n remains relatively constant during the test.

However, for expansive soils, n (and consequently e) varies as a function of volumetric changes given by changes in θ . Although this argument was partially resolved by [Askar & Jin \(2000\)](#), the model parameters have no physical meaning, and their mathematical resolution depends on the definition of the functions $k(\theta)$ and $\psi(\theta)$. Thus, since the parameters used in the [Cavalcante & Zornberg \(2017\)](#) model have definite physical meaning and are constant variables, in the proposed model, the swelling fraction of the [Askar & Jin \(2000\)](#) approach will be represented by a constant term with physical meaning. Therefore, by controlling the mechanical behaviour, the determined parameter will be responsible for regulating the properties of interest of the mathematical calculation that will be studied throughout the work. Fig. 3.2 presents an outline of the procedures adopted to formulate the model.

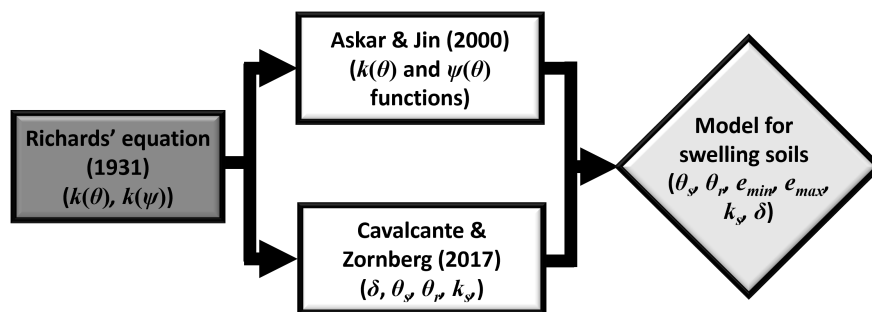


Figure 3.2: Schematic of model formulation for swelling soils in unsaturated porous media.

3.1.2 Analytical solutions

Once the model has been defined, the search for analytical solutions is carried out. Four analytical solutions are proposed that differ from each other and require two initial boundary conditions. In all four cases, the moisture content is kept uniform, and the boundary condi-

tion that controls the geometry of the column is varied. Thus, the resulting mathematical equation will be solved using the Laplace transform in the time domain for four cases using different initial conditions as schematized in Fig. 3.3. Table 3.1 presents the initial, upper and lower boundary and initial conditions for the four cases. In each case, *Mathematica 12.3* software was used to implement the code in all the formulations. On the other hand, the analytical solutions found will be evaluated in terms of their efficiency using the experimental results obtained by Azevedo (2016). The mathematical construction starts from the Richards equation in its classical form (Eq. 2.23) and the simplified equations of Cavalcante & Zornberg (2017) and Askar & Jin (2000).

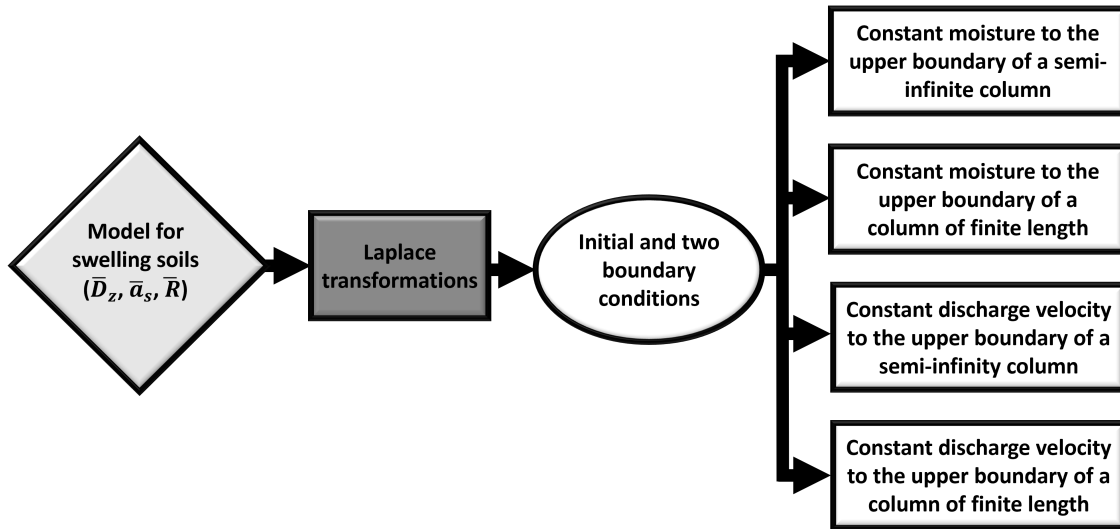


Figure 3.3: Formulation of the analytical solution for model of swelling soils.

Table 3.1: Initial and boundary conditions for each case.

Case	Initial condition	Upper boundary condition	Lower boundary condition
1		$\theta_0 = \text{const}$	$L = \infty$
2	$\theta_i = \text{const}$		$L = L$
3		$v_0 = \text{const}$	$L = \infty$
4			$L = L$

3.1.3 Validation with experimental results

The soil column device was structured to estimate θ values in soil under a wide range of ψ . The column shown in Fig. 3.4 consists of a 197 mm diameter, 1100 mm high acrylic column cell to contain the soil sample and a suction and water flow monitoring and control

system. The hydraulic assembly uses a top cap connected low-flow pump to deliver water at a constant rate of 0.40 ml/min. To guarantee the non-saturated condition throughout the test, the flow rate chosen was lower than the one at which the k_s value was reached. Additionally, the flow is evenly distributed through the entire compacted soil column by using filter paper at the top of the system.

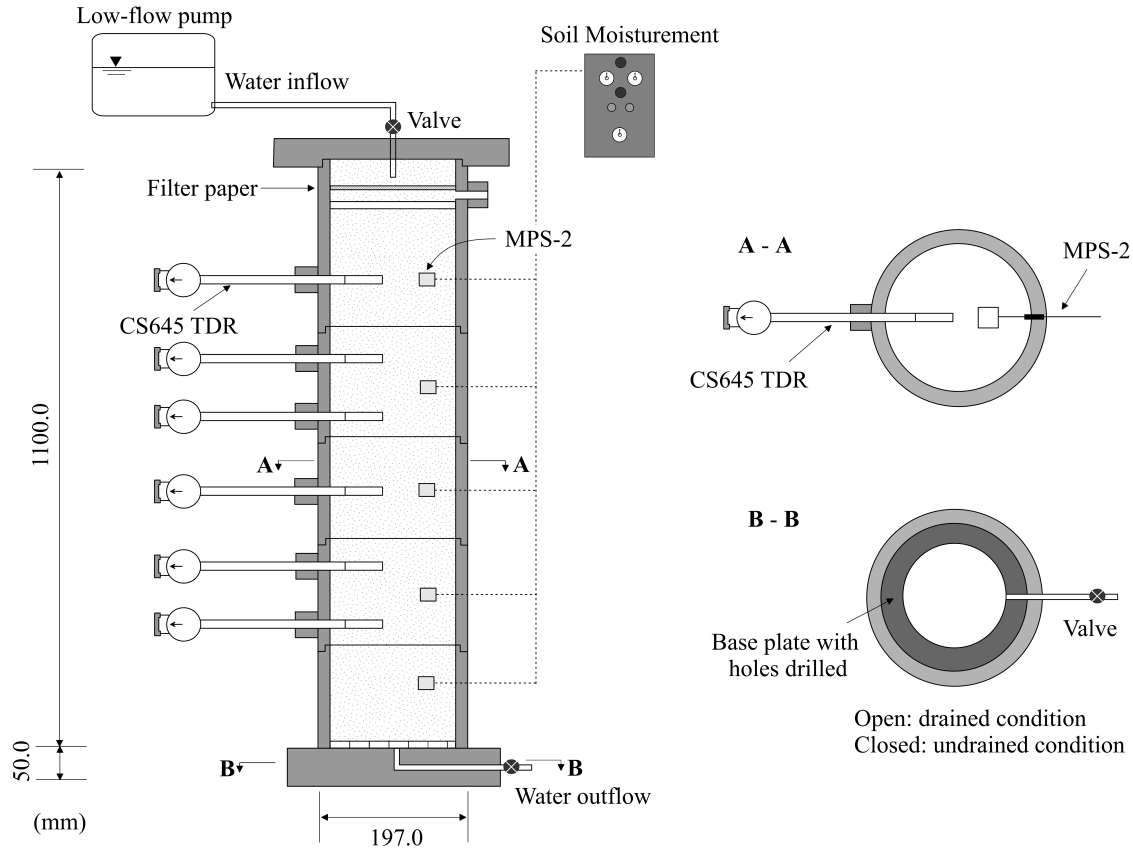


Figure 3.4: Schematic diagram of the soil column test.

The water used in the test is drained using a perforated base plate at the bottom of the column to a tipping bucket connected to the bottom of the container. The value of θ at which steady flow conditions were obtained in this test system was 0.30. Both the outflow and inflow of water into the soil pile are controlled using manual control valves, where the outflow valve controls the loading condition of the test. Several circular sections were cut along the length of the acrylic cell to mount the measuring and control instruments. Finally, the soil column was lined with a plastic liner to prevent moisture loss by evaporation.

Two different types of control sensors were installed in the monitoring equipment to evaluate the behaviour of ψ and θ . Fluctuations in θ were controlled and measured with seven CS645 time domain reflectometry (TDR) probes. On the other hand, suction was recorded using MPS-2 tensiometers. TDR- CS645 and MPS-2 were arranged horizontally, as

shown in Fig. 3.4, and the TDRs were arranged at 12, 34, 44, 56, 68, and 78 cm from the top of the soil column. In the case of the TDRs, a calibration process was performed to improve their accuracy to +/- 1% (Azevedo, 2012). The column tests were initially conceived to evaluate the effect of the capillary barrier on geosynthetics, so the results of θ vs t and ψ vs t were limited exclusively to those recorded at positions upstream of the capillary barrier. Therefore, to avoid this effect on the modelling and still have sufficient data to run the fitting routines, the TDR-7 results will be excluded from the analysis.

The four analytical solutions proposed in the previous item will be fitted to the results using two distinct and consecutive steps. The first step consists of fitting the RMA soil water retention curve and soil unsaturated conductivity curve utilising the model of Cavalcante & Zornberg (2017). With the flux parameters k_s , θ_r , θ_s , the model parameter δ is determined using curve fitting. In the second step, the above parameters are used together with the developed model parameters derived from the mathematical formulation (e_{max} and e_{min}) in the functions $k_s(\theta)$, $\theta(\psi)$ and $e(\theta)$.

3.1.4 Parametric calibration

It is necessary to show that the model can simulate results from selected experimental tests, so the model's performance is analyzed using parametric calibration. To achieve this purpose, data are used to demonstrate graphically the range in which the model can reproduce the variation of void ratio with increasing suction. In this way, the suction *versus* void ratio (e -log ψ curve) is derived from ψ values obtained from the SWRC in the drying path. According to Gallipoli (2012), the e -log ψ curve possesses a unique slope called the virgin line governed by the properties of the micropores.

As the suction increases, the void ratio decreases, which defines a shrinkage path in the e -log ψ curve on the drying path. However, in the curve e -log ψ , it is also possible to identify the wetting path, generated from the increase of e , and the decrease of ψ . Since the values of ψ are related to the e data, the inflexion point of the e -log ψ curve where the shrinkage is zero corresponds to the AEV of the SWRC. According to Fig. 3.5, the interval that exists between the value of ψ prior to the onset of shrinkage and the AEV defines both the virgin drying line of the SWRC and the virgin shrinkage line of the e -log ψ space. It is possible to observe that most shrinkage occurs within the fully saturated state, i.e., in the suction range before the soil starts desaturation. The e -log ψ curve is illustrated in Fig. 3.5 and can be interpreted in a unified framework.

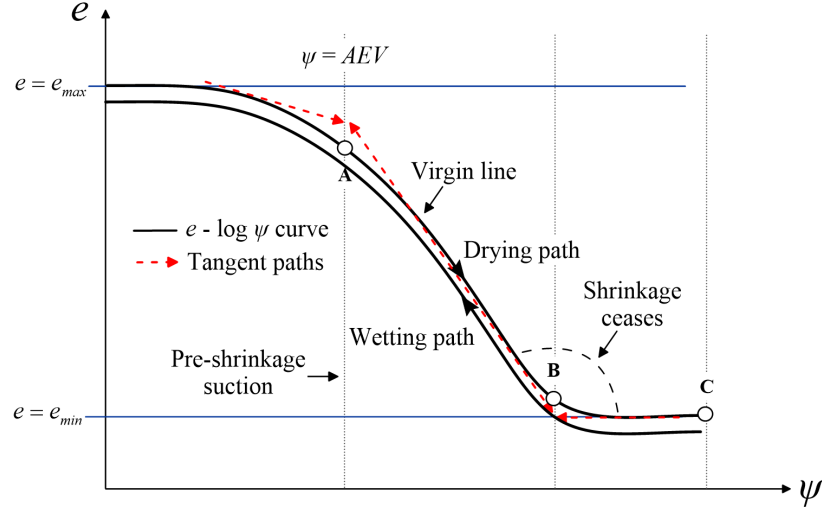


Figure 3.5: $e - \log \psi$ curve.

The experimental results of expansive clays reported by [Nowamooz & Masrouri \(2010\)](#), [Al-Dakheeli & Bulut \(2019\)](#), [Zhao et al. \(2021\)](#), and [Sarker & Wang \(2022\)](#) are adopted to verify the proposed model. To illustrate the model's accuracy, the numerical predictions and the raw data are given for comparison. The basis of comparison of the results is the e - $\log \psi$ curve, and the δ value is estimated from the mathematical fit of the model. Using the idealized curve presented in Fig. 3.5, the sensitivity of the parameters will be evaluated, as well as the capacity of the model to recreate both the drying and wetting paths.

3.2 MATERIALS

Experimental results used to evaluate the proposed model were performed by [Azevedo \(2012, 2016\)](#). Soil column tests were conducted using soil obtained from a borrow pit at the Rocky Mountain Arsenal (RMA) site in Denver, USA. Unaltered samples were collected from field exploration using invasive Shelby tube borings. Table 3.2 indicates the physical properties of the tested soil cores: specific gravity (S_g) [$ML^3M^{-1}L^{-3}$], dry unit weight (γ_d) [ML^{-3}], optimum moisture content (w_{opt}) [MM^{-1}], minimum void ratio (e_{min}) [L^3L^{-3}], and maximum void ratio (e_{max}) [L^3L^{-3}]. Additionally, the values of liquid limit (LL), plastic limit (PL), and plasticity index (PI) are presented.

Table 3.2: Physical properties of soil.

Property	S_g	γ_d (g/cm^3)	w_{opt} (%)	e_{min}	e_{max}	LL (%)	PL (%)	PI (%)
Value	2.71	1.90	15	0.45	0.89	32	12	20

The grain size distribution curve obtained from the tests is presented in Fig. 3.6. In grain sizes smaller than 0.075 mm, the soil samples showed *silty sand* textural mappings when tested using 4% sodium hexametaphosphate (SHMP), meaning that approximately 50% of the soil sample passed the No. 200 sieve (Azevedo, 2012, 2016). The separation method for clay ($<2 \mu\text{m}$), silt ($2\text{-}75 \mu\text{m}$), and sand ($75\text{-}2000 \mu\text{m}$), as well as the measurement techniques, were carried out following the international standard ASTM D422 (ASTM, 2007). The hydrometer used for the dispersed particle concentration controls was of the ASTM-H152-68°F type. This model is, in particular, a standard and universally approved. The suspension smaller than $75 \mu\text{m}$ was dispersed with SHMP at 40 g per liter of solution. To measure the concentration in suspension, the ASTM procedure requires using a compound correction for each hydrometer reading. A more detailed description of the material used in this study is summarized by Thompson (2009).

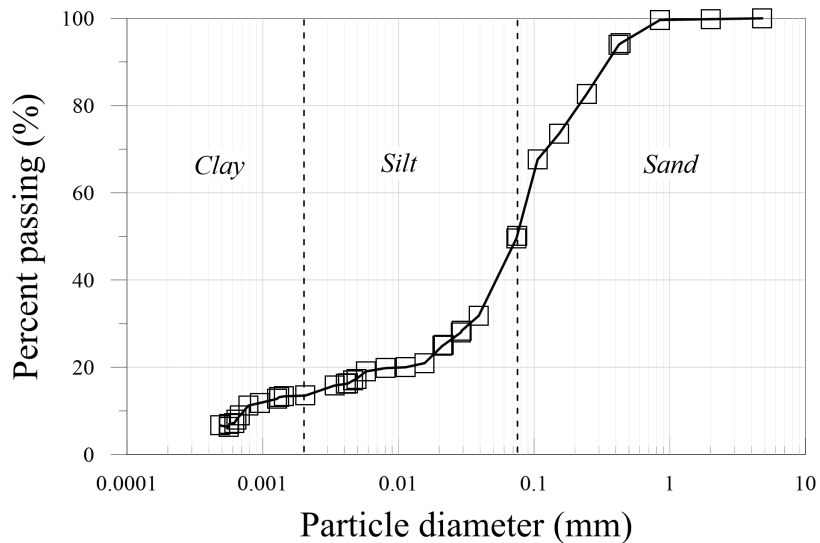


Figure 3.6: Particle Size Distribution of the soil.

Fig. 3.7 shows the typical bimodal SWRC of this material (Azevedo, 2012, 2016). The results were obtained using three different techniques at varying ranges: i) for a low suction range (0 to 10 kPa), the hanging column test method was used; ii) at moderate suction (5 to 500 kPa), the pressure plate testing according was employed, and iii) at high suction (over 500 kPa), thermodynamic methods were applied. The air entry value for the macropores (AEV_{macro}) in the curve was 0.30 kPa. Due to the use of various measurement systems, it was possible to obtain values greater than 10000 kPa of matric suction. According to Otálvaro Calle (2013), the mobilization of the water stored in the micropores requires increasing the suction until reaching values of 35 MPa. In this case, due to the joint use of different methods, it was possible to observe the AEV of the micropores (AV_{micro}) at 1100 kPa.

The data received from the experimental cycle were analyzed using a curve-fitting procedure proposed by Van Genuchten (1980). In the predictive process, a parametric comparison was resorted to using the θ_s data as the point of coincidence between the model and the laboratory results (Azevedo, 2012, 2016). Fig. 3.7 presents the typical SWRC of the evaluated material and the mathematical fit, and Table 3.3 shows the model fit parameters and experimental results. The van Genuchten model fits the data by employing a functional algorithm appropriate for small ψ values, which limits the model when there is a transition between porous systems.

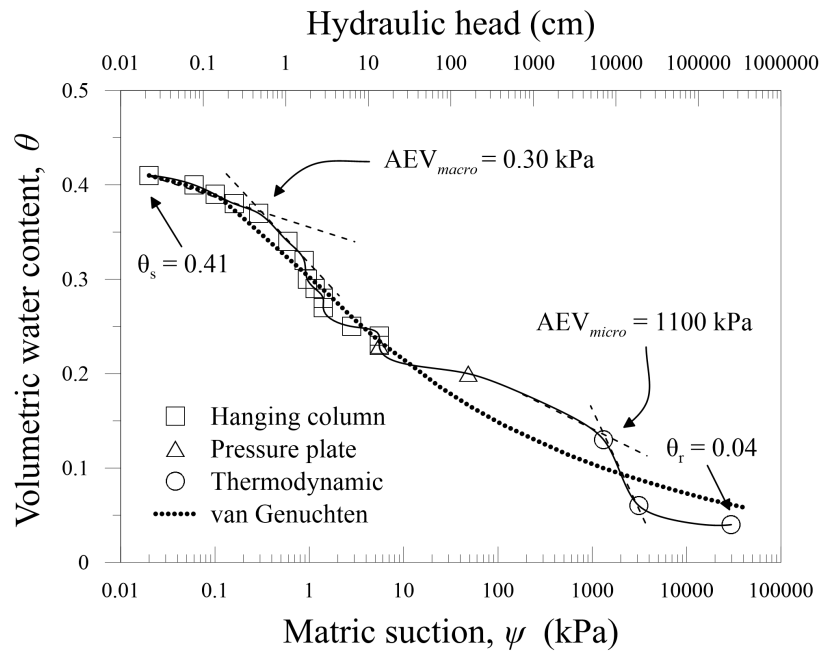


Figure 3.7: Soil Water Retention Curve.

Table 3.3: Summary of hydraulic fitting parameters of soil.

	θ_s	θ_r	AEV_{micro} (kPa)	AEV_{macro} (kPa)	n	α (cm^{-1})
Experimental	0.41	0.04	0.30	1100	-	-
Van Genuchten (1980)	0.41	0.05	-	-	1.16	0.69

In unsaturated soils, the value of hydraulic conductivity (k) varies with suction so that at a value of ψ of 0 kPa, k is equal to k_s . To observe the behaviour of k in different ranges of ψ , it is necessary to find the k -function of the soil. Though, as in the case of SWRC the k -function can be estimated by employing theoretical and experimental methods, many empirical techniques are time-consuming and prone to high levels of uncertainty. Therefore, mathematical models have been developed that allow k -functions to be predicted from SWRC results (Mualem, 1976).

The van Genuchten-Maulem model established by [Mualem \(1976\)](#) is the most approved for estimating the variation of k with respect to ψ , as it modifies the equations of [Van Genuchten \(1980\)](#) in a statistical way to determine the k -function. Fig. 3.8 presents the soil k -function obtained using the van Genuchten-Maulem model. Since the behaviour of the SWRC and k -function is theoretically linked, it is possible to establish a relationship between ψ , k , and θ being inversely proportional between ψ and k and directly proportional between k and θ . In Fig. 3.8, the value of k_s found was $8.2 \times 10^{-5} \text{ cm/s}$ which, when employed in the model of [Cavalcante & Zornberg \(2017\)](#), allows demonstrating that the fitting hydraulic parameter δ is proportional to the saturation slope.

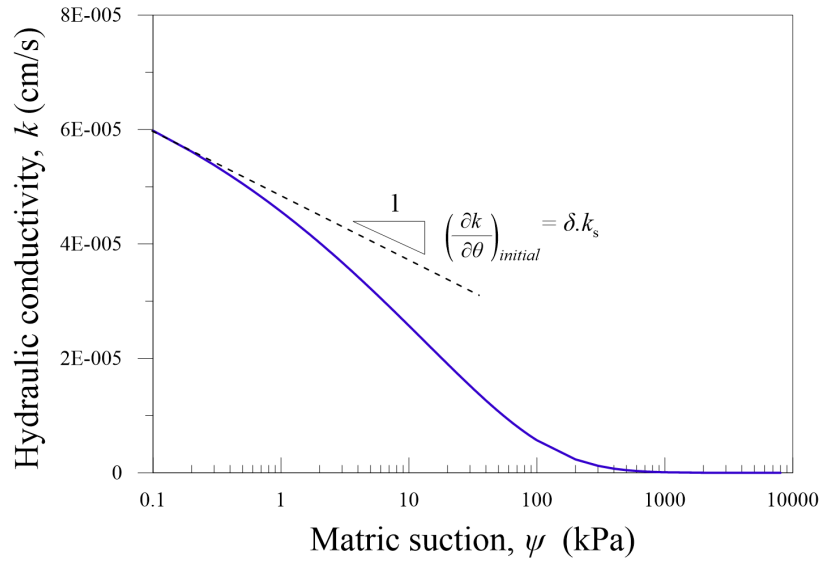


Figure 3.8: Soil k -function.

Chapter 4

RESULTS

4.1 MATHEMATICAL MODEL FORMULATION

In this section, the model of water flow in porous media with swelling potential is formulated. The way to obtain the equation is based on the classical mathematical definitions of the [Askar & Jin \(2000\)](#) and [Cavalcante & Zornberg \(2017\)](#) models. At the end of the formulation, a flow equation analogous to the classical one proposed by [Richards \(1931\)](#) is obtained, with terms of derivatives of the void ratio replacing the initial fraction of the original equation. Therefore, the resulting equation can be called the water flow equation in unsaturated media with swelling or the Richards equation for swelling soils.

There are two arguments to be considered to obtain the equation: one from the perspective of water movement in unsaturated porous media, where the arguments established by the law of continuity, the Darcy-Buckingham law and the Bernoulli equation must be fulfilled, and the other, assuming that any volumetric change experienced during swelling deforms the soil matrix, which can be expressed using a state variable. The equation proposed by [Askar & Jin \(2000\)](#) (Eq. 2.47) can be rewritten using the rate of change in water storage in a REV as:

$$m_{storage} = \frac{1}{1+e} \frac{\partial}{\partial t} [\rho_w(1+e)\theta] dx dy dz \quad (4.1)$$

The principle of continuity implies that for all fluids that are incompressible (i.e., ρ_w is constant in time) and homogeneous (i.e., ρ_w is constant in space), the difference between the total mass outflow and inflow rates must be equal to the change in water storage. Using the continuity equation (Eq. 2.8) Eq. 4.1 can represent this principle as:

$$\frac{1}{1+e} \frac{\partial}{\partial t} [\theta(1+e)] = -\frac{\partial v_x}{\partial x} - \frac{\partial v_y}{\partial y} - \frac{\partial v_z}{\partial z} \quad (4.2)$$

Employing the flow rate per unit of area (discharge velocity) in each direction can be defined using Darcy-Buckingham's law (Buckingham, 1907), which is expressed using Eqs. 2.16, 2.17, 2.18, the Eq. 4.2 can be rewrite as follows:

$$\frac{1}{1+e} \frac{\partial}{\partial t} [\theta(1+e)] = \frac{\partial}{\partial x} \left[\frac{k_x(\psi)}{\rho_w g} \frac{\partial \psi}{\partial x} \right] + \frac{\partial}{\partial y} \left[\frac{k_y(\psi)}{\rho_w g} \frac{\partial \psi}{\partial y} \right] + \frac{\partial}{\partial z} \left[k_z(\psi) \left(\frac{1}{\rho_w g} \frac{\partial \psi}{\partial z} - 1 \right) \right] \quad (4.3)$$

According to the θ -form of the Richards equation, the definition of unsaturated water diffusivity coefficient ($D(\theta)$) can be used to simplify Eq. 4.3 of the form:

$$\frac{1}{1+e} \frac{\partial}{\partial t} [\theta(1+e)] = \frac{\partial}{\partial x} \left(D_x(\theta) \frac{\partial \theta}{\partial x} \right) + \frac{\partial}{\partial y} \left(D_y(\theta) \frac{\partial \theta}{\partial y} \right) + \frac{\partial}{\partial z} \left(D_z(\theta) \frac{\partial \theta}{\partial z} \right) - \frac{\partial k_z(\theta)}{\partial z} \quad (4.4)$$

Eq. 4.4 can be referred to as an extension of the Fokker-Planck equation for soils with swelling potential. However, for the case of soil-column tests, it must be assumed that the flow direction is strictly vertical, following the orientation of the z -axis, so Eq. 4.4 can be simplified as:

$$\frac{1}{1+e} \frac{\partial}{\partial t} [\theta(1+e)] = \frac{\partial}{\partial z} \left(D_z(\theta) \frac{\partial \theta}{\partial z} \right) - \frac{\partial k_z(\theta)}{\partial z} \quad (4.5)$$

Joining Eq. 4.5 to the concept of unsaturated advective seepage (a_s), the following equation is obtained:

$$\frac{1}{1+e} \frac{\partial}{\partial t} [\theta(1+e)] = \frac{\partial}{\partial z} \left(D_z(\theta) \frac{\partial \theta}{\partial z} \right) - a_s(\theta) \frac{\partial \theta}{\partial z} \quad (4.6)$$

Applying the derivative rules to the first term of Eq. 4.6:

$$\frac{\theta}{1+e} \frac{\partial e}{\partial t} + \frac{\partial \theta}{\partial t} = \frac{\partial}{\partial z} \left(D_z(\theta) \frac{\partial \theta}{\partial z} \right) - a_s(\theta) \frac{\partial \theta}{\partial z} \quad (4.7)$$

Replacing $\partial e / \partial t$ by $(\partial e / \partial \theta)(\partial \theta / \partial t)$, Eq. 4.7 can be rewritten as:

$$R(e) \frac{\partial \theta}{\partial t} = \frac{\partial}{\partial z} \left(D_z(\theta) \frac{\partial \theta}{\partial z} \right) - a_s(\theta) \frac{\partial \theta}{\partial z} \quad (4.8)$$

with,

$$R(e) = 1 + \frac{\theta}{1+e} \frac{\partial e}{\partial \theta} \quad (4.9)$$

The function $R(e)$ allows evaluating the behaviour of expansive soils when exposed to wetting cycles under unsaturated conditions of transient flow. In terms of the second member of Eq. 4.8, the diffusive component ($D_z(\theta)$) corresponds to the flow of water advancing under gravitational action, and the diffusive component (a_s) defines the diffusively propagated water movement. The solution of Eq. 4.8 requires the definition of three additional relations because it involves four unknowns (θ , k_z , ψ and e). The relations $k(\theta)$ and $\psi(\theta)$ were mathematically deduced by Cavalcante and Zornberg (2017), and their proof is presented in Appendix A1 and A2 respectively. Accordingly, $k_z(\theta)$ and $\psi(\theta)$ are represented by:

$$k_z(\theta) = k_s \left(\frac{\theta - \theta_r}{\theta_s - \theta_r} \right) \quad (4.10)$$

$$\psi(\theta) = \frac{1}{\delta} \ln \left(\frac{\theta - \theta_r}{\theta_s - \theta_r} \right) \quad (4.11)$$

It can be demonstrated (Appendix A3) that the ratio $e(\theta)$ keeps its intrinsic meaning in e , and that its variation depends on the definition of a minimum and a maximum value:

$$e(\theta) = -1 + (1 + e_{min}) \left(\frac{1 + e_{max}}{1 + e_{min}} \right)^{\left(\frac{\ln \frac{\theta}{\theta_r}}{\ln \frac{\theta_s}{\theta_r}} \right)} \quad (4.12)$$

An essential consequence of adopting Eqs. 4.10, 4.11 and 4.12 into Eq. 4.8 is that the hydraulic expressions $D_z(\theta)$, $a_s(\theta)$ and $R(e)$ become constants. Specifically, the resulting parameters can be expressed as:

$$\bar{D}_z = \frac{k_s}{\delta(\theta_s - \theta_r)\rho_w g} \quad (4.13)$$

$$\bar{a}_s = \frac{k_s}{(\theta_s - \theta_r)} \quad (4.14)$$

$$\bar{R} = 1 + \frac{\ln\left(\frac{1 + e_{max}}{1 + e_{min}}\right)}{\ln\left(\frac{\theta_s}{\theta_r}\right)} \quad (4.15)$$

where \bar{D}_z is the constant unsaturated water diffusivity, \bar{a}_s is the constant unsaturated advective seepage, and \bar{R} is the constant swelling potential obtained when $k_z(\theta)$, $\psi(\theta)$ and $e(\theta)$ are represented by linear, logarithmic, and linear relationships, respectively. As can be seen, when the soil is non-swelling, i.e., when there is no variation in e (i.e. $e_{min} = e_{max}$), \bar{R} is equal to 1. In this case, the model is returned to the original version of the model proposed by [Cavalcante & Zornberg \(2017\)](#).

Therefore, by converting the generalized version of the model (4.8) into an easily applicable form using Eqs. 4.13, 4.14 and 4.15 the required parameters in the model are θ_s , θ_r , k_s , δ , e_{min} and e_{max} . Direct or indirect methods can obtain these parameters. θ_s and θ_r come from the SWRC, k_s can be obtained either experimentally or by using constitutive estimation models, δ is a fitting parameter that depends on the SWRC, and e_{min} and e_{max} by using physical characterization tests. Thus, the simplified form of the model corresponds to:

$$\bar{R} \frac{\partial \theta}{\partial t} = \bar{D}_z \frac{\partial^2 \theta}{\partial z^2} - \bar{a}_s \frac{\partial \theta}{\partial z} \quad (4.16)$$

For steady-state conditions, Eq. 4.16 becomes:

$$\frac{\bar{D}_z}{\bar{R}} \frac{d^2 \theta}{dz^2} - \frac{\bar{a}_s}{\bar{R}} \frac{d\theta}{dz} = 0 \quad (4.17)$$

In summary, the global framework for unsaturated transient flow in expansive media evaluated in this study is represented by Eq. 4.8 for the general case, where $k_z(\theta)$, $\psi(\theta)$ and $e(\theta)$ are functions of θ . In contrast, the problem related to swelling soils in unsaturated flows is easier to evaluate using Eq. 4.16, where \bar{D}_z , \bar{a}_s and \bar{R} are constant values. A particular feature of Eq. 4.16 is its analogy with the advection-dispersion contaminant transport equation:

$$R \frac{\partial c}{\partial t} = D_h \frac{\partial^2 c}{\partial z^2} - v_s \frac{\partial c}{\partial z} \quad (4.18)$$

4.2 ANALYTICAL SOLUTIONS

The development of analytical solutions considers the soil-atmosphere relationship, including three parameters dependent on these dynamics. To understand this unit, it is necessary to evaluate the mechanics of water distribution in the atmosphere, soil surface, and interior matrix. Most of these phenomena are due to the law of mass conservation generated during the hydrological cycle. For practical purposes, in most problems involving real geotechnical scenarios, the hydrologic cycle is simplified exclusively to the physical factors of precipitation, evapotranspiration, surface runoff and infiltration.

Infiltration caused by the external injection of water is the primary variable of analysis in the hydrological balance due to its influence on the definition of the physical processes of water distribution within the soil. To evaluate this phenomenon, it is necessary to establish a control field in which water follows a flow path in a vertically downward direction. On a global scale, during a rainfall event, the soil is in its maximum infiltration phase in the first periods, allowing it to absorb all the water on the surface. When passing from time $t = 0$ to time $t = t$, the porous matrix of the soil reduces its capacity due to saturation, initially of the macropores and subsequently of the micropores. Fig. 4.1a presents a synthesized scheme of the hydrological cycle and the atmosphere-water interaction on a macro scale. The rate at which water infiltrates into the soil mass is called the infiltration velocity (v_0) [LT^{-1}] and is inversely proportional to the hydraulic conductivity of the material. The relationship between $k(\theta)$ and (v_0) is presented in Fig. 4.1b.

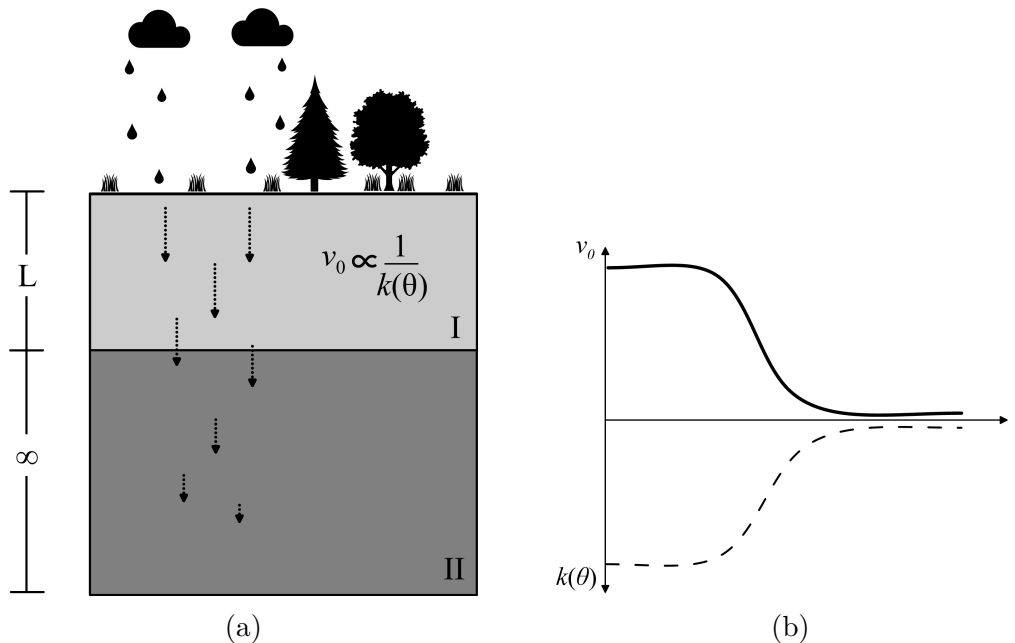


Figure 4.1: Synthesized scheme: (a) hydrological cycle; (b) functions $k(\theta)$ and v_0 with respect to time.

As rainwater accumulates in the upper layer (I), the water-filled pores find a continuous phase to flow, increasing permeability and reducing infiltration capacity; this relationship is appreciable in the upper layers. As soon as the moisture front advances and reaches the transition zone (II), the infiltration capacity of the soil increases due to the decrease in permeability as a result of running the unsaturated condition. From this point, the water table is assumed to reach deeper strata, which saturates the lower layers, giving rise to a type I scenario. The functional dynamics are similar in stages I and II, and the flow mechanism responds to same phenomena, infiltration in stages I and II.

It is possible to understand the behaviour of the parameter (v_0) , using the variation of θ as a function of time. For a value of $(v_0) = 0$, the value of θ remains constant at $\theta = \theta_i$, where θ_i is the initial volumetric water content [L^3L^{-3}]. As the flow is in phase I, $(v_0) = (v_0)$, which stimulates the variation of θ , from θ_i to θ_0 , where θ_0 is the volumetric water content measured at any instant t . Increasing the discharge gradient until $(v_0) = (v_{0,max})$ (where $v_{0,max}$ [LT^1] is maximum discharge), gives $\theta_i = \theta_s$. Fig. 4.2 shows the relationship between (v_0) , $(v_{0,max})$, θ_i , θ_0 , and θ_s , as well as the behaviour of the curves as a function of time.

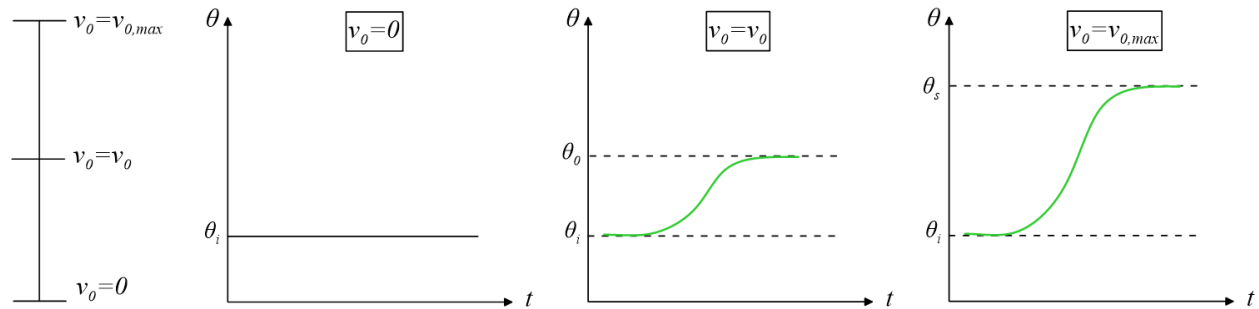


Figure 4.2: Graphical representation of the behaviour of θ_0 , θ_i , v_0 and $v_{0,max}$ with respect to time.

The unsaturated model defined by [Cavalcante & Zornberg \(2017\)](#) allows modelling moisture fronts at different depths to overcome some conceptual and numerical limitations. Thus, by adopting at the upper boundary of the domain a second-order boundary condition or Neumann flow condition, it was necessary to impose a constant value of (v_0) , as well as maximum $(v_{0,max})$ and minimum $(v_{0,min})$ [LT^1] discharge values. Both $(v_{0,max})$ and $(v_{0,min})$ are defined from the unsaturated hydraulic conductivity, the maximum wetting capacity and the initial state of soil moisture.

4.2.1 Case 1: Imposed constant moisture to the upper boundary of a semi-infinite column

For this case, it is established that the initial condition of the formulation considers the initial volumetric content (θ_i) uniform, so for a time $t=0$, the solution is given by:

$$\theta(z, 0) = \theta_i \quad (4.19)$$

where θ_i is constant. For this solution, a Dirichlet boundary condition is adopted, where the required value at the domain boundary corresponds to a constant value of θ at the upper boundary:

$$\theta(0, t) = \theta_0 \quad (4.20)$$

where θ_0 is constant. Considering that the domain corresponds to a semi-infinite column, the flow evaluated in space is described in the ∞ -scenario. Therefore, the lower boundary condition adopted in this case is described by:

$$\frac{\partial \theta}{\partial z}(\infty, t) = 0 \quad (4.21)$$

By adopting this condition, two situations arise simultaneously in the solution: i) upon reaching a certain depth within the domain, θ and ψ reach constant values, and ii) the hydraulic gradient in the z -direction equals 1 in depth. Thus, using the initial condition ($\theta_i=\text{constant}$), and the upper ($\theta=\text{constant}$) and lower ($z=\infty$) boundary conditions, the analytical solution of equation Eq. 4.16 for the case 1 is:

$$\theta(z, t) = \theta_i + (\theta_0 - \theta_i)A(z, t) \quad (4.22)$$

where A equals:

$$A(z, t) = \frac{1}{2} \left[\text{erfc}(Z_{-1}) + \exp\left(\frac{\bar{a}_s z}{\bar{D}_z}\right) \text{erfc}(Z_{+1}) \right] \quad (4.23)$$

and the term Z_{+1} equals:

$$Z_{\pm 1} = \frac{\bar{R}z \pm \bar{a}_s t}{2\sqrt{\bar{R}\bar{D}_z t}} \quad (4.24)$$

The complementary error function, $\text{erfc}(Z)$, is defined, for $z \geq 0$ as:

$$\text{erfc}(Z) = 1 - \frac{2}{\pi} \int_0^z \exp(-t^2) dt \quad (4.25)$$

In simple words, the function $\text{erfc}(Z)$ represents the area under the two tails of a zero-mean Gaussian probability density function with a variance (σ^2) value equal to $1/2$. For the particular case in which $\bar{a}_s=0$, i.e. $k_s=0$ (a completely impermeable or membrane-covered soil), the analytical solution reduces to:

$$\theta(z, t) = \theta_i + (\theta_0 - \theta_i) \text{erfc} \left(\frac{z}{2\sqrt{\frac{\bar{D}_z}{Rt}}} \right) \quad (4.26)$$

For the case in which $\bar{D}_z=0$, i.e. $k_s=0$, the analytical solution of Eq. 4.16 reduces to:

$$\theta(z, t) = \theta_i + (\theta_0 - \theta_i) \text{H} \left(\frac{\bar{a}_s}{Rt - z} \right) \quad (4.27)$$

where H is the Heaviside function, whose value is 0 for any negative argument, and 1 for any positive argument. Therefore, H is given by:

$$\text{H}(x) = \begin{cases} 0, & \text{if } x \leq 0. \\ 1, & \text{if } x > 0. \end{cases} \quad (4.28)$$

By employing the ordinary differential equation (4.17), the Richards equation is reduced to a steady-state condition. In this scenario, it is not necessary to use an initial condition, since the lower and upper boundary conditions in the domain are sufficient to find the solution. For this case, the Dirichlet boundary condition imposed on the upper boundary of the domain corresponds to:

$$\theta(0) = \theta_0 \quad (4.29)$$

where θ_0 is constant. For the semi-infinite column, the lower boundary condition is given by:

$$\frac{d\theta}{dz}(\infty) = 0 \quad (4.30)$$

Therefore, in the steady-state condition, the analytical solution of the Richards equation for evaluating swelling in soils is:

$$\theta(Z) = \theta_0 \quad (4.31)$$

4.2.2 Case 2: Imposed constant moisture to the upper boundary of a column of finite length

As in Case 1, Case 2 employs the same initial condition of $\theta_i = \text{constant}$, as described in Eq. 4.19. Similarly, the Dirichlet boundary condition imposed at the upper boundary of the domain corresponds to the same one used in Case 1, whose mathematical expression is given by Eq. 4.20. However, being a column of finite length, the lower boundary condition varies concerning Case 1. For this case, a column of length L is assumed in which the gradient of θ is equal to 0, which is expressed as:

$$\frac{\partial \theta}{\partial z}(L, t) = 0 \quad (4.32)$$

By employing this assumption, the same mathematical consequences are obtained: i) $\theta = \text{constant}$, ii) $\psi = \text{constant}$ and iii) hydraulic gradient equals 1. However, in this case, these reactions are recorded at a domain depth equal to L . Thus, the analytical solution of Eq. 4.16 under these initial and boundary conditions corresponds to:

$$\theta(z, t) = \theta_i + (\theta_0 - \theta_i)B(z, t) \quad (4.33)$$

where B is given by:

$$B(z, t) = 1 - \sum_{m=1}^{\infty} \frac{2\beta_m \sin\left(\frac{\beta_m z}{L}\right) \exp\left(\frac{\bar{a}_s z}{2\bar{D}_z} - \frac{\bar{a}_s^2 t}{4R\bar{D}_z} - \frac{\beta_m^2 \bar{D}_z t}{RL^2}\right)}{\left[\beta_m^2 + \frac{\bar{a}_s L}{2\bar{D}_z} + \left(\frac{\bar{a}_s L}{2\bar{D}_z}\right)^2\right]} \quad (4.34)$$

and the term β_m corresponds to the eigenvalues at the positive roots of the equation and is defined by:

$$\beta_m \cot(\beta_m) + \frac{\bar{a}_s L}{2\bar{D}_z} = 0 \quad (4.35)$$

To achieve accurate results of the analytical solution, approximately four terms of the series defined in Eq. 4.34 can be employed. Therefore, using the definitions of $Z_{\pm 1}$ and the complementary error function, $\text{erfc}(Z)$, Eq. 4.34 reduces to:

$$\begin{aligned} B(z, t) = & \frac{1}{2} \text{erfc}(Z_{-1}) + \frac{1}{2} \exp\left(\frac{\bar{a}_s z}{\bar{D}_z}\right) \text{erfc}(Z_{+1}) \\ & + \frac{1}{2} \left[2 + \frac{\bar{a}_s(2L - z)}{\bar{D}_z} + \frac{\bar{a}_s^2 t}{\bar{R}\bar{D}_z} \right] \exp\left(\frac{\bar{a}_s L}{\bar{D}_z}\right) \text{erfc} \left[\frac{\bar{R}(2L - z) + \bar{a}_s t}{2\sqrt{\bar{D}_z \bar{R} t}} \right] \\ & - \sqrt{\frac{\bar{a}_s^2 t}{\pi \bar{R} \bar{D}_z}} \exp\left(\frac{\bar{a}_s L}{\bar{D}_z} - \frac{\bar{R}}{4\bar{D}_z t} (2L - z + \bar{a}_s t)^2\right) \end{aligned} \quad (4.36)$$

In order to simplify the domain of analysis, the same hypotheses used in Case 1 are applied. Thus, for the scenario in which $\bar{a}_s=0$, i.e. $k_s=0$, the analytical solution solving Eq. 4.16 under this particular boundary condition reduces to:

$$\theta(z, t) = \theta_i + (\theta_0 - \theta_i) \left(1 + \sum_{m=1}^{\infty} \frac{4}{\pi} \sin\left(\frac{\pi z}{2L}\right) \exp\left(-\frac{\pi^2 \bar{D}_z t}{4\bar{R}L^2}\right) \right) \quad (4.37)$$

When considering the influence of the eigenvalues on the dynamics of the results, the two possible roots ($\beta_m = \pm\pi/2$) were evaluated. However, only the positive β_m value gives a feasible solution in Case 2. Thus, including this argument in the simplification process of Eq. 4.37, the approximate expression of the analytical solution is given by:

$$\theta(z, t) = \theta_i + (\theta_0 - \theta_i) \left[\text{erfc}\left(\frac{\bar{R}z}{2\sqrt{\bar{D}_z \bar{R} t}}\right) + \text{erfc}\left(\frac{\bar{R}(2L - z)}{2\sqrt{\bar{D}_z \bar{R} t}}\right) \right] \quad (4.38)$$

For the case in which $\bar{D}_z=0$, i.e. $k_s=0$, the analytical solution of Eq. 4.16 reduces to Eq. 4.27. Precisely, the Dirichlet condition adopted to the upper boundary of the domain corresponds to Eq. 4.29. In the case of the lower boundary condition, the assumption of a column with length L results in a zero volumetric water content gradient, which is expressed as:

$$\frac{d\theta}{dz}(L) = 0 \quad (4.39)$$

Using these conditions, the solution obtained for Case 2 in the steady-state is the same as in Case 1 (Eq. 4.31).

4.2.3 Case 3: Imposed constant discharge velocity to the upper boundary of a semi-infinity column

As in Cases 1 and 2, the initial condition adopted in Case 3 is given by a constant value θ_i . However, unlike Cases 1 and 2, in this case a second-type boundary condition (also called the Neumann boundary condition) is used for the upper boundary. This assumes that the upper boundary will not be dominated by a constant value θ but by a constant discharge velocity (v_0) as follows:

$$\left(\bar{D}_z \frac{\partial \theta}{\partial z} - k_z \right) \Big|_{z=0} = v_0 \quad (4.40)$$

where v_0 is constant. The mathematical behaviour of v_0 is dominated by k_s . Thus, the maximum value that can be reached by v_0 corresponds to the value of k_s . However, the fluctuation of k_s is dominated by the value of θ_s and θ_r , so the maximum imposed discharge velocity ($v_{0,max}$) is:

$$v_{0,max} = \frac{\theta_s k_s}{(\theta_s - \theta_r)} \quad (4.41)$$

Being a semi-infinite column, the lower boundary condition in Case 3 is given by Eq. 4.21. Some analytical solutions to partial differential equations under similar initial and boundary conditions have been reported in the literature (Gershon & Nir, 1969; Lindstrom et al., 1967). The analytical solution of Eq. 4.16 for Case 3 is given by:

$$\theta(z, t) = \theta_i + \left(\frac{v_0}{k_s} (\theta_s - \theta_r) - \theta_i \right) C(z, t) \quad (4.42)$$

where C equals:

$$\begin{aligned} C(z, t) = & \frac{1}{2} \operatorname{erfc}(Z_{-1}) + \sqrt{\frac{\bar{a}_s^2 t}{\pi \bar{R} \bar{D}_z}} \exp\left(-\frac{(\bar{R}z - \bar{a}_s t)^2}{4 \bar{D}_z \bar{R} t}\right) \\ & - \frac{1}{2} \left(-1 + \frac{\bar{a}_s z}{\bar{D}_z} + \frac{\bar{a}_s^2 t}{\bar{R} \bar{D}_z} \right) \exp\left(\frac{\bar{a}_s z}{\bar{D}_z}\right) \operatorname{erfc}(Z_{+1}) \end{aligned} \quad (4.43)$$

For the scenario in which $\bar{a}_s=0$, the analytical solution solving Eq. 4.16 under this particular boundary condition reduces to:

$$\theta(z, t) = \theta_i + \left(\frac{v_0}{k_s} (\theta_s - \theta_r) - \theta_i \right) \operatorname{erfc} \left(\frac{\bar{R}z}{2\sqrt{\bar{D}_z \bar{R}t}} \right) \quad (4.44)$$

For the case in which $\bar{D}_z=0$, the analytical solution of Eq. 4.16 reduces to:

$$\theta(z, t) = \theta_i + \left(\frac{v_0}{k_s} (\theta_s - \theta_r) - \theta_i \right) \operatorname{H} \left(\frac{\bar{a}_s}{\bar{R}t - z} \right) \quad (4.45)$$

where H is the Heaviside function and is given by Eq. 4.28. For this case, the steady-state solution is obtained by solving Eq. 4.17. Unlike Case 1 and 2, Case 3 employs the Neumann flux boundary condition which includes a constant v_0 value at the upper boundary of the domain:

$$\left(\bar{D}_z \frac{d\theta}{dz} - k_z \right) \Big|_{z=0} = v_0 \quad (4.46)$$

For the lower boundary of the domain, Eq. 4.30 is used for the case of a semi-infinite column. Finally, the analytical solution of Eq. 4.17 for Case 3 corresponds to:

$$\theta(z) = \frac{v_0}{k_z} (\theta_s - \theta_r) \quad (4.47)$$

4.2.4 Case 4: Imposed constant discharge velocity to the upper boundary of a column of finite length

Case 4 can be categorized as a union of Cases 1, 2 and 3, so the initial condition is given by Eq. 4.19. As in Case 3, Case 4 employs the Neumann condition in the upper boundary of the domain, whose main argument assumes v_0 as constant, and $v_{0,max}$ is defined using Eq. 4.41. Additionally, being a finite column of length L, the lower boundary condition is the same as that used in Case 2 (Eq. 4.32). Therefore, the analytical solution of Eq. 4.16 for these initial and boundary conditions were derived as follows:

$$\theta(z, t) = \theta_i + \left(\frac{v_0}{k_s} (\theta_s - \theta_r) - \theta_i \right) D(z, t) \quad (4.48)$$

where D equals:

$$D(z, t) = 1 - \sum_{m=1}^{\infty} \frac{\frac{2\bar{a}_s L}{\bar{D}_z} \beta_m \left[\beta_m \cos\left(\frac{\beta_m z}{L}\right) + \frac{\bar{a}_s L}{2\bar{D}_z} \sin\left(\frac{\beta_m z}{L}\right) \right] \exp\left(\frac{\bar{a}_s z}{2\bar{D}_z} - \frac{\bar{a}_s^2 t}{4\bar{R}\bar{D}_z} - \frac{\beta_m^2 \bar{D}_z t}{\bar{R}L^2}\right)}{\left[\beta_m^2 + \frac{\bar{a}_s L}{\bar{D}_z} + \left(\frac{\bar{a}_s L}{2\bar{D}_z}\right)^2 \right] \left[\beta_m^2 + \left(\frac{\bar{a}_s L}{2\bar{D}_z}\right)^2 \right]} \quad (4.49)$$

In this case, only the positive values of the root of the eigenvalues β_m were used:

$$\beta_m \cot(\beta_m) - \frac{\beta_m^2 \bar{D}_z}{\bar{a}_s L} + \frac{\bar{a}_s L}{4\bar{D}_z} = 0 \quad (4.50)$$

As in Case 3, the mathematical simplification process was performed, so that from Eq. 4.50 only four terms are necessary to obtain a certain solution. Therefore, the optimized form of Eq. 4.50 is given by:

$$\begin{aligned} D(z, t) = & \frac{1}{2} \operatorname{erfc}(Z_{-1}) + \sqrt{\frac{\bar{a}_s^2 t}{\pi \bar{R} \bar{D}_z}} \exp\left(-\frac{(\bar{R}z - \bar{a}_s t)^2}{4\bar{D}_z \bar{R} t}\right) \\ & - \frac{1}{2} \left(-1 + \frac{\bar{a}_s x}{\bar{D}_z} + \frac{\bar{a}_s^2 t}{\bar{R} \bar{D}_z}\right) \exp\left(\frac{\bar{a}_s z}{\bar{D}_z}\right) \operatorname{erfc}(Z_{+1}) \\ & + \sqrt{4 \frac{\bar{a}_s^2 t}{\pi \bar{R} \bar{D}_z}} \left[1 + \frac{\bar{a}_s}{4\bar{D}_z} \left(2L - z + \frac{\bar{a}_s}{\bar{R}} t\right)\right] \exp\left(\frac{\bar{a}_s L}{\bar{D}_z} - \frac{\bar{R}}{4\bar{D}_z t} \left(2L - z + \frac{\bar{a}_s}{\bar{R}} t\right)^2\right) \\ & - \frac{\bar{a}_s}{\bar{D}_z} \left[2L - z + \frac{3\bar{a}_s t}{2\bar{R}} + \frac{\bar{a}_s}{4\bar{D}_z} \left(2L - z + \frac{\bar{a}_s}{\bar{R}} t\right)^2\right] \exp\left(-\frac{\bar{a}_s L}{\bar{D}_z}\right) \operatorname{erfc}\left(\frac{\bar{R}(2L - z) + \bar{a}_s}{2\sqrt{\bar{D}_z \bar{R} t}}\right) \end{aligned} \quad (4.51)$$

For the scenario in which $\bar{a}_s=0$, the analytical solution solving Eq. 4.16 under this particular boundary condition reduces to Eq. 4.44 in Case 3. Also, For the case in which $\bar{D}_z=0$, the analytical solution of Eq. 4.16 reduces to Eq. 4.45 in Case 3. The derivation of the steady-state solution in Case 4 applied the Neumann flux boundary condition at the upper boundary of the domain resulting in Eq. 4.46 of Case 3. Likewise, the lower boundary condition imposes a null gradient of θ for a finite column of length L, resulting in Eq. 4.39 of Case 2. Applying these boundary conditions together yields Eq. 4.47, the same obtained in Case 3.

4.3 DECISION JUSTIFICATION ON CASE CHOICE

A comparative analysis of the finite and semi-infinite domain solutions was carried out to establish the cases to evaluate the experimental results. In this case, the selection was based on two main criteria. First, a significant agreement between cases was observed when analysing a small L range. Since a one-dimensional space limited to $L = 1.1$ m was evaluated, the results obtained for the finite solutions (Cases 2 and 4) were very similar to those obtained in the semi-infinite cases (Cases 1 and 3). However, for values of L of considerable magnitude, the numerical correspondence between values is reduced since it is bound exclusively for the initial interval. Second, it is much more practical to use the equations of the semi-infinite solutions (for small L values) because they do not use infinite summations. Therefore, it was decided to use Cases 1 and 3 to evaluate the proposed model using the experimental results.

Some results obtained using Cases 2 and 4 are shown to exemplify the correspondence between cases. Fig. 4.3 presents the volumetric water fronts estimated by the model in the soil column using Case 2. In Fig. 4.3a and 4.3b, the time history of θ at different locations and the profiles of θ at increasing times are presented. Additionally, Fig. 4.4 presents the void ratio estimated by the model in the soil column using Case 2 for time history at different locations (Fig. 4.4a) and the profiles increasing times (Fig. 4.4b). At values of L greater than 1.1 m, the model limits the presentation of results due to the lower boundary condition $L = L$. As shown below, the results obtained for each z -position in Case 2 are identical to those obtained for Case 1.

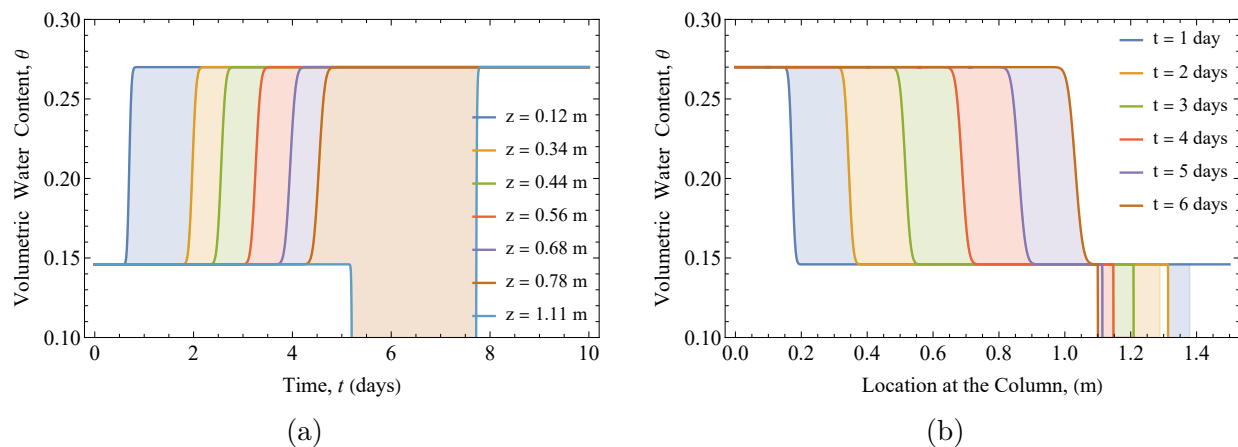


Figure 4.3: Predicted volumetric water content for Case 2 using $\delta=0.639$ kPa $^{-1}$: (a) time history at different locations; (b) profiles at increasing times.

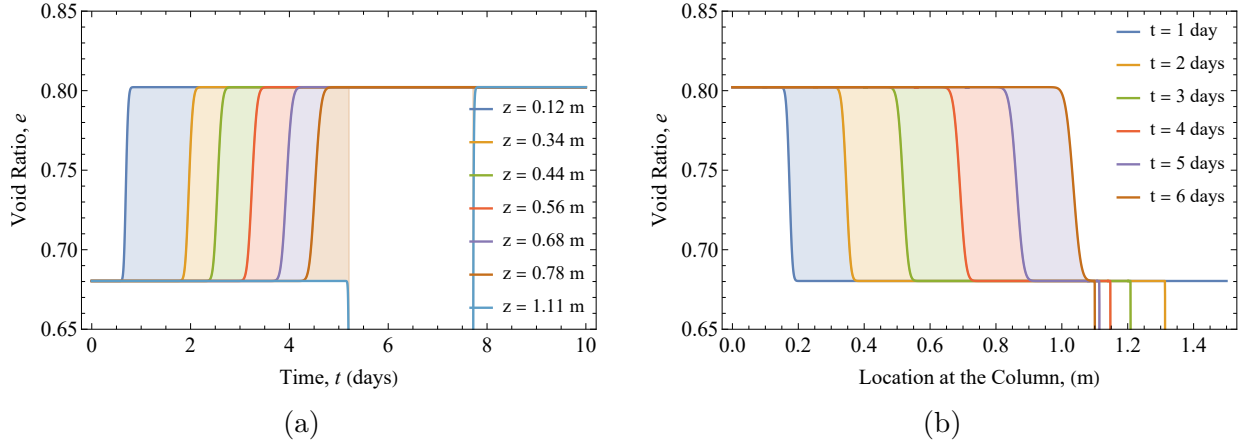


Figure 4.4: Predicted void ratio for Case 2 using $\delta=0.639 \text{ kPa}^{-1}$: (a) time history at different locations; (b) profiles at increasing times.

In Fig. 4.5a and 4.5b, the void ratio and per cent swelling were evaluated for different t and z settings considering Case 4. In this scenario, the dynamics of the results are less perceptible for a limited space that $L = L$ controls since only the data obtained in the first layers of the soil column are presented. However, as will be observed later, the results obtained for Case 4 are identical, for this analysed swath, to those estimated using Case 3.

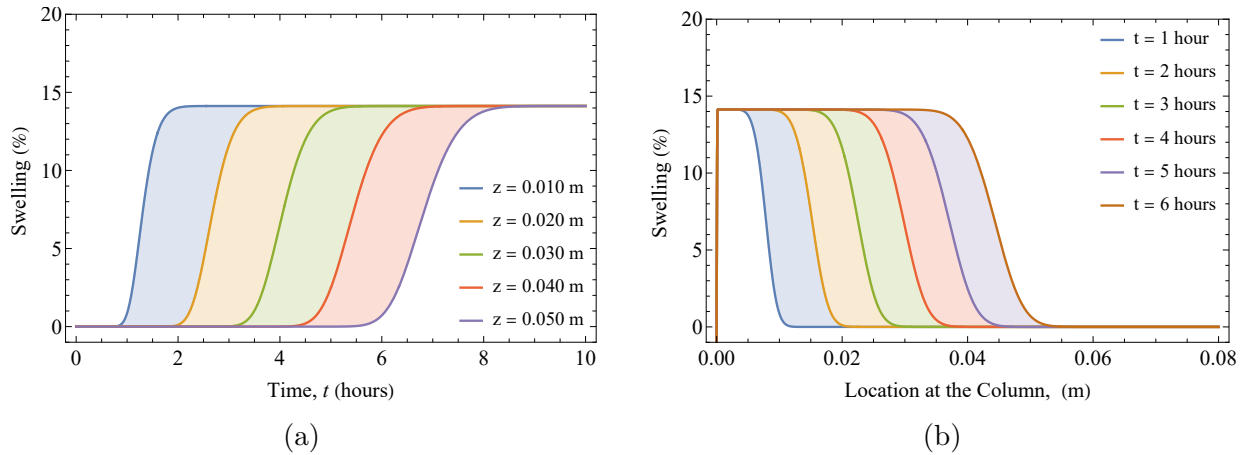


Figure 4.5: Predicted swelling for Case 4 using $\delta=0.639 \text{ kPa}^{-1}$: (a) time history at different locations; (b) profiles at increasing times.

4.4 VALIDATION WITH EXPERIMENTAL RESULTS

In the following section, the numerical predictions of the model are grouped into two stages of test results applying the hydromechanically coupled model for unsaturated swelling soils. The first group corresponds to the results obtained using the mathematical derivation of

the model exclusively. The other is the model’s results applying the analytical solutions for cases 1 and 3. It is important to emphasize that the parameters are the same for the first and second phases and come from the experimental tests performed by [Azevedo \(2016\)](#). The coupling between the model and constitutive parameters allows identifying the limitations of the model, as well as the range in which the results are accurate and in which the model estimates numerical atypicalities.

The model parameters can be determined by employing a relatively limited number of easy-to-run laboratory experiments. Therefore, according to the methodology performed by [Azevedo \(2016\)](#), it was possible to extract the values of the five constitutive parameters of the model (θ_s , θ_r , e_{max} , e_{min} and k_s). Table 4.1 summarizes the parameter values used in all modelling for phases 1 and 2 of the validation section.

Table 4.1: Parameters of the analyzed model.

Parameter	θ_s	θ_r	e_{max}	e_{min}	k_s (m/s)
Value	0.41	0.04	0.89	0.45	$8.2e^{-5}$

The hydraulic fitting parameter δ , was calculated from the SWRC results using both the unimodal model proposed by [Cavalcante & Zornberg \(2017\)](#) and the bimodal model proposed by [Costa & Cavalcante \(2021\)](#). Since δ is a parameter derived adequately from mathematical fitting, it was necessary to explore the variation between a unimodal and bimodal framework. The estimation of δ depends on the SWRC because, although it is a parameter specific to the proposed model, its derivation was performed by adapting the mathematical and physical arguments of [Cavalcante & Zornberg \(2017\)](#). Therefore, its intrinsic applicability in both models makes the functionality equivalent.

The model proposed by [Costa & Cavalcante \(2021\)](#) is based on the superposition of two unimodal models, so it is possible to find two hydraulic fitting parameters, δ and δ_2 , continuous with each other, which allows generating values for two different peaks in the SWRC. The δ from the [Costa & Cavalcante \(2021\)](#) model is used as a hypothesis for the δ value used in this study. The adjustment employing δ allows adjusting the SWRC taking as reference the AEV value of the micropores since this value corresponds to the range of suction and moisture variation applied during the test. On the other hand, the δ_2 value is defined by the AEV of the macropores, i.e. if this value is utilized to fit SWRC, the suction range achieved would be less than 1 kPa. Table 4.2 presents the numerical comparison of the fit performed for SWRC.

Table 4.2: Sensitivity of the δ parameter for unimodal and bimodal SWRC.

Model	Cavalcante & Zornberg (2017)	Costa & Cavalcante (2021)
δ (kPa ⁻¹)	0.639	1.004
δ_2 (kPa ⁻¹)	-	0.009
λ (kPa ⁻¹)	-	0.829

Note: hydraulic fitting parameter micropores (δ), hydraulic fitting parameter macropores (δ_2), additional fitting parameter for bimodal SWRC (λ).

By implementing Eq. 4.16 in *Wolfram Mathematica 12.3* using the parameter values in Tables 4.1 and 4.2, the following hydromechanical relationships were obtained: i) $\theta - \log \psi$, ii) $k_s - \log \psi$ and iii) $e - \log \psi$. In the case of the $\theta - \log \psi$ relationship, the best fit obtained concerning the experimental results was evaluated. However, since, in the soil microstructure, macropores and micropores are in equal proportion, the [Costa & Cavalcante \(2021\)](#) model recreates the SWRC path more accurately. The value of this fit was $\delta = 1.004 \text{ kPa}^{-1}$, a numerically higher value than that obtained by implementing [Cavalcante & Zornberg \(2017\)](#) ($\delta = 0.639 \text{ kPa}^{-1}$).

Fig. 4.6 and 4.7 show the experimental SWRC and the numerical fits for unimodal and bimodal schemes. Using the δ value for bimodal curves allows for identifying an accurate correlation with the laboratory values. In the case $\delta = 1.004 \text{ kPa}^{-1}$, the agreement can be considered as good, but certainly not perfect for the SWRC. It can also be observed that although δ possesses the same physical meaning for both models, the estimation of [Cavalcante & Zornberg \(2017\)](#) does not directly affect the prediction quality of [Costa & Cavalcante \(2021\)](#) for the same data set.

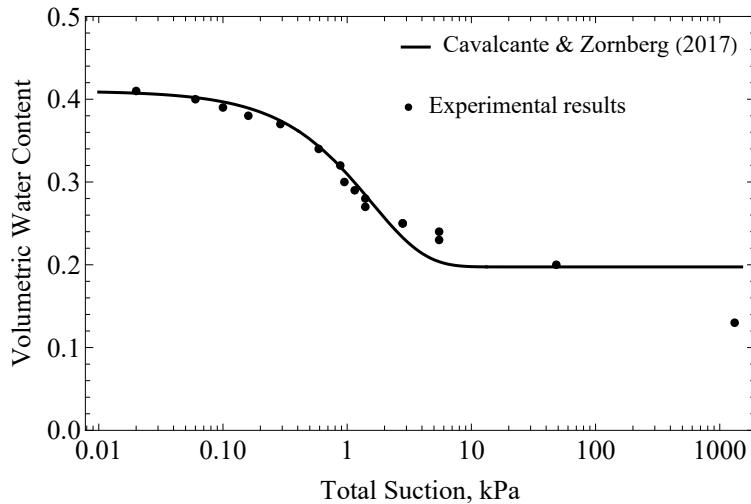


Figure 4.6: Fitting SWRC to obtain the δ value.

The experimental results of the SWRC presented in Fig. 3.7 indicate a bimodal behaviour. Although the proposed model depends on the parameter δ obtained from the model of Cavalcante & Zornberg (2017), whose formulation was based on unimodal SWRC, it is possible to establish a fit based on θ_i and θ_0 . Fig. 4.7 presents the SWRC fit employing the model proposed by Costa & Cavalcante (2021) for soils with bimodal porosity. The value of θ_i limits the fit and defines the maximum ψ value the model will reach to generate the suction front. In contrast, the value of θ_0 represents the minimum ψ value the model can estimate. This range of ψ applies exclusively to the estimate generated by the analytical solutions since, in that case, the suction is strongly dependent on θ_i and θ_0 .

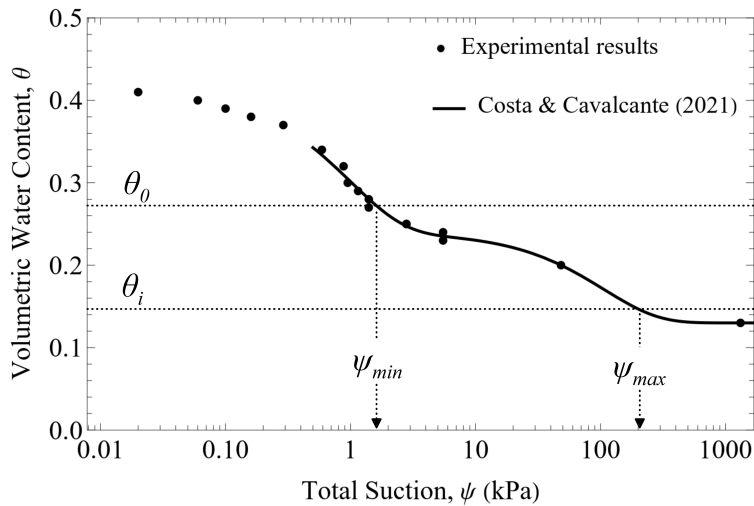


Figure 4.7: Fitting of bimodal SWRC to obtain the δ value.

The available measurements and predicted curves for the unsaturated hydraulic conductivity are compared in Fig. 4.8. In this case, only the scenario $\delta = 0.639 \text{ kPa}^{-1}$ was analyzed since the experimental results define an almost idealized unimodal k -function when increasing ψ . While allowing the unimodal graphical path to be determined, the fit varies significantly concerning the experimental residual ψ value (ψ value reached the minimum value of k_z) and moderately with respect to k_s .

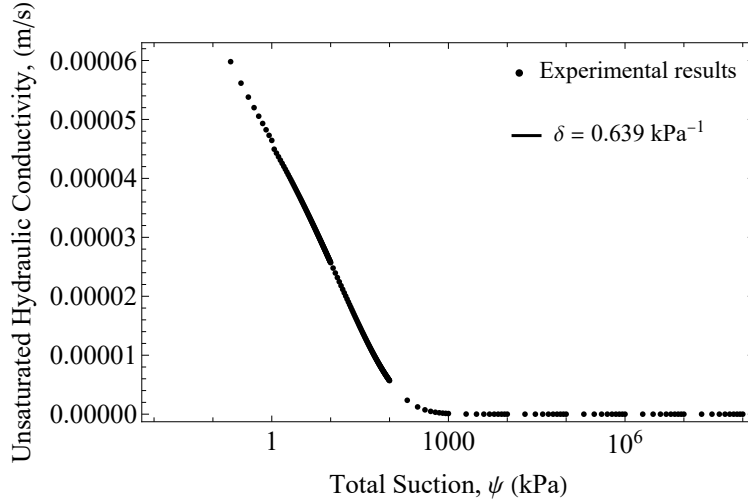


Figure 4.8: Comparison of the experimental results of unsaturated hydraulic conductivity with the k -function fitting model.

Inspection of Fig. 3.5 indicates that the AEV controls the rate at which the minimum void ratio changes for a given suction value. To corroborate this argument, the $e - \log \psi$ curve presented in Fig. 4.9 with different values of δ is considered. The value of AEV obtained experimentally was 0.5 kPa (Fig. 3.7), and the results in Fig. 4.9 for $\delta = 0.639 \text{ kPa}^{-1}$ indicate that the value of ψ at which shrinkage ceases is approximately 0.8 kPa. The estimated e_{min} value was the same for all δ values evaluated and corresponds to the experimental e_{min} value. This means that gradually with decreasing suction, the soil abruptly stopped swelling deformation during the hydration stage.

In the process of coding Eq. 4.16, three values of δ were explored to determine the sensitivity of the results. It was observed that the path of e with increasing ψ changed significantly with decreasing δ , indicating that the deformation caused by swelling decreases with decreasing δ . Fig. 4.9 also shows that the curves estimated by the model are of idealized character, i.e., their typical shape is defined respectively in Fig. 3.5. Table 4.3 shows the values of the advective (\bar{a}_s), diffusive (\bar{D}_z) and swelling (\bar{R}) components obtained by running the model with the parameters of the experimental results.

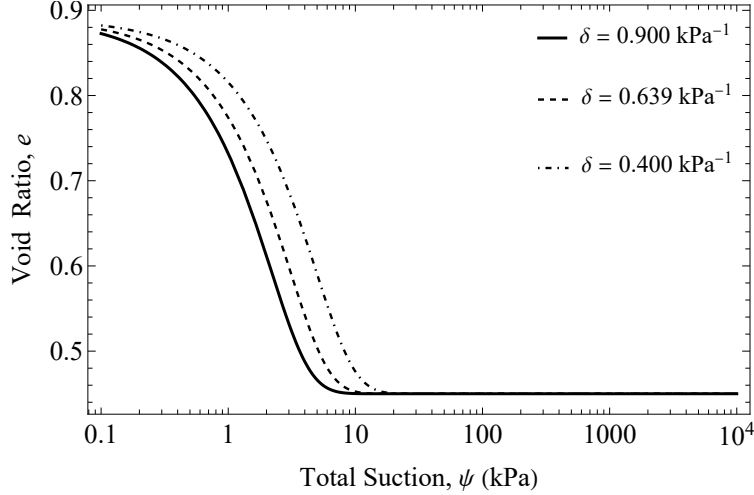


Figure 4.9: Sensitivity of hydraulic parameter (δ) in the $e - \log \psi$ curve.

Table 4.3: \bar{R} , \bar{D}_z and \bar{a}_s components obtained from the experimental fitting.

Parameter	\bar{R}	\bar{D}_z (m ² /s)	\bar{a}_s (m/s)
Value	1.27	1.90e ⁻⁸	1.60e ⁻⁴

Exploring the analytical solutions proposed to evaluate the hydromechanical mechanism of swelling soils in unsaturated flow problems of porous media is particularly beneficial in determining the behaviour of the parameters involved. Accordingly, this section provides a detailed analysis of the sensitivity of θ_s , θ_r , e_{min} , e_{max} , k_s , and δ . The parametric study was conducted considering a constant initial volumetric content condition (Case 1) and constant discharge velocity (Case 3) for semi-infinite columns. The adopted values of each parameter in the two scenarios are presented in Table 4.4.

Table 4.4: Parametric values used in the analytical solutions for Cases 1 and 3.

Parameter	g (m/s ²)	δ (kPa ⁻¹)	ρ_w (N/m ³)	θ_0	θ_i	v_0 (m/s)	L (m)
Value	9.80	0.639	1000	0.27	0.15	2.18e ⁻⁷	1.10

Note: gravitational acceleration (g), hydraulic fitting parameter (δ), density of water (ρ_w), volumetric content at time t (θ_0), initial volumetric content (θ_i), discharge velocity (v_0) and soil-column length (L).

The value of $\delta = 0.639$ kPa⁻¹ was maintained in all stages of the solution because it presented a better fit in the SWRC results. For Case 1, an initial and boundary condition corresponding to $\theta_i = 0.15$, and $\theta_0 = 0.27$, respectively, was adopted. For Case 3, the solution was based on the criterion of $\theta_i = 0.15$ as initial and $v_0 = 2.18e^{-7}$ m/s and $L = \infty$ as boundary conditions. Fig. 4.10 shows the θ -fronts for Case 1 at different values of z (corresponding to

the location of each of the tensiometers) and at different times. In Fig. 4.10a and 4.10b, the advective (\bar{a}_s) and diffusive (\bar{D}_z) flow components of Eq. 4.16 are relevant and control the behaviour of the curves.

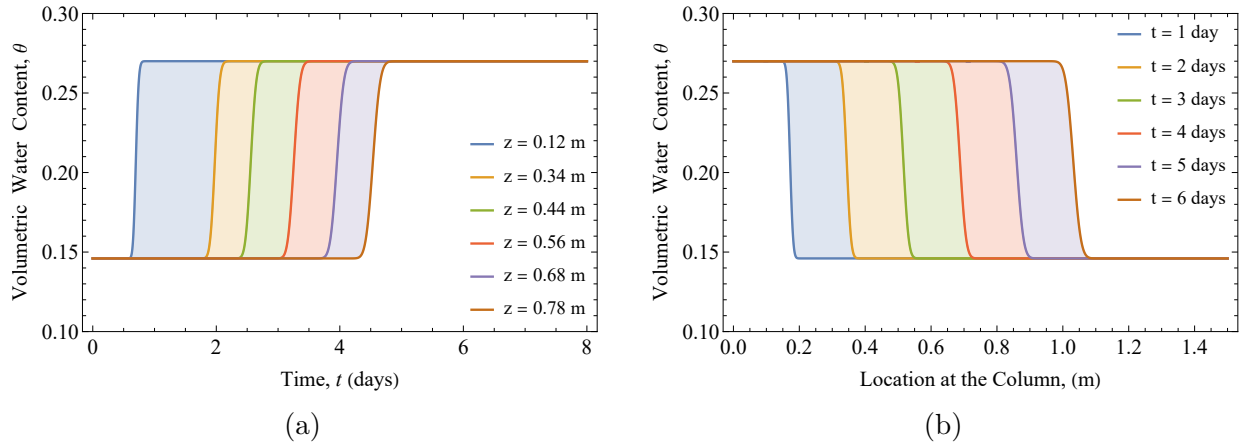


Figure 4.10: Predicted volumetric water content for Case 1 using $\delta=0.639 \text{ kPa}^{-1}$: (a) time history at different locations; (b) profiles at increasing times.

The experimental results obtained to analyze the moisture front in the soil column are presented in Fig. 4.11. The comparison of the data recorded by each tensiometer with the model estimation observed in Fig. 4.10a indicates that the model accuracy was approximate, reaching the maximum rate of moisture change $[(\partial\theta/\partial t)_{max}]$ at 0.27, compared to the experimental value of 0.30. Since Case 1 was used to evaluate these results, in all tensiometers $\theta_i = 0.15$, corresponding to the value estimated in the modelling. Both experimental results and model estimation indicate that θ propagates with increasing vertical distance in the column due to the \bar{a}_s component. This means that $(\partial\theta/\partial z)_{max}$ (Fig. 4.10b) decreases with increasing depth.

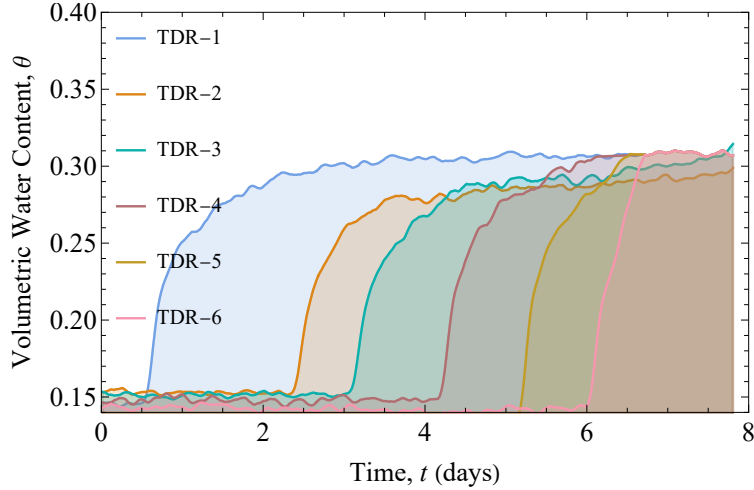


Figure 4.11: Experimental results for time history of volumetric water content.

In the case of the suction front estimation, the solution was implemented to determine the behaviour of ψ along the soil column with $L = 1.10$ m. Fig. 4.12 shows the ψ fronts estimated by the model for a time $t = 8$ days in the five depths of the MPS. Also, in Fig. 4.12a and 4.12b the time history of ψ at different locations, and the profiles of ψ at increasing times, respectively, are presented. The Fig. 4.12a shows that the maximum ψ value calculated in all the MPS is constant, corresponding to approximately 200 kPa. However, the time required for the suction to begin to decrease beyond the initial value increases with increasing z .

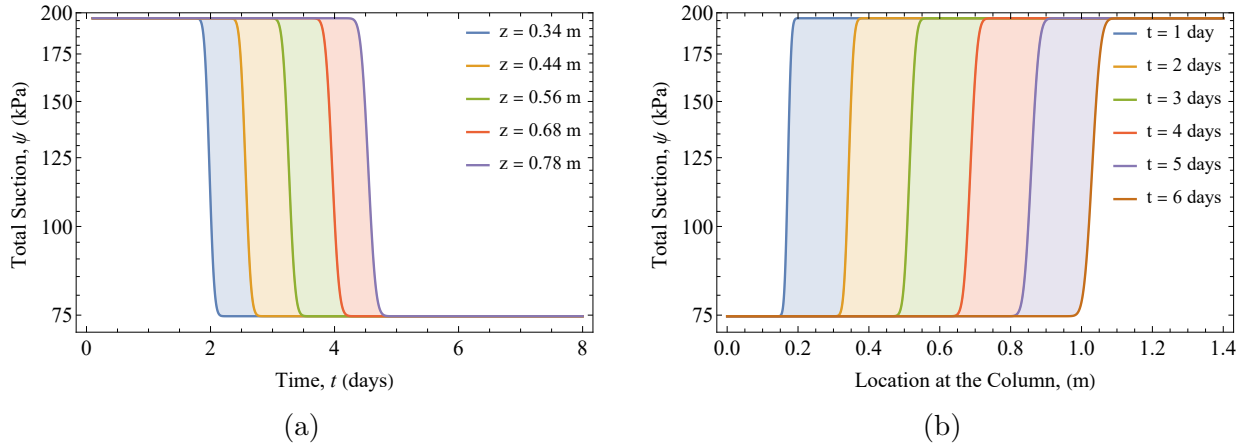


Figure 4.12: Predicted suction for Case 1 using $\delta=0.639$ kPa⁻¹: (a) time history at different locations; (b) profiles at increasing times.

Fig. 4.13 presents the experimental results to analyse the soil column's suction front. Comparison of the data recorded by each MPS with the model estimate observed in Fig. 4.12a indicates that the model accuracy was approximate, reaching a residual value of suction

equals to 0.075 MPa, compared to the experimental value of 0.0075 MPa. This difference, although significant in terms of tension between soil menisci, in numerical terms, represents a deviation of less than 15%. The experimental results and the model estimation indicate that ψ propagates decreasingly with increasing vertical distance in the column and with increasing time. The soil starts the test with a value of ψ corresponding to ψ_{max} due to at values of θ close to 0, ψ tends to ∞ . As θ gradually increases, ψ decreases, since according to the SWRC at $\theta = \theta_s$, $\psi = 0$, which explains the inversely proportional relationship between θ and ψ as z and t increase.

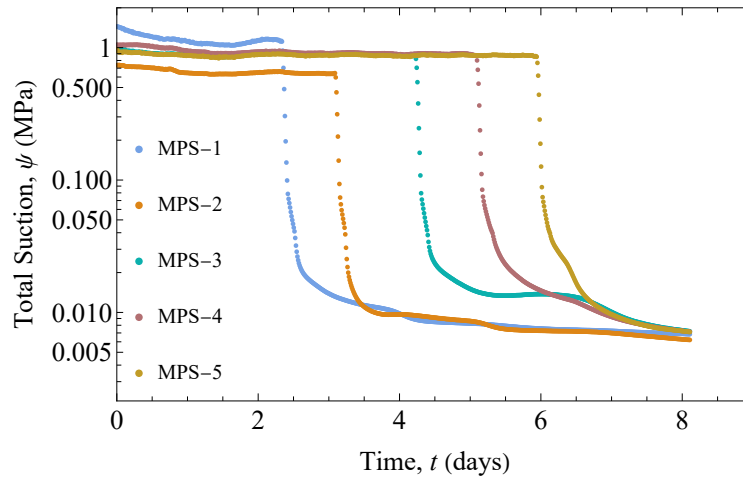


Figure 4.13: Experimental results for time history of total suction.

Fig. 4.14 presents the estimates of k_z recorded by the model, and Fig. 4.14a and 4.14b show the change in k_z concerning time and depth, respectively. In this case, although the tensiometers do not record the change in k_z , it was considered to use these same locations to evaluate the behaviour of the results in a homogeneous way. The point of comparison of the experimental results observed in Fig. 4.8 corresponds to the value of $k_s = 8.2 \text{ e-}5 \text{ m/s}$.

The estimate presented for the two cases in Fig. 4.14 fluctuates in velocities from $2.5\text{e}^{-7} \text{ m/s}$ to $5\text{e}^{-7} \text{ m/s}$. In this case, although the difference is in magnitudes of the order of $1\text{e}^{-2} \text{ m/s}$, which in theory is insubstantial, in the case of swelling soils, this difference is significant. In evaluating the graphical framework of Fig. 4.14a, k_z increases with increasing t , which is physically correct since as ψ decreases, the pore diameter expands. Due to the relationship between ψ and k_z is inversely proportional, in Fig. 4.14b, k_z decreases with increasing depth because, as θ does not propagate rapidly in the bottom of the column, theoretically ψ tends to ∞ , which reduces the pore spacing and k_z .

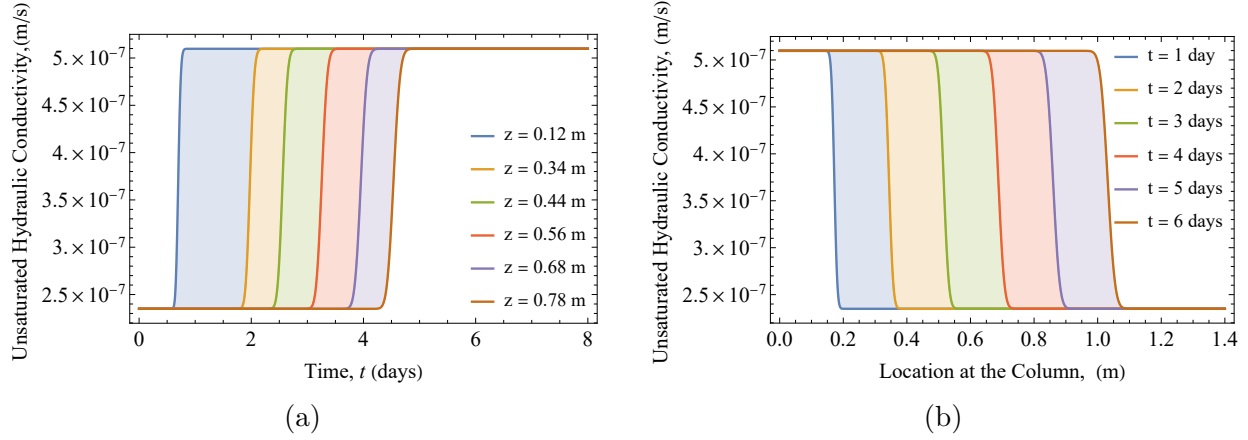


Figure 4.14: Predicted unsaturated hydraulic conductivity for Case 1 using $\delta=0.639 \text{ kPa}^{-1}$: (a) time history at different locations; (b) profiles at increasing times.

Fig. 4.15 presents the saturation fronts estimated by the model in the soil column. Also, in Fig. 4.15a and 4.15b the time history of S_r at different locations and the profiles of S_r at increasing times, respectively, are presented. Since the relationship between S_r and θ is directly proportional, as SWRC is often presented in terms of S_r , the relationship with ψ is inversely proportional. Inspection of Fig. 4.15a indicates that the model estimate for the saturation phase was 65%, which value represents the unsaturated state of the modelling. This value was achieved for all control points, and the range of S_r fluctuation was 30%.

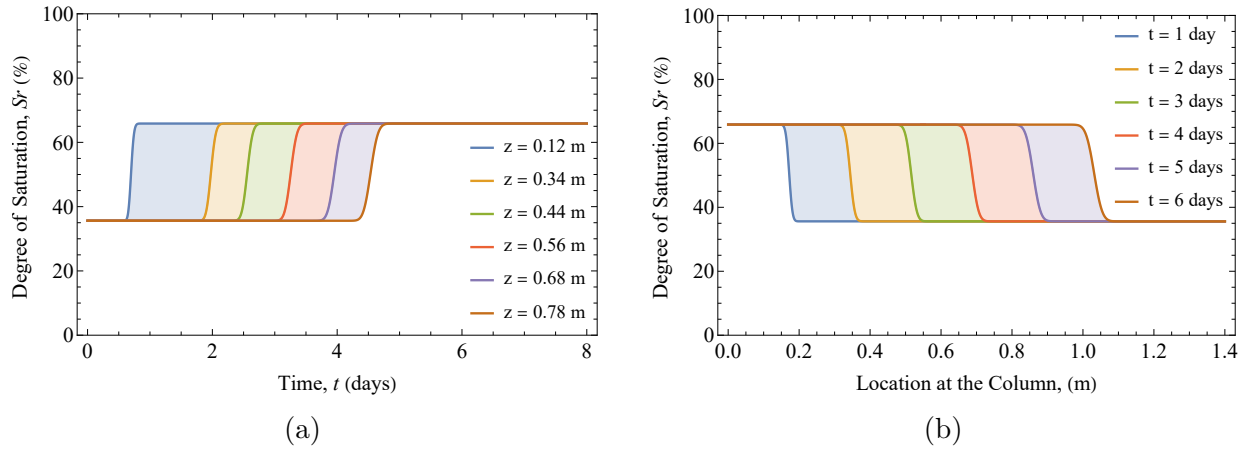


Figure 4.15: Predicted saturation degree for Case 1 using $\delta=0.639 \text{ kPa}^{-1}$: (a) time history at different locations; (b) profiles at increasing times.

Fig. 4.16 shows the void ratio profiles at different times for Case 1 (considering $\delta = 0.639 \text{ kPa}^{-1}$). Fig. 4.16a and 4.16 correspond to the case in which the swelling (\bar{R}), advective (\bar{a}_s) and diffusive (\bar{D}_z) components within Eq. 4.16 are relevant. Inspection in Fig. 4.16a reveals that $(\partial e / \partial t)_{max}$ decreases with increasing z values, indicating that e increases with time at

the first layers of the column due to the \bar{R} component of the non-saturated flow, i.e., when swelling occurs. The e_{max} value estimated by the model corresponds to 0.80. Although this value does not compare to the experimental e_{max} value of 0.87, it is worth noting that the model did not estimate the results up to the value of θ_s , which explains the variation. In contrast, Fig. 4.16b indicates that $(\partial e/\partial z)_{max}$ decreases with increasing t , i.e., e decreases with time because, in the lower layers at the initial stage of the test, ψ is high and θ is low.

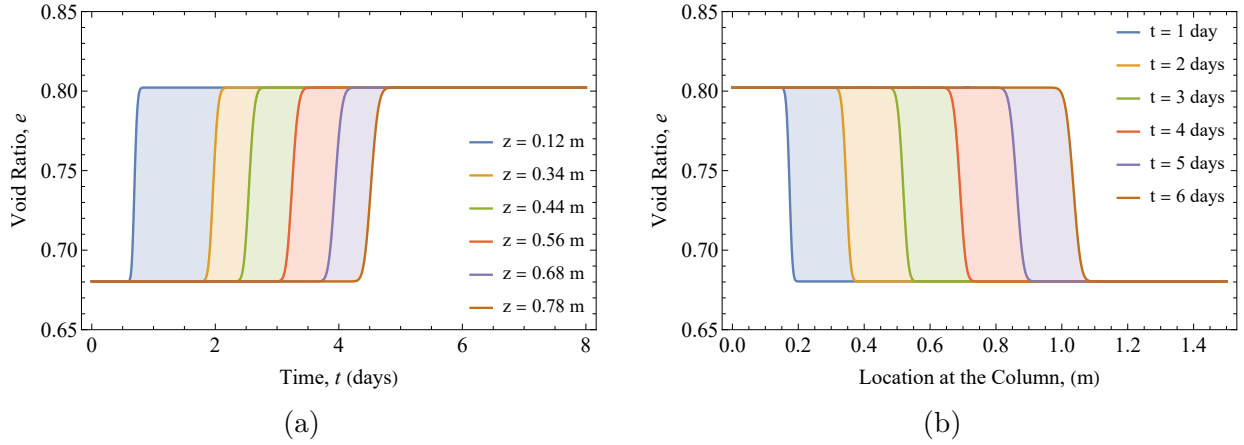


Figure 4.16: Predicted void ratio for Case 1 using $\delta=0.639 \text{ kPa}^{-1}$: (a) time history at different locations; (b) profiles at increasing times.

Fig. 4.17 shows the percent swelling estimated by the model for: i) time history at different locations (Fig. 4.17a), and ii) profiles at increasing times (Fig. 4.17b). The percentage swelling, in this case, is understood as a deformation expressed in millimeters over the initial height of the sample (i.e., the soil column). By comparing Fig. 4.17a with Fig. 4.16a, it is possible to establish that the order of magnitude of the estimated swelling is 15% for a change of $e = 0.125$. This indicates that the adsorption generated by the clay laminae accumulates water in the interlaminal spaces, producing a volumetric increase.

In contrast, Fig. 4.17b shows that with increasing ψ , the tension between the meniscus increases, which reduces the area in the microstructure and macrostructure, generating a process of shrinkage of the soil matrix. This indicates that both Fig. 4.16b and 4.17b estimate the volumetric reduction, which suggests that the model can also predict the shrinkage paths. The explanation for this estimate is due to the fact that the difference between e_{max} and e_{min} controls the swelling component (\bar{R}) in Eq. 4.16. Therefore, upon an increase in ψ , the model reproduces the inverse path to that observed in Fig. 4.16b and 4.17b, since in Case 1, the flow is dominated by the \bar{D}_z and \bar{a}_s components.

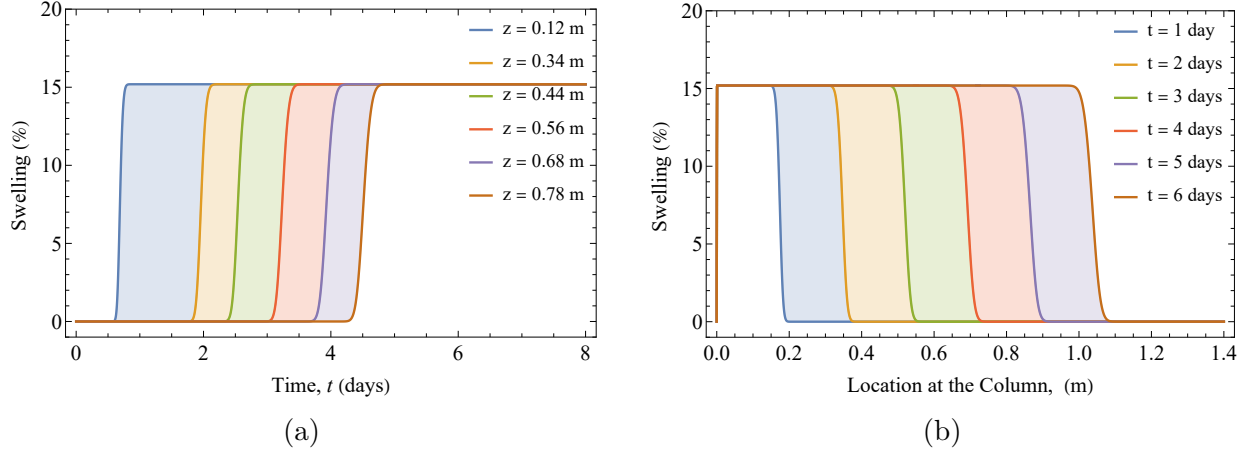


Figure 4.17: Predicted swelling for Case 1 using $\delta=0.639 \text{ kPa}^{-1}$: (a) time history at different locations; (b) profiles at increasing times.

The last scenario explored using Case 1 is presented in Fig. 4.18. The results in Fig. 4.18a illustrate the time history of void ratio ($\partial e/\partial t$) for Case 1 ($\delta = 0.639 \text{ kPa}^{-1}$) for a problem with \bar{R} , \bar{D}_z and \bar{a}_s components. For a given position z , the rate of void ratio change is zero for an initial period where $\theta = \theta_i$. The rate of void ratio change begins to increase until it reaches a peak value equal to $(\partial e/\partial t)_{max}$ at a specific time t . Beyond the time corresponding to the peak rate, the rate of void ratio change reaches the zero value. The results of Fig. 4.18a also indicate that the peak rate of void ratio change decreases with increasing t .

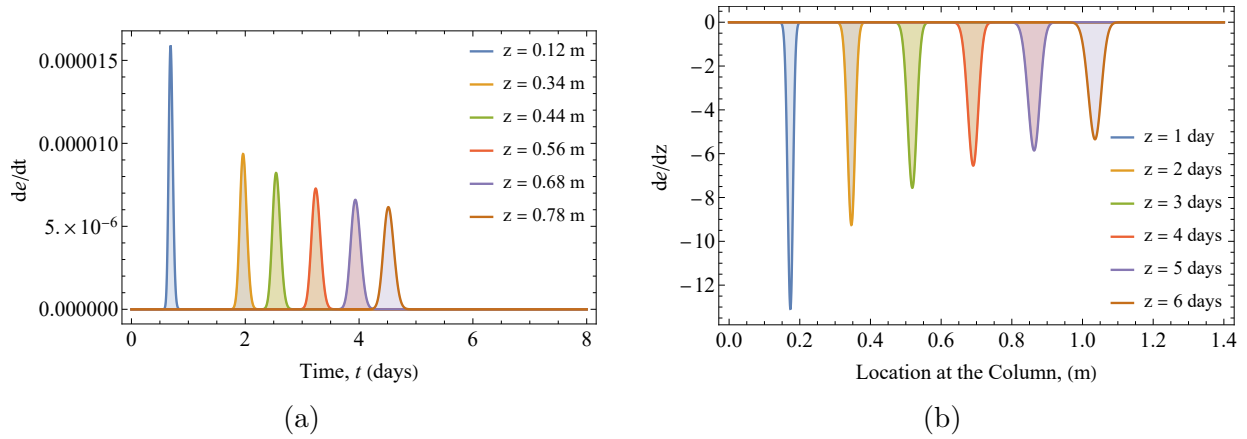


Figure 4.18: Predicted results for Case 1 using $\delta=0.639 \text{ kPa}^{-1}$: (a) time history of void ratio rates (b) void ratio gradient profiles.

From the visual and numerical exploration of Fig. 4.18a, it was possible to observe two important pieces of evidence: i) that the distance between tails for each curve increases with increasing z , and ii) the area under the curves is the same for each z value. In addition, the

\bar{a}_s component controls both the increase in the distance between tails and the decrease in the peak value $(\partial e/\partial t)_{max}$. In contrast, Fig. 4.18b presents the void ratio gradient profiles for the case where \bar{R} , \bar{D}_z and \bar{a}_s components are relevant. In Fig. 4.18b, upon reaching a specific time t , the void ratio gradients are equal to 0. Subsequently, they increase (in absolute value), getting a peak value $(\partial e/\partial z)_{max}$ at a particular time t . The observation of this graph is similar to that observed in Fig. 4.18a. However, the analysis must be performed under absolute value.

Fig. 4.19, 4.20 and 4.21 present the results obtained when the boundary condition corresponding to Case 3 was used. Specifically, a constant discharge velocity value corresponding to $v_0 = 2.8 \text{ e}^{-7} \text{ m/s}$ to the upper boundary of a semi-infinite column was imposed. In this case, because the relationship between v_0 and k_z is appreciable considerably in the first 40 cm of depth, given that the soil behaves like a sponge, the estimates were restricted to this range to assess the behaviour of the results.

In the case of Fig. 4.19 and 4.20, the void ratio and percent swelling were evaluated for different t and z settings. As shown in Case 3, Fig. 4.19a presents that $(\partial e/\partial t)_{max}$ decreases with increasing z , and Fig. 4.19b shows that $(\partial e/\partial z)_{max}$ decreases with increasing t . Indeed, the value of $v_0 = 2.82 \text{ e}^{-7} \text{ m/s}$ adopted in the analysis presented in Fig 4.19a corresponds to an imposed swelling that could generate $e_\infty = 0.79$, i.e., a value close to the e adopted in Case 1. A similar behaviour is observable in Fig. 4.20a and 4.20b, delivering consistent and comparable results with those obtained in Fig. 4.17a and 4.17b. Case 3 was considered within the analytical solutions since, during the soil-column test, a constant discharge velocity of 0.40 mL/min was imposed. The two estimated responses can be attributed to the \bar{R} , \bar{D}_z and \bar{a}_s components within Eq. 4.43.

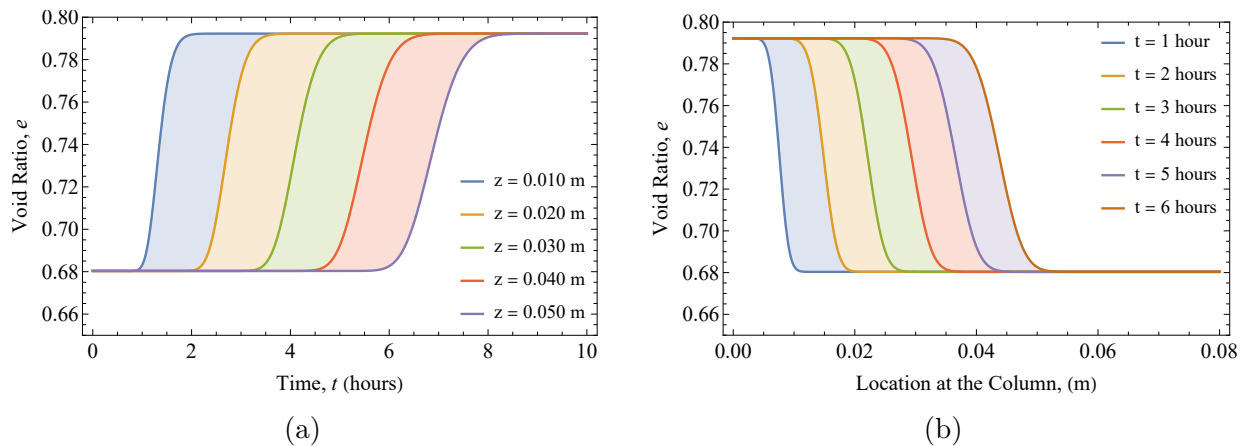


Figure 4.19: Predicted void ratio for Case 3 using $\delta=0.639 \text{ kPa}^{-1}$: (a) time history at different locations; (b) profiles at increasing times.

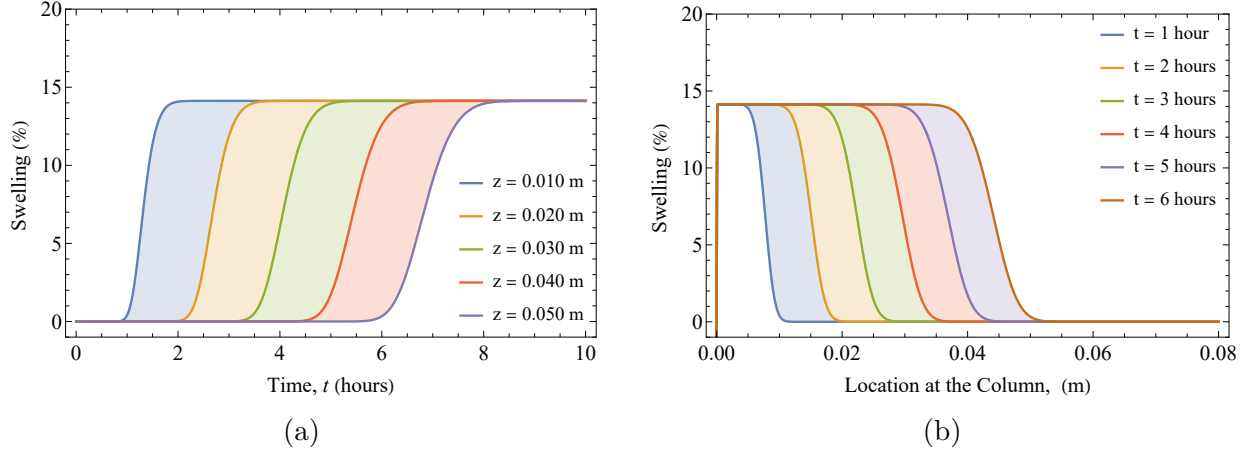


Figure 4.20: Predicted swelling for Case 3 using $\delta=0.639 \text{ kPa}^{-1}$: (a) time history at different locations; (b) profiles at increasing times.

The estimated results in Fig. 4.21 correspond to the time history of void ratio rates (Fig. 4.21a) and void ratio gradient profiles (Fig. 4.21b) for Case 3 considering $\delta = 0.639 \text{ kPa}^{-1}$. However, three relevant things can be evaluated when implementing Case 3: i) when decreasing the evaluation depth, the peak $(\partial e/\partial t)_{max}$ and $(\partial e/\partial z)_{max}$ values reached in Fig. 4.21a and 4.21b, respectively, are more significant than those obtained in Fig. 4.18a and 4.18b, ii) the width between the initial and final tails of all curves increases with increasing t , and iii) the total area under all curves is greater than the one observed applying Case 1. These differences may be mainly due to two reasons: i) the fluctuation of θ depends on the value of v_0 , or ii) as $L < L_{exp}$, both the flow and the swelling process occur faster, which increases the numerical value of $(\partial e/\partial t)_{max}$ and $(\partial e/\partial z)_{max}$.

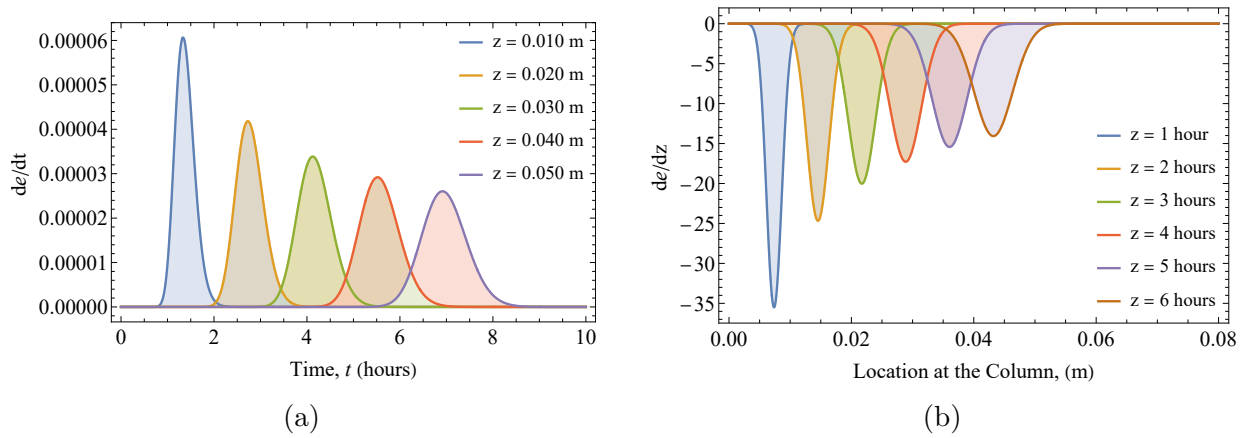


Figure 4.21: Predicted results for Case 3 using $\delta=0.639 \text{ kPa}^{-1}$: (a) time history of void ratio rates (b) void ratio gradient profiles.

4.5 PARAMETRIC CALIBRATION

4.5.1 Wetting path

Parametric calibration of the model is performed using the experimental results obtained by [Nowamooz & Masrouri \(2010\)](#). The model is calibrated using the initial parameters (θ_s , θ_r , e_{max} , e_{min} , δ) to get the value of δ that generates the best fit to the curve $e - \log \psi$. In this case, the ability of the model to reproduce the results during the wetting phase, i.e., when the soil increases its void ratio and enters the swelling process, will be evaluated. Table 4.5 presents the initial values used to compare the model and the literature results. Also, Table 4.5 shows the adjustment obtained considering $\delta = 0.6937 \text{ kPa}^{-1}$.

Table 4.5: Calibration parameters for the wetting path.

Model	θ_s	θ_r	e_{max}	e_{min}	$\delta \text{ (kPa}^{-1}\text{)}$
Nowamooz & Masrouri (2010)	0.43	0.08	1.16	0.44	0.6937

The study performed by [Nowamooz & Masrouri \(2010\)](#) focuses on the swelling activity of two expansive clays obtained from the Mignaloux-Beauvoir region near Le Deffend in France. The $e - \log \psi$ curves were obtained from laboratory tests with wetting and drying paths varying the suction from 1000 to 0 MPa. The soil shows significant swelling since the difference between e_{max} and e_{min} is 0.72. Fig. 4.22 presents the model fit for the swelling curve considering the value of $\delta = 0.6937 \text{ kPa}^{-1}$, i.e., the value estimated by the proposed model.

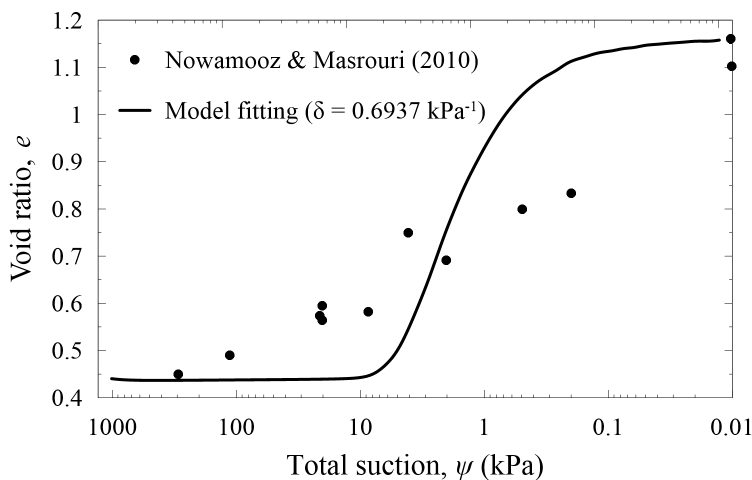


Figure 4.22: $e - \log \psi$ curve (wetting path) comparison between model simulation and experiment data ([Nowamooz & Masrouri, 2010](#)).

In this case, the fit was performed by applying a nonlinear regression analysis to the evaluated data set, which allowed for recreating the swelling path. However, the estimated results were defined in the framework of an idealized curve, which explains that, although the wetting path is recreated, the regression fit does not pass through all the experimental points. In this case, the difference between the fit and the experimental data is because the authors used wetting and drying paths for the same soil sample. Therefore, it is not possible to reproduce the hysteresis phenomenon between experimental curves, which explains the fit obtained.

The comparative process was performed using a simple regression analysis between the estimated and experimental data. To understand the behaviour of the results, the coefficient of determination (R^2) was calculated, which is interpreted on a scale from 0 to 1, where values close to 1 indicate an excellent numerical fit. Table 4.6 presents the R^2 values obtained for the case studied by Nowamooz & Masrouri (2010) in the parametric calibration. Likewise, Table 4.6 also shows the values of the \bar{R} component obtained for the wetting path. In the scenario explored, the value of R^2 was higher than 0.95, indicating that the model correctly reproduces the swelling process for any configuration of e_{max} and e_{min} . Also, from the values of \bar{R} , it is possible to interpret that the numerical fluctuation of this parameter depends significantly on the difference between e_{max} and e_{min} , so it increases when the difference is more significant. By comparing the values of Table 4.6 with the value of \bar{R} obtained from the fit with the data of RMA soil (Table 4.3), it is possible to conclude that the RMA soil correspond to a material of expansivity similar to that observed by Nowamooz & Masrouri (2010).

Table 4.6: Statistical fit and estimated \bar{R} component for the wetting path.

Model	\bar{R}	R^2
Nowamooz & Masrouri (2010)	1.27	0.96

4.5.2 Drying path

The parametric calibration of the model is performed using the experimental results obtained by Al-Dakheeli & Bulut (2019), Zhao et al. (2021) and Sarker & Wang (2022). From the initial model parameters ($\theta_s, \theta_r, e_{max}, e_{min}, \delta$), the model is calibrated to obtain the value of δ that generates the best fit to the $e - \log \psi$ curve. On the other hand, δ belongs to the value obtained using the proposed model. The selection of the results to construct the comparative analysis was based on the difference between e_{min} and e_{max} to determine the capacity of the model to estimate the results when the difference is very high or not very significant. Table 4.7 presents the initial values used to compare the model and the literature results. Also, Table 4.7 presents the fit recorded for δ for each set analyzed.

Table 4.7: Calibration parameters for the drying path.

Model	θ_s	θ_r	e_{max}	e_{min}	δ (kPa $^{-1}$)
Al-Dakheeli & Bulut (2019)	0.19	0.06	1.80	0.05	0.0889
Zhao et al. (2021)	0.28	0.03	0.74	0.32	0.0005
Sarker & Wang (2022)	0.34	0.10	0.94	0.77	0.0480

The study by Al-Dakheeli & Bulut (2019) focuses on the swelling activity of expansive soils obtained from the Lake Hefner and Ardmore sites in Oklahoma. The e - $\log \psi$ curves were obtained from laboratory tests of MP_4 and $UMS-T5$ for the SWRC, and the volume change and the basic volume-mass relationships were used to determine the void ratio. The soil exhibits a drying path since the difference between e_{max} and e_{min} is 1.30. Fig. 4.23 presents the model fit for the e - $\log \psi$ curve considering the value of $\delta = 0.0889$ kPa $^{-1}$. In this case, the fit was performed by applying a nonlinear regression analysis to the evaluated data set, which allowed recreating of the drying path.

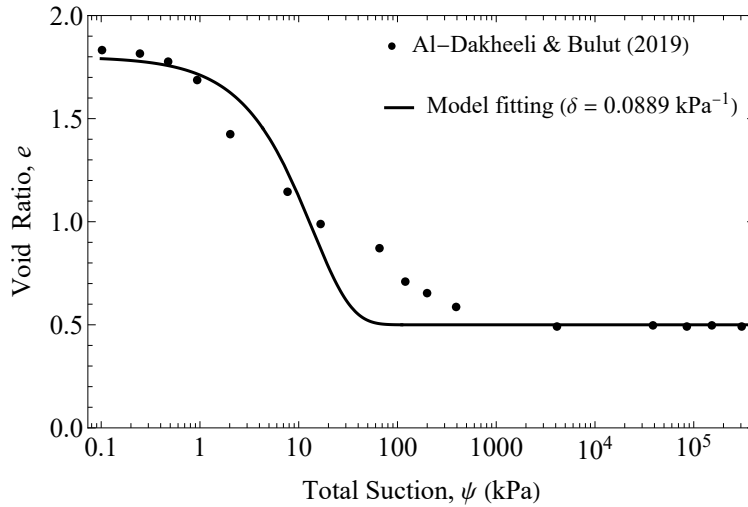


Figure 4.23: e - $\log \psi$ curve (drying path) comparison between model simulation and experiment data (Al-Dakheeli & Bulut, 2019).

Fig. 4.24 presents the fit between the model and the experimental results obtained by Zhao et al. (2021). In this study, the hydromechanical behaviour of compacted clays that were subjected to wetting and drying cycles was explored. Thus, the experimental e - $\log \psi$ curve was structured from a value $e_{max} = 0.74$ to $e_{min} = 0.32$.

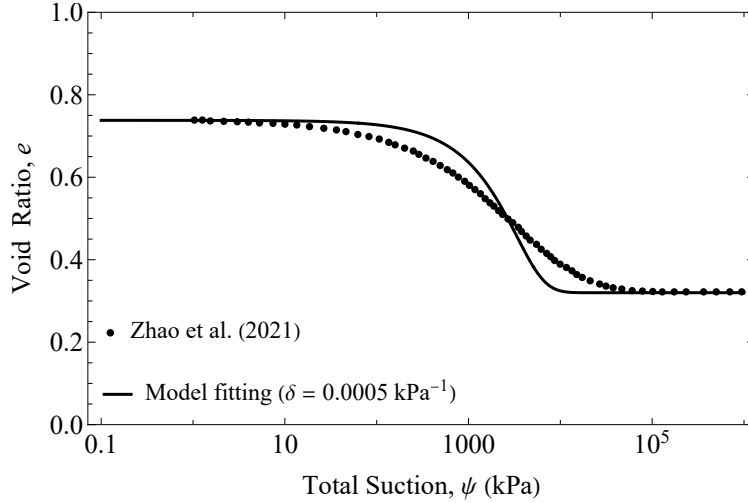


Figure 4.24: $e - \log \psi$ curve (drying path) comparison between model simulation and experiment data (Zhao et al., 2021).

The use of the results shown by Zhao et al. (2021) allows for exploring whether the model can reproduce data from soils in which the difference between e_{max} and e_{min} could be more representative. This means that if the difference between e_{max} and e_{min} is not significant, the parameter $\bar{R} = 1$, which would return Eq. 4.16 to its original form, i.e. the Cavalcante & Zornberg (2017) equation. The parametric estimation executed in this case considered $\delta = 0.0005 \text{ kPa}^{-1}$, so the obtained fit recreates the drying path and accurately estimates the experimental e_{max} and e_{min} values.

The last study used to determine the sensitivity of the model corresponds to that carried out by Sarker & Wang (2022). The material used corresponds to compacted Moreland clay, a highly expansive soil which can reach LL values higher than 80%. The $e - \log \psi$ curve for the drying path was determined to interrelate the elastic deformation and the SWRC of Moreland clay. Although this fit presents the same argument as the previous case, i.e., the difference between e_{max} and e_{min} is not significant, it was considered since the soil is highly expansive. Fig. 4.25 shows the fit between the estimated and experimentally obtained data. The parametric estimation, in this case, considered $\delta = 0.0480 \text{ kPa}^{-1}$, the mean value of δ in all the analyses performed.

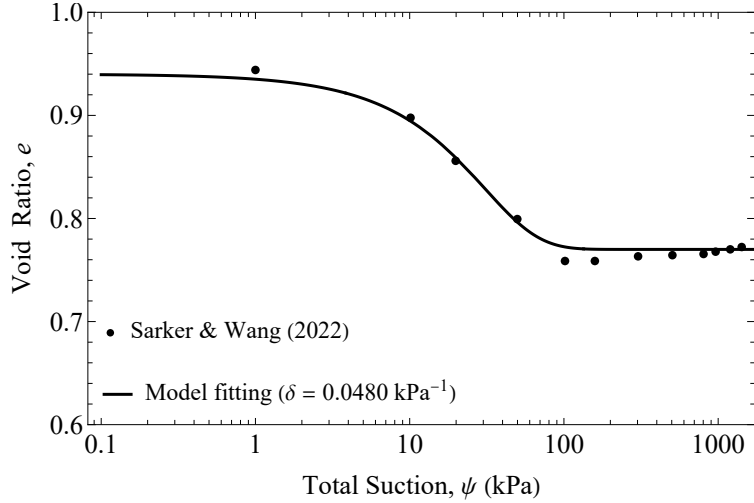


Figure 4.25: $e - \log \psi$ curve (drying path) comparison between model simulation and experiment data (Sarker & Wang, 2022).

Table 4.8 presents the R^2 values for each case evaluated in the parametric calibration. Likewise, Table 4.8 also shows the \bar{R} component values obtained for each data set. In each of the scenarios explored, the value of R^2 was more significant than 0.97, indicating that the model correctly reproduces the drying path for any configuration of e_{max} and e_{min} , i.e., compacted soils, with low or high expansivity, among others. Also, from the values of \bar{R} , it is possible to interpret that the numerical fluctuation of this parameter depends significantly on the difference between e_{max} and e_{min} , so it increases when the difference is significant. By comparing the values of Table 4.8 with the value of \bar{R} obtained from the fit with the experimental data (Table 4.3), it is possible to conclude that the RMA soil corresponds to a material of medium-low expansivity.

Table 4.8: Statistical fit and estimated \bar{R} component for the drying path.

Model	\bar{R}	R^2
Al-Dakheeli & Bulut (2019)	1.59	0.98
Zhao et al. (2021)	1.14	0.99
Sarker & Wang (2022)	1.32	0.99

Chapter 5

CONCLUDING REMARKS

5.1 CONCLUSIONS

Numerically simulating the behaviour of expansive soils is still a challenge for geotechnical researchers due to the high complexity of the mechanical-hydraulic phenomena involved. Nevertheless, this work generates new knowledge by trying to reproduce the response of these soils in terms of suction potential when different variables are modified. A numerical-mathematical approach that solves and extends the application of the Richards equation for soils with expansive potential is presented. Analytical solutions were constructed to determine the parametric sensitivity and the behaviour of the variables involved for different positions and times. On the other hand, experimental results were used to assess the ability of the model to reproduce the swell-shrink paths. During the parametric calibration, it was explored whether the model could estimate the wetting and drying paths of soils with different e_{min} and e_{max} settings.

The evaluation of the model in unimodal SWRC was performed using theoretical results in bimodal SWRC employing experimental data from soil-column tests. Using the graphical fit given by θ_0 and θ_i , it was possible to corroborate that the dynamics of the results fluctuate according to the range offered by these two parameters in the SWRC. This intrinsic behaviour of the model responds mainly to the fact that in bimodal SWRC, the model is limited in determining the AEV of the micropores. For this reason, it is necessary to include at least two different δ values that respond to these suction peaks, macroporous and microporous.

When comparing the values of δ in the drying path with those obtained for the wetting path, it is possible to infer that: i) δ depends on the difference between e_{max} and e_{min} , and ii) in the wetting path, the estimated value of δ is significantly higher, i.e. δ depends on the type of process to be evaluated. Although it could have been expected that the model would present some difficulty in compacted soils because the difference between e_{max} and e_{min} is

not significant, it was possible to evaluate that the model managed to reproduce the data with a correlation factor higher than 0.96.

The parametric calibration allowed to determine the sensitivity of the variables involved and the conditions under which the model can be applied. By recovering high correlation values from the statistical analysis, it is possible to conclude that the model can satisfactorily reproduce the hydromechanical behaviour of expansive soils with different suction potentials. However, it is necessary to explore the cases in which the expansivity is null and in the circumstances in which it is extreme.

5.2 LIMITATIONS OF THE MODEL

- The main limitation of the model centres on the fact that the mechanical part addressed in the mathematical formulation comprises exclusively the change in the void ratio, which in theory, relates the volumetric variation directly to the shear strength. However, although it was possible to estimate the wetting and drying paths on the $e - \log \psi$ curve with high statistical closeness, it is necessary to clarify that this model is based on a simplified procedure, which considers a limited number of parameters.
- Regarding the parametric definition, the limitation is that estimating the value of δ is necessary using the model of [Cavalcante & Zornberg \(2017\)](#). Although it facilitates the numerical calculation, this process implies that before using the model proposed here, it is required to adjust the unimodal SWRC with the equation of [Cavalcante & Zornberg \(2017\)](#) and determine the best value of δ .
- As a last limitation, it is presented that, as in this case, when having bimodal SWRC, the suction range estimated by the model using the analytical solutions is restricted to a spectrum of values delimited by θ_i and θ_0 . This restriction of the model is due to the use of the [Cavalcante & Zornberg \(2017\)](#) model, which is formulated for unimodal SWRCs.

5.3 RECOMMENDATIONS

Based on the results and discussions generated from this work, it is possible to develop the following recommendations for improving the approach and continue studying expansive soils from a hydromechanical perspective.

- Optimize the model in the field of soils with bimodal SWRC by proposing a new solution that includes the [Costa & Cavalcante \(2021\)](#) model in the mathematical formulation or adapting the existing one for soils with this behaviour.

- Extend the methodology developed here by including the change in volumetric deformation and strength properties generated by moisture variation.
- Extend the mathematical formulation of the analytical solutions to include cases controlled exclusively by the initial conditions of the void ratio.
- Evaluate the model with experimental results of soils with extreme expansivity, e.g., clays with high montmorillonite and illite content.

References

- Aitchison, G., & Holmes, J. (1953). Aspects of swelling in the soil profile.
- Al-Dakheeli, H., & Bulut, R. (2019). Interrelationship between elastic deformation and soil-water characteristic curve of expansive soils. *Journal of Geotechnical and Geoenvironmental Engineering*, 145(4), 04019005. doi: [https://doi.org/10.1061/\(ASCE\)GT.1943-5606.0002020](https://doi.org/10.1061/(ASCE)GT.1943-5606.0002020)
- Alonso, E., Vaunat, J., & Gens, A. (1999). Modelling the mechanical behaviour of expansive clays. *Engineering geology*, 54(1-2), 173–183. doi: [https://doi.org/10.1016/S0013-7952\(99\)00079-4](https://doi.org/10.1016/S0013-7952(99)00079-4)
- Alonso, E. E., Gens, A., & Josa, A. (1990). A constitutive model for partially saturated soils. *Géotechnique*, 40(3), 405–430. doi: <https://doi.org/10.1680/geot.1990.40.3.405>
- Al-Rawas, A. A., & Goosen, M. F. (2006). Expansive soils: recent advances in characterization and treatment.
- Al-Yaqoub, T. H., Parol, J., & Znidarcic, D. (2017). Experimental investigation of volume change behavior of swelling soil. *Applied Clay Science*, 137, 22–29. doi: <https://doi.org/10.1016/j.clay.2016.11.018>
- Ameta, N., Purohit, D., & Wayal, A. S. (2007). Characteristics, problems and remedies of expansive soils of rajasthan, india. *EJGE*, 13, 1–7.
- Anastasopoulos, I. (2013). Structural damage of a 5-storey building: differential settlement due to construction of an adjacent building or because of construction defects. In *International conference on case histories in geotechnical engineering, chicago*.
- Askar, A., & Jin, Y.-C. (2000). Macroporous drainage of unsaturated swelling soil. *Water Resources Research*, 36(5), 1189–1197. doi: <https://doi.org/10.1029/2000WR900023>
- Assouline, S. (2013). Infiltration into soils: Conceptual approaches and solutions. *Water Resources Research*, 49(4), 1755–1772. doi: <https://doi.org/10.1002/wrcr.20155>
- ASTM. (2007). Standard test method for particle-size analysis of soils.
- Asuri, S., & Keshavamurthy, P. (2016). Expansive soil characterisation: an appraisal. *INAE Letters*, 1(1), 29–33. doi: <https://doi.org/10.1007/s41403-016-0001-9>
- Azevedo, M. M. d. (2012). *Anti-capillary barrier performance of wicking geotextiles* (Unpublished doctoral dissertation).
- Azevedo, M. M. d., et al. (2016). *Performance of geotextiles with enhanced drainage* (Unpublished doctoral dissertation).
- Bachmat, Y. (1965). Basic transport coefficients as aquifer characteristics. In *Iash symposium hydrology of fractured rocks* (Vol. 1, p. 63).

- Bear, J. (1972). Dynamics of fluid in porous media dover, new york. *ISBN*, 10(0486656756), C50.
- Bendahgane, M., Nechnech, A., Taibi, S., & Abou-Bekr, N. (2017). Hydromechanical behaviour of an unsaturated algiers clay. *European Journal of Environmental and Civil Engineering*, 21(9), 1093–1113. doi: <https://doi.org/10.1080/19648189.2016.1150897>
- Biot, M. A. (1941). General theory of three-dimensional consolidation. *Journal of applied physics*, 12(2), 155–164. doi: <https://doi.org/10.1063/1.1712886>
- Bishop, A. W., Alpan, I., Blight, G., & Donald, I. (1960). Factors controlling the strength of partly saturated cohesive soils.
- Bronswijk, J. (1990). Shrinkage geometry of a heavy clay soil at various stresses. *Soil Science Society of America Journal*, 54(5), 1500–1502. doi: <https://doi.org/10.2136/sssaj1990.03615995005400050048x>
- Brooks, R., & Corey, A. (1964). Hydraulic properties of porous media. hydrology paper no. 3. *Civil Engineering Department, Colorado State University, Fort Collins, CO*.
- Buckingham, E. (1907). Studies on the movement of soil moisture.
- Buzzi, O. (2010). On the use of dimensional analysis to predict swelling strain. *Engineering Geology*, 116(1-2), 149–156. doi: <https://doi.org/10.1016/j.enggeo.2010.08.005>
- Buzzi, O., Fityus, S., & Sloan, S. (2007). A proposition for a simple volume change model for saturated expansive soils. *Numerical Models in Geomechanics—NUMOG X, Rhodos*, 99–104.
- Buzzi, O., Giacomini, A., & Fityus, S. (2011). Towards a dimensionless description of soil swelling behaviour. *Géotechnique*, 61(3), 271–277. doi: <https://doi.org/10.1680/geot.7.00194>
- Castro Cuba Valencia, M. E. (1992). Suelos expansivos en talara.
- Cavalcante, A., Ozelim, L., Swamee, P., & Rathie, P. (2013). Explicit numerical iterative methods applied to the three-parameter infiltration equation. *a a*, 2(2), 2.
- Cavalcante, A. L. B., & Zornberg, J. G. (2017). Efficient approach to solving transient unsaturated flow problems. i: Analytical solutions. *International Journal of Geomechanics*, 17(7), 04017013. doi: [https://doi.org/10.1061/\(ASCE\)GM.1943-5622.0000875](https://doi.org/10.1061/(ASCE)GM.1943-5622.0000875)
- Chapman, D. L. (1913). Li. a contribution to the theory of electrocapillarity. *The London, Edinburgh, and Dublin philosophical magazine and journal of science*, 25(148), 475–481. doi: <https://doi.org/10.1080/14786440408634187>
- Chen, J.-M., Tan, Y.-C., & Chen, C.-H. (2003). Analytical solutions of one-dimensional infiltration before and after ponding. *Hydrological Processes*, 17(4), 815–822. doi: <https://doi.org/10.1002/hyp.1202>
- Chen, J.-M., Tan, Y.-C., Chen, C.-H., & Parlange, J.-Y. (2001). Analytical solutions for linearized richards equation with arbitrary time-dependent surface fluxes. *Water Resources Research*, 37(4), 1091–1093. doi: <https://doi.org/10.1029/2000WR900406>
- Childs, E. C., & Collis-George, N. (1950). The permeability of porous materials. *Proceedings of the Royal Society of London. Series A. Mathematical and Physical Sciences*, 201(1066), 392–405. doi: <https://doi.org/10.1098/rspa.1950.0068>

- Considine, M. (1984). Soils shrink, trees drink, and houses crack. *ECOS Magazine*, 41, 13–15.
- Cornelis, W. M., Khlosi, M., Hartmann, R., Van Meirvenne, M., & De Vos, B. (2005). Comparison of unimodal analytical expressions for the soil-water retention curve. *Soil Science Society of America Journal*, 69(6), 1902–1911. doi: <https://doi.org/10.2136/sssaj2004.0238>
- Costa, M. B. A. d., & Cavalcante, A. L. B. (2021). Bimodal soil–water retention curve and k-function model using linear superposition. *International Journal of Geomechanics*, 21(7), 04021116. doi: [https://doi.org/10.1061/\(ASCE\)GM.1943-5622.0002083](https://doi.org/10.1061/(ASCE)GM.1943-5622.0002083)
- Darcy, H. (1856). *Les fontaines publiques de la ville de dijon: Exposition et application des principes à suivre et des formules à employer dans les questions de distribution d'eau: Ouvrage terminé par un appendice relatif aux fournitures d'eau de plusieurs villes, au filtrage des eaux et à la fabrication des tuyaux de fonte, de plomb, de tôle et de bitume* (Vol. 2). V. Dalmont.
- Day, R. W. (1992). Damage to two apartment buildings due to moisture variation of expansive soil. *Journal of performance of constructed facilities*, 6(3), 169–176. doi: [https://doi.org/10.1061/\(ASCE\)0887-3828\(1992\)6:3\(169\)](https://doi.org/10.1061/(ASCE)0887-3828(1992)6:3(169))
- Dormieux, L., Barboux, P., Coussy, O., & Dangla, P. (1995). A macroscopic model of the swelling phenomenon of a saturated clay. *European journal of mechanics. A. Solids*, 14(6), 981–1004.
- Dueck, A., & Börgesson, L. (2007). Model suggested for an important part of the hydro-mechanical behaviour of a water unsaturated bentonite. *Engineering geology*, 92(3-4), 160–169. doi: <https://doi.org/10.1016/j.enggeo.2007.04.004>
- Erguler, Z. A., & Ulusay, R. (2003). A simple test and predictive models for assessing swell potential of ankara (turkey) clay. *Engineering Geology*, 67(3-4), 331–352. doi: [https://doi.org/10.1016/S0013-7952\(02\)00205-3](https://doi.org/10.1016/S0013-7952(02)00205-3)
- Ewing, R. C. (2011). Foundation repairs due to expansive soils: Eudora welty house, jackson, mississippi. *Journal of performance of constructed facilities*, 25(1), 50–55. doi: [https://doi.org/10.1061/\(ASCE\)CF.1943-5509.0000159](https://doi.org/10.1061/(ASCE)CF.1943-5509.0000159)
- Eyo, E. U., Ngambi, S., & Abbey, S. J. (2017). Investigative modelling of behaviour of expansive soils improved using soil mixing technique. *International Journal of Applied Engineering Research*, 12(13), 3828–3836.
- Farthing, M. W., & Ogden, F. L. (2017). Numerical solution of richards' equation: A review of advances and challenges. *Soil Science Society of America Journal*, 81(6), 1257–1269. doi: <https://doi.org/10.2136/sssaj2017.02.0058>
- Fityus, S., & Buzzi, O. (2009). The place of expansive clays in the framework of unsaturated soil mechanics. *Applied Clay Science*, 43(2), 150–155. doi: <https://doi.org/10.1016/j.clay.2008.08.005>
- Fredlund, D. G., & Rahardjo, H. (1993). *Soil mechanics for unsaturated soils*. John Wiley & Sons.
- Fredlund, D. G., & Xing, A. (1994). Equations for the soil-water characteristic curve. *Canadian geotechnical journal*, 31(4), 521–532. doi: <https://doi.org/10.1139/t94-061>

- Fukue, M., Minato, T., Taya, N., & Chida, T. (2001). Thickness of adsorbed water layer for clay particles. In *Clay science for engineering. proceeding of the international symposium on suction, swelling, permeability and structure of clays* (pp. 423–427).
- Gallipoli, D. (2012). A hysteretic soil-water retention model accounting for cyclic variations of suction and void ratio. *Geotechnique*, *62*(7), 605–616. doi: <https://doi.org/10.1680/geot.11.P.007>
- Gardner, W. (1936). *The role of the capillary potential in the dynamics of soil moisture...* US Department of agriculture.
- Gardner, W. (1958). Some steady-state solutions of the unsaturated moisture flow equation with application to evaporation from a water table. *Soil science*, *85*(4), 228–232.
- Gens, A., & Alonso, E. (1992). A framework for the behaviour of unsaturated expansive clays. *Canadian Geotechnical Journal*, *29*(6), 1013–1032. doi: <https://doi.org/10.1139/t92-120>
- Gershon, N., & Nir, A. (1969). Effects of boundary conditions of models on tracer distribution in flow through porous mediums. *Water Resources Research*, *5*(4), 830–839. doi: <https://doi.org/10.1029/WR005i004p00830>
- Gongora, C. H. F., Osorio, Z. K. C., Caballero, R. Z., & Ortíz, B. A. C. (2008). Estabilización química de suelos expansivos de san José de Cúcuta (colombia) usando cenizas volantes. *Respuestas*, *13*(2), 19–31.
- Gouy, M. (1910). Sur la constitution de la charge électrique à la surface d'un électrolyte. *J. Phys. Theor. Appl.*, *9*(1), 457–468.
- Grant, R., Christian, J. T., & Vanmarcke, E. H. (1974). Differential settlement of buildings. *Journal of the Geotechnical Engineering Division*, *100*(9), 973–991. doi: <https://doi.org/10.1061/AJGEB6.0000101>
- Hall, W. A. (1956). An analytical derivation of the darcy equation. *Eos, Transactions American Geophysical Union*, *37*(2), 185–188. doi: <https://doi.org/10.1029/TR037i002p00185>
- Hernández, V., Olarte, M. C., Ruge, J. C., Gabriel Bastidas, J., Herrera, C. E., & Fernando Otálvaro, I. (2022). Evaluation of water retention curves in soils with different fines content. *Arabian Journal of Geosciences*, *15*(9), 1–8. doi: <https://doi.org/10.1007/s12517-022-10189-0>
- Hogarth, W., & Parlange, J. (2000). Application and improvement of a recent approximate analytical solution of richards' equation. *Water Resources Research*, *36*(7), 1965–1968. doi: <https://doi.org/10.1029/2000WR900042>
- Holtz, R., & Kovacs, W. (1981). An introduction to geotechnical engineering prentice-hall, inc. *New Jersey, NY, USA*, 733.
- Holtz, W. G., & Gibbs, H. J. (1956). Engineering properties of expansive clays. *Transactions of the American Society of Civil Engineers*, *121*(1), 641–663. doi: <https://doi.org/10.1061/TACEAT.0007325>
- Houston, S. L., Dye, H. B., Zapata, C. E., Walsh, K. D., & Houston, W. N. (2011). Study of expansive soils and residential foundations on expansive soils in arizona. *Journal of performance of constructed facilities*, *25*(1), 31–44.
- Hubbert, M. K. (1956). Darcy's law and the field equations of the flow of underground fluids. *Transactions of the AIME*, *207*(01), 222–239. doi: <https://doi.org/10.2118/749-G>

- Hueckel, T. A. (1992). Water–mineral interaction in hygromechanics of clays exposed to environmental loads: a mixture-theory approach. *Canadian Geotechnical Journal*, 29(6), 1071–1086. doi: <https://doi.org/10.1139/t92-124>
- Ikeagwuani, C. C., & Nwonu, D. C. (2019). Emerging trends in expansive soil stabilisation: A review. *Journal of Rock Mechanics and Geotechnical Engineering*, 11(2), 423–440. doi: <https://doi.org/10.1016/j.jrmge.2018.08.013>
- Jones, L. D., & Jefferson, I. (2012). Expansive soils.
- Langroudi, A. A., & Yasrobi, S. S. (2009). A micro-mechanical approach to swelling behavior of unsaturated expansive clays under controlled drainage conditions. *Applied Clay Science*, 45(1-2), 8–19. doi: <https://doi.org/10.1016/j.clay.2008.09.004>
- Lempinen, A. (2011). Coupling swelling and water retention processes in compacted bentonite. *Chemical Product and Process Modeling*, 6(1). doi: <https://doi.org/10.2202/1934-2659.1516>
- Lew, B. (2010). Structure damage due to expansive soils: A case study. *Electronic Journal of Geotechnical Engineering*, 15, 1317–1324.
- Li, J., & Cameron, D. A. (2002). Case study of courtyard house damaged by expansive soils. *Journal of performance of constructed facilities*, 16(4), 169–175. doi: [https://doi.org/10.1061/\(ASCE\)0887-3828\(2002\)16:4\(169\)](https://doi.org/10.1061/(ASCE)0887-3828(2002)16:4(169))
- Li, J., Cameron, D. A., & Ren, G. (2014). Case study and back analysis of a residential building damaged by expansive soils. *Computers and Geotechnics*, 56, 89–99. doi: <https://doi.org/10.1016/j.compgeo.2013.11.005>
- Li, J., & Guo, L. (2017). Field investigation and numerical analysis of residential building damaged by expansive soil movement caused by tree root drying. *Journal of Performance of Constructed Facilities*, 31(1), D4016003. doi: [https://doi.org/10.1061/\(ASCE\)CF.1943-5509.0000908](https://doi.org/10.1061/(ASCE)CF.1943-5509.0000908)
- Liakopoulos, A. C. (1964). *Transient flow through unsaturated porous media*. University of California, Berkeley.
- Likos, W. J., & Lu, N. (2004). Hysteresis of capillary stress in unsaturated granular soil. *Journal of Engineering mechanics*, 130(6), 646–655. doi: [https://doi.org/10.1061/\(ASCE\)0733-9399\(2004\)130:6\(646\)](https://doi.org/10.1061/(ASCE)0733-9399(2004)130:6(646))
- Lindstrom, F. T., Haque, R., Freed, V. H., & Boersma, L. (1967). The movement of some herbicides in soils. linear diffusion and convection of chemicals in soils. *Environmental science & technology*, 1(7), 561–565. doi: <https://doi.org/10.1021/es60007a001>
- List, F., & Radu, F. A. (2016). A study on iterative methods for solving richards' equation. *Computational Geosciences*, 20(2), 341–353. doi: <https://doi.org/10.1007/s10596-016-9566-3>
- Liu, L. (2013). Prediction of swelling pressures of different types of bentonite in dilute solutions. *Colloids and Surfaces A: Physicochemical and Engineering Aspects*, 434, 303–318. doi: <https://doi.org/10.1016/j.colsurfa.2013.05.068>
- Loret, B., Hueckel, T., & Gajo, A. (2002). Chemo-mechanical coupling in saturated porous media: elastic–plastic behaviour of homoionic expansive clays. *International Journal of Solids and Structures*, 39(10), 2773–2806. doi: [https://doi.org/10.1016/S0020-7683\(02\)00151-8](https://doi.org/10.1016/S0020-7683(02)00151-8)

- Low, P. F. (1961). Physical chemistry of clay-water interaction. *Advances in agronomy*, 13, 269–327. doi: [https://doi.org/10.1016/S0065-2113\(08\)60962-1](https://doi.org/10.1016/S0065-2113(08)60962-1)
- Low, P. F., & Margheim, J. F. (1979). The swelling of clay: I. basic concepts and empirical equations. *Soil Science Society of America Journal*, 43(3), 473–481. doi: <https://doi.org/10.2136/sssaj1979.03615995004300030010x>
- Lytton, R. L. (1970). Design criteria for residential slabs and grillage rafts on reactive clay. *Rep. Prepared for CSIRO, Division of Applied Geomechanics*.
- Macht, F., Eusterhues, K., Pronk, G. J., & Totsche, K. U. (2011). Specific surface area of clay minerals: Comparison between atomic force microscopy measurements and bulk-gas (n₂) and-liquid (egme) adsorption methods. *Applied Clay Science*, 53(1), 20–26. doi: <https://doi.org/10.1016/j.clay.2011.04.006>
- Mašín, D., & Khalili, N. (2015). Swelling phenomena and effective stress in compacted expansive clays. *Canadian Geotechnical Journal*, 53(1), 134–147. doi: <https://doi.org/10.1139/cgj-2014-0479>
- Miller, E. E. (1975). Physics of swelling and cracking soils. *Journal of Colloid and Interface Science*, 52(3), 434–443. doi: [https://doi.org/10.1016/0021-9797\(75\)90268-4](https://doi.org/10.1016/0021-9797(75)90268-4)
- Moore, R., et al. (1939). Water conduction from shallow water tables. *Hilgardia*, 12(6), 383–426. doi: <https://doi.org/10.3733/hilg.v12n06p383>
- Mualem, Y. (1976). A new model for predicting the hydraulic conductivity of unsaturated porous media. *Water resources research*, 12(3), 513–522.
- Mualem, Y. (1986). Hydraulic conductivity of unsaturated soils: Prediction and formulas. *Methods of Soil Analysis: Part 1 Physical and Mineralogical Methods*, 5, 799–823. doi: <https://doi.org/10.2136/sssabookser5.1.2ed.c31>
- Nelson, J., & Miller, D. J. (1997). *Expansive soils: problems and practice in foundation and pavement engineering*. John Wiley & Sons.
- Neuman, S. P. (1977). Theoretical derivation of darcy's law. *Acta mechanica*, 25(3), 153–170. doi: <https://doi.org/10.1007/BF01376989>
- Norrish, K. (1954). The swelling of montmorillonite. *Discussions of the Faraday society*, 18, 120–134. doi: <https://doi.org/10.1039/DF9541800120>
- Nowamooz, H., & Masrouri, F. (2010). Relationships between soil fabric and suction cycles in compacted swelling soils. *Engineering geology*, 114(3-4), 444–455. doi: <https://doi.org/10.1016/j.enggeo.2010.06.005>
- Olarte, M. C., Ruge, J. C., & Rocha de Albuquerque, P. J. (2021). Influence of the inclusion of synthetic compounds on the plasticity of kaolinitic clays. *Arabian Journal of Geosciences*, 14(16), 1–11. doi: <https://doi.org/10.1007/s12517-021-08042-x>
- Otálvaro Calle, I. F. (2013). Comportamento hidromecânico de um solo tropical compactado.
- Padilla-Corona, E. (2008). Foundations on expansive soils in mexico. *Foundations*, 5, 15pm–6.

- Parcher, J. V., & Liu, P.-C. (1965). Some swelling characteristics of compacted clays. *Journal of the Soil Mechanics and Foundations Division*, 91(3), 1–18. doi: <https://doi.org/10.1061/JSFEAQ.0000733>
- Parker, J., & Lenhard, R. (1987). A model for hysteretic constitutive relations governing multiphase flow: 1. saturation-pressure relations. *Water Resources Research*, 23(12), 2187–2196. doi: <https://doi.org/10.1029/WR023i012p02187>
- Parlange, M., Prasad, S., Parlange, J.-Y., & Römkens, M. (1992). Extension of the heat-conduction technique to arbitrary soil water diffusivities. *Water resources research*, 28(10), 2793–2797. doi: <https://doi.org/10.1029/92WR01683>
- Philip, J. (1969). Hydrostatics and hydrodynamics in swelling soils. *Water Resources Research*, 5(5), 1070–1077. doi: <https://doi.org/10.1029/WR005i005p01070>
- Philip, J. R. (1957). The theory of infiltration: 4. sorptivity and algebraic infiltration equations. *Soil science*, 84(3), 257–264.
- Philip, J. R. (1969). Theory of infiltration. In *Advances in hydroscience* (Vol. 5, pp. 215–296). Elsevier. doi: <https://doi.org/10.1016/B978-1-4831-9936-8.50010-6>
- Phillips, A., & Tripathy, S. (2011). Swelling pressures of some initially saturated and compacted saturated bentonites. *International Journal of Advanced Technology in Civil Engineering*, 1(1), 64–69.
- Richards, L. A. (1931). Capillary conduction of liquids through porous mediums. *Physics*, 1(5), 318–333. doi: <https://doi.org/10.1063/1.1745010>
- Sander, G., Parlange, J.-Y., Kühnel, V., Hogarth, W., Lockington, D., & O’kane, J. (1988). Exact nonlinear solution for constant flux infiltration. *Journal of Hydrology*, 97(3-4), 341–346. doi: [https://doi.org/10.1016/0022-1694\(88\)90123-0](https://doi.org/10.1016/0022-1694(88)90123-0)
- Santamarina, J., Klein, K., Wang, Y.-H., & Prencke, E. (2002). Specific surface: determination and relevance. *Canadian Geotechnical Journal*, 39(1), 233–241. doi: <https://doi.org/10.1139/t01-077>
- Sarker, D., & Wang, J. X. (2022). Experimental study on soil–water retention properties of compacted expansive clay. In *Advances in transportation geotechnics iv: Proceedings of the 4th international conference on transportation geotechnics volume 3* (pp. 433–445). doi: https://doi.org/10.1007/978-3-030-77238-3_33
- Scheidegger, A. E. (2020). The physics of flow through porous media. In *The physics of flow through porous media (3rd edition)*. University of Toronto press.
- Sheng, D., Gens, A., Fredlund, D. G., & Sloan, S. W. (2008). Unsaturated soils: from constitutive modelling to numerical algorithms. *Computers and Geotechnics*, 35(6), 810–824. doi: <https://doi.org/10.1016/j.compgeo.2008.08.011>
- Shi, B., Jiang, H., Liu, Z., & Fang, H. (2002). Engineering geological characteristics of expansive soils in china. *Engineering Geology*, 67(1-2), 63–71. doi: [https://doi.org/10.1016/S0013-7952\(02\)00145-X](https://doi.org/10.1016/S0013-7952(02)00145-X)
- Šimnek, J., Van Genuchten, M. T., & Šejna, M. (2006). The hydrus software package for simulating two-and three-dimensional movement of water, heat, and multiple solutes in variably-saturated media. *Technical manual, version, 1*, 241.

- Skempton, A. W., & MacDonald, D. H. (1956). The allowable settlements of buildings. *Proceedings of the Institution of Civil Engineers*, 5(6), 727–768. doi: <https://doi.org/10.1680/ipeds.1956.12202>
- Snethen, D. R., Townsend, F. C., Johnson, L. D., Patrick, D. M., Vedros, P. J., et al. (1975). A review of engineering experiences with expansive soils in highway subgrades.
- Sridharan, A., & Jayadeva, M. (1982). Double layer theory and compressibility of clays. *Geotechnique*, 32(2), 133–144. doi: <https://doi.org/10.1680/geot.1982.32.2.133>
- Swamee, P. K., Rathie, P. N., de SM Ozelim, L. C., & Cavalcante, A. L. (2014). Recent advances on solving the three-parameter infiltration equation. *Journal of Hydrology*, 509, 188–192. doi: <https://doi.org/10.1016/j.jhydrol.2013.11.032>
- Tang, C., Tang, A. M., Cui, Y.-J., Delage, P., Schroeder, C., & Shi, B. (2011). A study of the hydro-mechanical behaviour of compacted crushed argillite. *Engineering geology*, 118(3-4), 93–103. doi: <https://doi.org/10.1016/j.enggeo.2011.01.004>
- Terzaghi, K. (1923). Die berechnung der durchlässigkeit des tones aus dem verlauf der hydromechanischen spannungserscheinungen. *Sitzungsber. Akad. Wiss.(Wien). Math.-Naturwiss. Kl., Abt. Iia*, 132, 125–138.
- Thompson, N. E. (2009). *Small soil column investigation of soil-geotextile capillary barrier systems* (Unpublished doctoral dissertation). University of Texas.
- Van der Waals, J. D. (1873). *Over de continuïteit van den gas-en vloeïstoofstand* (Vol. 1). Sijthoff.
- Van Genuchten, M. T. (1980). A closed-form equation for predicting the hydraulic conductivity of unsaturated soils. *Soil science society of America journal*, 44(5), 892–898. doi: <https://doi.org/10.2136/sssaj1980.03615995004400050002x>
- Van Olphen, H. (1986). An introduction to clay colloid chemistry, 1977. *National Academy of Sciences, Washington, DC*.
- Wheeler, S., Sharma, R., & Buisson, M. (2003). Coupling of hydraulic hysteresis and stress-strain behaviour in unsaturated soils. *Géotechnique*, 53(1), 41–54. doi: <https://doi.org/10.1680/geot.2003.53.1.41>
- Williams, A., Pidgeon, J. T., & Day, P. W. (1985). Expansive soils: problem soils in south africa-state of the art. *Civil Engineer in South Africa*, 27(7), 367–401. doi: <https://doi.org/abs/10.10520/EJC24998>
- Wind, G. (1955). A field experiment concerning capillary rise of moisture in a heavy clay soil. *Netherlands Journal of Agricultural Science*, 3(1), 60–69. doi: <https://doi.org/10.18174/njas.v3i1.17827>
- Yong, R., Taylor, L. O., & Warkentin, B. P. (1962). Swelling pressures of sodium montmorillonite at depressed temperatures. *Clays and Clay Minerals*, 11(1), 268–281. doi: <https://doi.org/10.1346/CCMN.1962.0110126>
- Yong, R. N., & Warkentin, B. P. (1966). *Introduction to soil behavior* (Tech. Rep.).
- Zha, Y., Yang, J., Shi, L., & Song, X. (2013). Simulating one-dimensional unsaturated flow in heterogeneous soils with water content-based richards equation. *Vadose Zone Journal*, 12(2), 1–13. doi: <https://doi.org/10.2136/vzj2012.0109>

- Zhang, F., Zhang, Z., Low, P., & Roth, C. (1993). The effect of temperature on the swelling of montmorillonite. *Clay Minerals*, 28(1), 25–31. doi: <https://doi.org/10.1180/claymin.1993.028.1.03>
- Zhao, G.-t., Zou, W.-l., Han, Z., Wang, D.-x., & Wang, X.-q. (2021). Evolution of soil-water and shrinkage characteristics of an expansive clay during freeze-thaw and drying-wetting cycles. *Cold Regions Science and Technology*, 186, 103275. doi: <https://doi.org/10.1016/j.coldregions.2021.103275>
- Zumrawi, M. (2015). Construction problems of light structures founded on expansive soils in sudan. *International Journal of Science and Research*, 4(8), 896–902.

Appendix A

MATHEMATICAL DERIVATION

The following appendix presents the derivation of each of the three relationships used in the derivation of the model: $k_z(\theta)$, $\psi(\theta)$ and $e(\theta)$. These functions' definitions allow finding the constants \bar{D}_z , \bar{a}_s and \bar{R} .

A.1 DEFINITION OF $k_z(\theta)$

The impact of the saturated conductivity (k_s) on the mathematical formulation of the model is demonstrated below. The physical meaning of k_s controls the advective part of Eq. 4.16, so it is necessary to equal \bar{a}_s to k_s using the definition of \bar{a}_s as a constant c_1 :

$$a_s(\theta) = c_1 = \frac{\partial k_z(\theta)}{\partial \theta} \quad (\text{A.1})$$

For the sake of integrating both parts, it is necessary to make a restrictive assumption based on the definition of the limits. For any value of $k_s = 0$ at the lower boundary, the function $\bar{a}_s(\theta)$ is at the residual value θ_r . Thus, when k_s reaches a specific value, the integral of $\theta = \theta$, as follows:

$$\int_0^{k_z} dk_z(\theta) = \int_{\theta_r}^{\theta} c_1 d\theta \quad (\text{A.2})$$

By integrating the left-hand term of Eq. A.2, $k_z(\theta)$ is obtained, and since c_1 is constant, it is possible to extract it from the integral:

$$k_z(\theta) = c_1 \int_{\theta_r}^{\theta} d(\theta) \quad (\text{A.3})$$

Evaluating the integral of θ between θ and θ_r yields:

$$k_z(\theta) = c_1(\theta - \theta_r) \quad (\text{A.4})$$

In the function $k_z(\theta)$, when $\theta = \theta_s$, $k_z = k_s$. Therefore:

$$k_s = c_1(\theta_s - \theta_r) \quad (\text{A.5})$$

Solving c_1 from Eq. A.5:

$$c_1 = \frac{k_s}{\theta_s - \theta_r} \quad (\text{A.6})$$

Although according to Eq. A.1, c_1 represents the definition of the function $\bar{a}_s(\theta)$, in Eq. A.6 $c_1 = \bar{a}_s$. Therefore, substituting Eq. A.6 in Eq. A.4 gives the solution for the function $k_z(\theta)$:

$$k_z(\theta) = k_s \frac{(\theta - \theta_r)}{(\theta_s - \theta_r)} \quad (\text{A.7})$$

A.2 DEFINITION OF $\psi(\theta)$

In order to define the advective part of Eq. 4.16, it is necessary to determine the function $\psi(\theta)$, whose deduction, together with the function $k_z(\theta)$, represents the term $\bar{D}_z(\theta)$. To obtain both the solution of $\psi(\theta)$ and of \bar{D}_z as a constant, it is necessary to establish that:

$$D_z(\theta) = \frac{k_z(\theta)}{\rho_w g} \frac{\partial \psi}{\partial \theta} = c_2 \quad (\text{A.8})$$

Using the definition of $k_z(\theta)$ obtained in Eq. A.7, Eq. A.8 can be rewritten as:

$$\frac{k_s}{\rho_w g} \frac{(\theta - \theta_r)}{(\theta_s - \theta_r)} \frac{\partial \psi}{\partial \theta} = c_2 \quad (\text{A.9})$$

where $c_2 = \bar{D}_z(\theta)$. To integrate both parts, it is necessary to make a restrictive assumption based on the definition of the limits. In this case, the integral is divided into two sections, one dependent on the suction and the other on the volumetric water content. Now, when $\psi = 0$, $\theta = \theta_s$, since when $\theta = \theta_r$, ψ tends to ∞ . Thus, when the suction reaches a certain value ψ , $\theta = \theta$:

$$\frac{k_s}{\rho_w g(\theta_s - \theta_r)} \int_0^\psi d\psi = c_2 \int_{\theta_s}^\theta \frac{d\theta}{\theta - \theta_r} \quad (\text{A.10})$$

The algebraic handling performed to solve Eq. A.10 is found in the following set of equations:

$$\begin{aligned} v &= \theta - \theta_r \\ dv &= d\theta \\ \frac{k_s}{\rho_w g(\theta_s - \theta_r)} \int_0^\psi d\psi &= c_2 \int_{\theta_s}^\theta \frac{dv}{v} \\ \frac{k_s}{\rho_w g(\theta_s - \theta_r)} \psi \Big|_0^\psi &= c_2 \ln(\theta - \theta_r) \Big|_{\theta_s}^\theta \end{aligned} \quad (\text{A.11})$$

When solving the integral of each term of the equation, taking into consideration the upper and lower limit, one obtains:

$$\frac{k_s}{\rho_w g(\theta_s - \theta_r)} \psi(\theta) = c_2 (\ln(\theta - \theta_r) - \ln(\theta_s - \theta_r)) \quad (\text{A.12})$$

Solving $\psi(\theta)$:

$$\psi(\theta) = c_2 \frac{\rho_w g(\theta_s - \theta_r)}{k_s} \ln \left(\frac{\theta - \theta_r}{\theta_s - \theta_r} \right) \quad (\text{A.13})$$

At this point, it is possible to find the definition of δ into the Eq. A.13 as:

$$\delta = \frac{k_s}{c_2 \rho_w g(\theta_s - \theta_r)} \quad (\text{A.14})$$

where:

$$c_2 = \frac{k_s}{\delta \rho_w g(\theta_s - \theta_r)} = \bar{D}_z \quad (\text{A.15})$$

Substituting Eq. A.14 into Eq. A.13, the mathematical definition of $\psi(\theta)$ is obtained:

$$\psi(\theta) = \frac{1}{\delta} \ln \left(\frac{\theta - \theta_r}{\theta_s - \theta_r} \right) \quad (\text{A.16})$$

It is possible to represent Eq. A.16 in terms of $\theta(\psi)$ as follows:

$$\theta(\psi) = \theta_r + (\theta_s - \theta_r) \exp(-\delta|\psi(\theta)|) \quad (\text{A.17})$$

A.3 DEFINITION OF $e(\theta)$

The function $e(\theta)$ controls the swelling process in Eq. 4.16 using the e_{min} and e_{max} values obtained from simple laboratory tests. To get the solution of $e(\theta)$, it is necessary to establish that the ratio of $R(e)$ is equal to a constant c_3 :

$$R(e) = 1 + \frac{\theta}{1+e} \frac{de}{d\theta} = c_3 \quad (\text{A.18})$$

However, to facilitate the mathematical derivation, it was assumed that $c_3 - 1 = c_4$. Therefore, by rearranging Eq. A.18:

$$c_4 \frac{d\theta}{\theta} = \frac{de}{1+e} \quad (\text{A.19})$$

For the sake of integrating both parts, it is necessary to make a restrictive assumption based on the definition of the limits. In this case, the integral is divided into two sections, one dependent on the volumetric water content and the other on the void ratio. To establish the range in which the integral of Eq. A.19 is going to be evaluated, it is assumed that when $\theta = \theta_r$, $e = e_{min}$, which is correct in the first phase of the swelling process. As θ gradually increases, the deformation produced by the increase in volume causes e to increase. This can be expressed mathematically by assuming that when $\theta = \theta$, $e = e$, i.e., any value greater than e_{min} :

$$c_4 \int_{\theta_r}^{\theta} \frac{d\theta}{\theta} = \int_{e_{min}}^e \frac{de}{1+e} \quad (\text{A.20})$$

To solve Eq. A.20 the following mathematical property was used:

$$\begin{aligned} v &= 1 + e \\ dv &= de \end{aligned} \quad (\text{A.21})$$

When evaluating the Eq. A.20 in the proposed limits was obtained:

$$c_4 \left(\ln \frac{\theta}{\theta_r} \right) = \ln \frac{1+e}{1+e_{min}} \quad (\text{A.22})$$

In order to determine the constant \bar{R} , it is necessary to assume that, during the swelling process, the soil reaches a value of $\theta = \theta_s$ at $e = e_{max}$. Therefore, Eq. A.22 can be rewritten as:

$$c_4 \left(\ln \frac{\theta_s}{\theta_r} \right) = \ln \frac{1+e_{max}}{1+e_{min}} \quad (\text{A.23})$$

Solving c_4 :

$$c_4 = \left(\frac{\ln \frac{1+e_{max}}{1+e_{min}}}{\ln \frac{\theta_s}{\theta_r}} \right) \quad (\text{A.24})$$

Since $1 + c_4 = c_3$, the constant \bar{R} is defined as:

$$1 + c_4 = 1 + \left(\frac{\ln \frac{1+e_{max}}{1+e_{min}}}{\ln \frac{\theta_s}{\theta_r}} \right) = \bar{R} \quad (\text{A.25})$$

Substituting Eq. A.25 into Eq. A.22:

$$\left(\frac{\ln \frac{\theta}{\theta_r}}{\ln \frac{\theta_s}{\theta_r}} \right) \left(\ln \frac{1+e_{max}}{1+e_{min}} \right) = \ln \frac{1+e}{1+e_{min}} \quad (\text{A.26})$$

By applying the power rule of logarithms to Eq. A.26:

$$\left(\ln \frac{1+e_{max}}{1+e_{min}} \right) \left(\frac{\ln \frac{\theta}{\theta_r}}{\ln \frac{\theta_s}{\theta_r}} \right) = \ln \frac{1+e}{1+e_{min}} \quad (\text{A.27})$$

By applying the natural logarithm rule of exp to both sides of Eq. 2.22:

$$\left(\frac{1 + e_{max}}{1 + e_{min}}\right) \begin{pmatrix} \ln \frac{\theta}{\theta_r} \\ -\frac{\theta_s}{\theta_r} \end{pmatrix} = \frac{1 + e}{1 + e_{min}} \quad (\text{A.28})$$

Solving (θ) from Eq. A.28 gives the mathematical solution for the function $e(\theta)$:

$$e(\theta) = -1 + (1 + e_{min}) \left(\frac{1 + e_{max}}{1 + e_{min}}\right) \begin{pmatrix} \ln \frac{\theta}{\theta_r} \\ -\frac{\theta_s}{\theta_r} \end{pmatrix} \quad (\text{A.29})$$